Naval Command,
Control and Ocean
Surveillance Center RDT&E Division San Diego, CA
92152-5001

Evaluation of Nondestructive Inspection Techniques for Quality Control of Alumina-Ceramic Housing Components

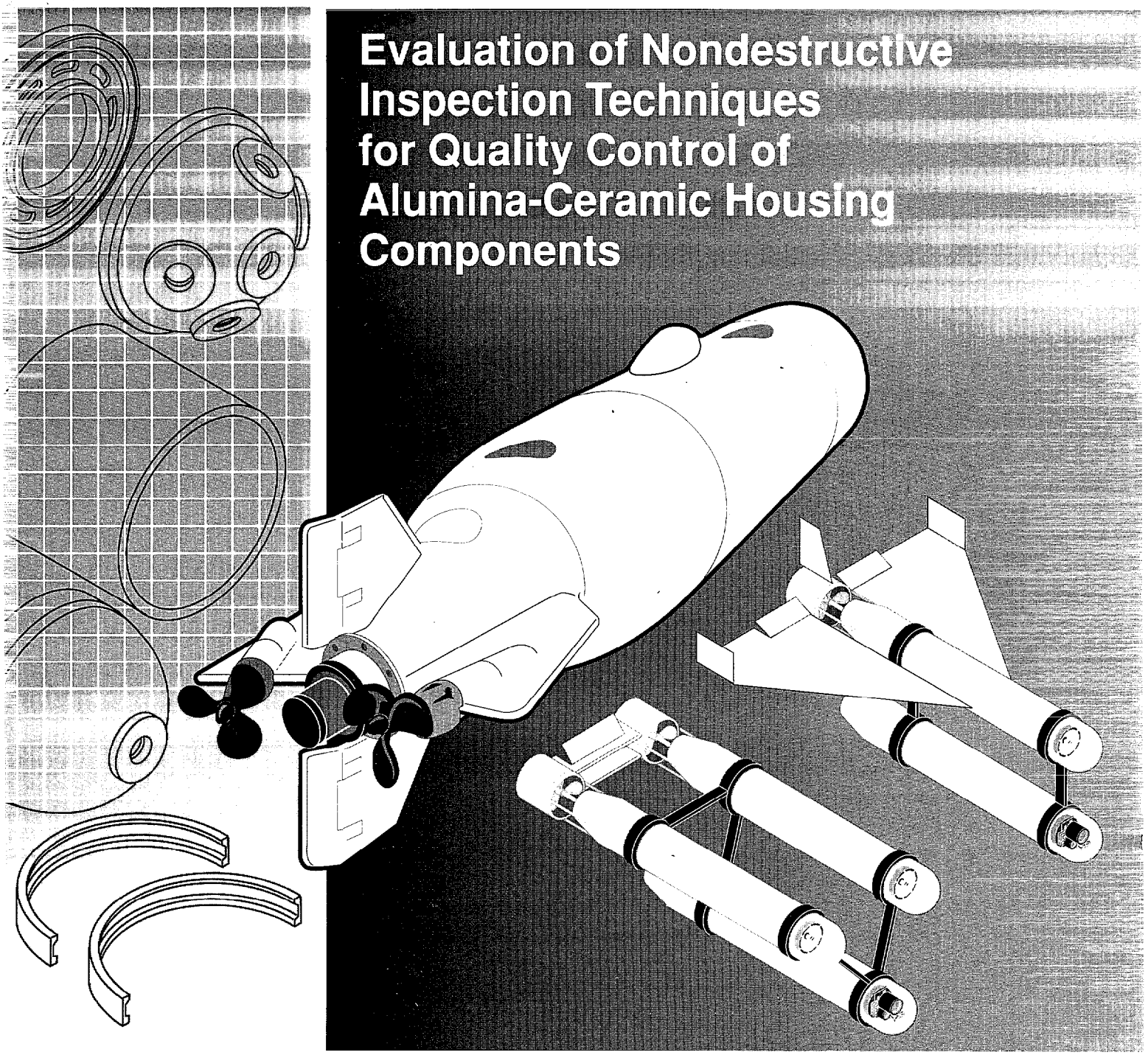

R. R. Kurkchubasche
R. P. Johnson
J. D. Stachiw

Technical Report 1588
September 1993
Approved for public release; distribution is unlimited.

Technical Report 1588
September 1993

Evaluation of Nondestructive Inspection Techniques for Quality Control of Alumina-Ceramic Housing Components

R. R. Kurkchubasche
R. P. Johnson
J. D. Stachiw

NAVAL COMMAND, CONTROL AND OCEAN SURVEILLANCE CENTER
RDT&E DIVISION
San Diego, California 92152–5001

K. E. EVANS, CAPT, USN
Commanding Officer

R. T. SHEARER
Executive Director

ADMINISTRATIVE INFORMATION

This work was performed by the Marine Materials Technical Staff, RDT&E Division of the Naval Command, Control and Ocean Surveillance Center, for the Naval Sea Systems Command, Washington, DC 20362.

SUMMARY

Alumina-ceramic pressure housings designed for a service depth of 20,000 feet have been shown to be feasible alternatives to heavier housings made from more traditional materials such as titanium, aluminum, and steel. The improvement in pressure hull weight to displacement ratio when alumina ceramic is substituted for titanium results in a three-fold increase in the payload weight capacity. The successful design, fabrication, and testing of large housings at the Naval Command, Control and Ocean Surveillance Center (NCCOSC) RDT&E Division (NRaD) such as the 26-inch-diameter housing shows that alumina-ceramic housings will soon make a transition from the developmental stage to the operational environment. One of the requirements brought on by this transition is the capability to nondestructively inspect alumina-ceramic housing components for gross fabrication flaws before they are incorporated into underwater vehicles and for operational damage during their service lives.

Several radiographic and ultrasonic inspection methods were evaluated to determine their ability to detect defects in ceramic components, determine defect location, and characterize defect size and shape.

Curved and flat 96-percent alumina-ceramic specimens having a variety of predictable defects were fabricated for NRaD and were forwarded to vendors of nondestructive evaluation (NDE) services for inspection.

The inspection methods evaluated included X-ray film radiography, digitization and enhancement of film radiographs, digital radiography, computed tomography, full-immersion pulse-echo ultrasonic inspection, waterjet through-transmission ultrasonic inspection, and acoustic scanning microscopy.

While radiographic methods such as film radiography had difficulty detecting planar defects and equi-axed or spherical defects smaller than 0.050 inch, they gave a good two-dimensional indication of the defect size for defects larger than 0.050 inch. Digitization and enhancement of film radiographs did not aid in the detection of defects, but may be instrumental in their characterization. Digital radiography, due to its higher contrast resolution, was capable of picking up planar defects. While computer tomography is very expensive, several radiographic scans taken of a defect region surrounding a defect revealed the true defect size and shape, although this information is only useful if it can be correctly interpreted.

Both of the ultrasonic methods evaluated by NRaD performed well in defect detection. The pulse-echo method was capable of finding smaller defects than the waterjet through-transmission technique. The method to choose depends on the fabrication stage of the ceramic component and the availability of NDE suppliers. The pulse-echo method has the advantage of providing the depth of the defect inside the ceramic wall. The advantages of the waterjet through-transmission method are that it is not depth sensitive and it does not suffer from a blinding effect at the wall surfaces, which effectively hides defects. Scanning acoustic microscopy provides a magnified ultrasonic scan of the defect. However, it suffers from a depth effect much like that of an optical microscope, and is only useful for small defects whose entirety lies in a very narrow focal plane.

A combination of ultrasonic and radiographic methods is recommended for the nondestructive inspection of large ceramic components. The component should first be scanned for the presence of defects by either pulse-echo or through-transmission ultrasonic C-scan. Should more information be required on any of the defects, either film radiography, digital radiography, or computed tomography should be used to investigate further. Digital radiography will give a much clearer image of the defect than film radiography. For three-dimensional location, size, and shape characterization of defects, computed tomography is recommended.

CONTENTS

INTRODUCTION 1

BACKGROUND 1

DEFECT TYPES AND THEIR CAUSES 1

AVAILABLE NDE METHODS 2

SELECTION OF NDE METHOD 3

OBJECTIVE 4

APPROACH 4

METHODS FOR PRE-SERVICE INSPECTION 4

METHODS FOR IN-SERVICE INSPECTION 5

RESULTS 5

RADIOGRAPHIC METHODS 5

Film Radiography 5

Computer Digitization and Enhancement of Film Radiographs 6

Digital Radiography (DR) 7

Computed Tomography (CT) 8

ULTRASONIC INSPECTION METHODS 9

Full-Immersion Pulse-Echo 9

Waterjet Through-Transmission 11

Scanning Acoustic Microscopy 12

CONCLUSIONS 13

RECOMMENDATIONS 14

RECOMMENDATIONS FOR FURTHER RESEARCH 15

REFERENCES 16

GLOSSARY 17

FIGURES

1. Schematic of typical deep submergence housing assembly designed by NRaD 19
2. Photo of cylindrical hull section of 25-inch-diameter alumina-ceramic housing 19

3. Fabrication process outline for typical alumina-ceramic component 20
4. Internal cracking in alumina-ceramic cylinders 20
5. Fatigue crack at ceramic bearing surface 21
6. External spalling on alumina-ceramic cylinder (reference 13) 22
7. Shards resulting from spalling (reference 13) 23
8. Cross-section of ceramic component end enclosed by U-shaped metallic end ring 24
9. Defect found in wall of 12-inch OD alumina-ceramic cylinder (reference 13) 24
10. Typical void shape (reference 13) 25
11. Engineering drawing for flat and curved calibration standards 26
12. Engineering drawing for 25-inch-diameter aluminum rings onto which curved ceramic specimens were mounted 27
13. Engineering drawing of assembled ring fixture 28
14. Assembled ring fixture containing as-fired curved ceramic specimens with cast-in defects 29
15. Setup for conventional film radiography of ceramic cylinder 30
16. X-ray film radiograph of as-fired flat alumina tile (D2) containing 1-inch-long by 0.028-inch-diameter rod-shaped defects 31
17. X-ray film radiograph of as-fired flat alumina tile (E2) containing 0.052-inch-diameter spherical defects 31
18. X-ray film radiograph of as-fired flat alumina tile (F2) containing 0.105-inch-diameter spherical defects 32
19a. Digitized image of finish-ground flat tile (E2) as displayed on a computer screen 33
19b. Digitized image of finish-ground flat tile (E2) displayed via logarithmic grey scale on a computer screen to simulate how the human eye would see it 33
20. Digitized image of x-ray film radiograph taken of as-fired flat alumina-ceramic tile (D2) containing 1-inch-long by 0.028-inch-diameter rod-shaped defects 34
21. Digitized image of x-ray film radiograph taken of as-fired flat alumina-ceramic tile (E2) containing 0.052-inch-diameter spherical defects 35
22. Digitized image of x-ray film radiograph taken of as-fired flat alumina-ceramic tile (F2) containing 0.105-inch-diameter spherical defects 36
23. Digitized image of x-ray film radiograph taken of as-fired flat alumina-ceramic tile (H2) containing 0.210-inch-square by 0.005-inch-thick planar defects 37
24. Digitized image of x-ray film radiograph taken of finish ground flat alumina-ceramic tile (H1) containing 0.210-inch-square by 0.005-inch-thick planar defects 38
25. Enhanced and embossed images of defects in as-fired flat alumina-ceramic tiles (a) D2 and (b) E2 39

26. Enhanced and embossed images of defects in as-fired flat alumina-ceramic tiles (a) F2 and (b) G2 ____ 40
27. Inspection setup for digital radiography and computed tomography ____ 41
28. Enlarged digital radiograph showing superposed images of as-fired curved specimens (a) A2 and E2, and (b) B2 and F2 ____ 43
29. Enlarged digital radiograph showing superposed images of as-fired curved tiles (a) C2 and G2, and (b) D2 and H2 ____ 45
30. CT slices of as-fired curved specimen (C2) enhanced by subtracting the average of each image from each image ____ 47
31. Non-enhanced CT slices of as-fired curved specimen (D2) ____ 49
32. CT slices of as-fired curved specimen (D2) enhanced by subtracting the average of each image from each image ____ 51
33. CT slices of as-fired curved specimen (E2) enhanced by subtracting the average of each image from each image ____ 53
34. CT slices of as-fired curved specimen (F2) enhanced by subtracting the average of each image from each image ____ 55
35. CT slices of as-fired curved specimen (G2) enhanced by subtracting the average of each image from each image ____ 57
36. CT slices of as-fired curved specimen (H2) enhanced by subtracting the average of each image from each image ____ 59
37. Setup for ultrasonic inspection ____ 61
38. C-scan obtained by full-immersion pulse-echo method of as-fired curved specimen (B2) containing 0.015-inch-diameter spherical defects ____ 63
39. C-scan obtained by full-immersion pulse-echo method of as-fired curved specimen (C2) containing 0.030-inch-diameter spherical defects ____ 63
40. C-scan obtained by full-immersion pulse-echo method of as-fired curved specimen (D2) containing 1-inch-long by 0.028-inch-diameter rod-shaped defects ____ 63
41. C-scan obtained by full-immersion pulse-echo method of as-fired curved specimen (E2) containing 0.052-inch-diameter spherical defects ____ 65
42. C-scan obtained by full-immersion pulse-echo method of as-fired curved specimen (F2) containing 0.105-inch-diameter spherical defects ____ 65
43. C-scan obtained by full-immersion pulse-echo method of as-fired curved specimen (G2) containing 0.105-inch-square by a 0.005-inch-thick planar defects ____ 65
44. C-scan obtained by full-immersion pulse-echo method of as-fired curved specimen (H2) containing 0.210-inch-square by 0.005-inch-thick planar defects ____ 67
45. C-scan obtained by full-immersion pulse-echo technique of 12-inch-OD by 14-inch-long alumina-ceramic cylinder having internal circumferential cracks caused by cyclic pressurization (reference 14) ____ 67

46. C-scan obtained by full-immersion pulse-echo method of a 1.25-inch alumina-ceramic tile containing defects at various depths 69

47. C-scan obtained by waterjet through-transmission method of as-fired curved ceramic specimen (A2) containing no known defects 71

48. C-scan obtained by waterjet through-transmission method of as-fired curved ceramic specimen (B2) containing 0.015-inch equi-axed defects 71

49. C-scan obtained by waterjet through-transmission method of as-fired curved ceramic specimen (C2) containing 0.030-inch equi-axed defects 71

50. C-scan obtained by waterjet through-transmission method of as-fired curved ceramic specimen (D2) containing 1-inch-long by 0.028-inch-diameter rod-shaped defects 72

51. C-scan obtained by waterjet through-transmission method of as-fired curved ceramic specimen (E2) containing 0.052-inch-diameter spherical defects 72

52. C-scan obtained by waterjet through-transmission method of as-fired curved ceramic specimen (F2) containing 0.105-inch-diameter spherical defects 72

53. C-scan obtained by waterjet through-transmission method of as-fired curved ceramic specimen (G2) containing 0.105-inch-square by 0.005-inch-thick planar defects 73

54. C-scan obtained by waterjet through-transmission method of as-fired curved ceramic specimen (H2) containing 0.210-inch-square by 0.005-inch-thick planar defects 73

55. C-scan obtained by SAM of one column of defects found in as-fired curved ceramic specimen (B2) containing 0.015-inch equi-axed defects. The area shown represents a 0.5-inch by 3-inch area on the specimen, each pixel measures 0.0065 x 0.0065 inch 75

56. Magnified C-scan obtained by SAM of one defect in as-fired curved ceramic specimen (B2). The area shown measures 0.096 x 0.096 inch, each pixel measures 0.0002 x 0.0002 inch 75

57. C-scan obtained by SAM of one column of defects found in as-fired curved ceramic specimen (D2) containing 1-inch-long by 0.028-inch-diameter rod-shaped defects. The area shown represents a 2.25-inch by 1.5-inch area on the specimen 77

58. C-scan obtained by SAM of as-fired curved ceramic specimen (F2) containing 0.105-inch-square by 0.005-inch-thick planar defects. The area shown measures 3 x 3 inches 77

59. C-scan obtained by SAM of as-fired curved ceramic specimen (G2) containing 0.210-inch-square by 0.005-inch-thick planar defects. The area shown measures 3 x 3 inches 79

60. C-scan obtained by SAM of one column of defects found in as-fired curved ceramic specimen (G2) containing 0.105-inch-square by 0.005-inch-thick planar defects. The area shown represents a 0.5-inch by 2.25-inch area on the specimen 79

61. C-scan obtained by SAM of one column of defects found in as-fired curved ceramic specimen (H2) containing 0.210-inch-square by 0.005-inch-thick planar defects. The area shown represents a 0.5-inch by 2.25-inch area on the specimen 79

TABLES

1. Nondestructive evaluation specimen defect code (reference 12) 81
2. Nondestructive evaluation method summary table 82

INTRODUCTION

Alumina ceramic is a material ideally suited for use in pressure-resistant housings for unmanned underwater vehicles (UUVs) because of its corrosion resistance, heat conductivity, impermeability to water, and non-magnetic characteristics. Furthermore, its high specific compressive strength and modulus make possible deep submergence housings with ratings in excess of 20,000 feet and weight-to-displacement (W/D) ratios lower than 0.60 at that depth. Traditionally, materials such as steel, titanium, and aluminum have been used for the construction of pressure resistant hulls, but their W/D ratios exceed 0.85. This difference accounts for a tripling of the payload weight capacity of a housing when alumina ceramic is substituted for titanium. A more complete explanation of the advantages of alumina ceramic or any other ceramic can be found in reference 1, which gives an outline of the program under which this work was completed.

A typical deep submergence housing as designed at the Naval Command, Control and Ocean Surveillance Center (NCCOSC) RDT&E Division (NRaD) is shown in figures 1 and 2.* This housing consists of alumina-ceramic cylinders and hemispheres joined to each other by metallic end rings, typically machined from titanium or aluminum. The metallic end rings are epoxy-bonded to the ceramic components. Design details on typical NRaD designed housings may be found in references 2 and 3.

Testing completed on these housings has shown that their structural performance is predictable (references 3, 4, and 5). NRaD has gained sufficient experience in the finite element modeling of stress and buckling to be able to predict ultimate failure of housings to within a few-hundred psi based on material properties taken from co-processed alumina parts. This predictability may be attributed to alumina's almost completely linear behavior and to the high dimensional tolerances to which the large ceramic components can be machined. This leads to excellent predictability in regard to elastic stability.

The only unpredictability is the effect of defects such as cracks, voids, and inclusions on the structural performance of the ceramic components.

The transition of alumina-ceramic pressure housing components from the developmental stage to the operational environment brings on the requirement for the nondestructive (ND) inspection of these components prior to and during service. The goal of the ND inspection of alumina-ceramic components is to discard and replace those components having gross fabrication defects or service-related damage, thus preventing the possibility of catastrophic failure.

This report defines some nondestructive evaluation (NDE) requirements and identifies which NDE methods fulfill these requirements.

BACKGROUND

DEFECT TYPES AND THEIR CAUSES

Defect types in alumina-ceramic components may be broken into two categories: *surface* and *internal*. Surface defects include cracks, regions of porosity, regions of residual stress, and other visible defects such as dings, chips, and scratches. Internal defects include voids and inclusions, as well as cracks, regions of porosity, and regions of residual stress.

The origins of these defects vary. Cracks may occur at almost every step of the component fabrication process. Figure 3 shows an outline of the fabrication process for large alumina-ceramic components. Cracks may occur after isostatic pressing, when the "green" part is pulled from its isopress mandrel. Cracks also may occur during the firing process: nonuniform rates of shrinkage or of cooling may lead to stresses too great for the part to withstand without cracking. Discontinuities in component geometry may also lead to high localized stresses, leading to cracks.

Operational use of ceramic components also may cause cracks. The component may receive a shock load which causes an internal crack, but

*Figures and tables are placed at the end of the text.

does not cause the part to break up. Furthermore, the component may contain fatigue cracks. NRaD engineers have observed internal cracks caused by cyclic pressurization to design depth. Figure 4 shows diagrammatically how these internal circumferencial cracks look. Observation has shown that the cracks always start at the bearing surface of ceramic components (figure 5) and progress away from the bearing surface, running parallel to the cylinder's inner and outer diameter. Tests show that the extent of internal cracking is related to the number of pressure cycles to which a ceramic component has been subjected and the stress to which it is loaded.

Internal circumferential cracks limit the lifetime of ceramic components being used repeatedly to design depth as they may cause shards to peel away from the component eventually (see figures 6 and 7), causing leakage or catastrophic failure. While NRaD is working to eliminate the occurrence of spalling in ceramic components altogether, it is considered safe practice to use cylinders having internal spalls as long as they have not progressed past the metallic end ring epoxied to the component end as shown in figure 8.

Voids and inclusions in ceramic components may be caused by debris that fall into the powder mix and become part of the pressed component. Voids result when these contaminants pyrolyze during firing leaving empty spaces in their places. Inclusions result when the foreign matter does not pyrolyze, but remains inside the part.

Regions of porosity may be the result of incomplete compaction during isostatic pressing, or a group of contaminants in the ceramic mix.

Residual stress regions may result from nonuniform shrinkage of the component during firing, or nonuniform cooling rates after firing, or they may be induced on the component surface during the final machining of the material.

Dings, chips, and scratches result from component mishandling.

It is beyond the scope of this study to determine what defect types, locations, sizes, and shapes are critical in determining the component's structural performance or nonperformance. Exercises in fracture mechanics may provide answers, but these generally are not practical because they assume that the void has some perfect geometry (i.e., spherical). In the past, the NDE of ceramic components has focused on defects with sizes ranging down to 25 microns. This size of defect may be critical for ceramic components loaded in tension, but the housings designed at NRaD typically are not loaded in tension. The operational stresses in these housings are almost exclusively compressive, with the exception of local regions on the ceramic bearing surface. Reference 6 deals with defect characterization and prevention in these areas of the ceramic component.

The purpose of ND inspection of the alumina-ceramic components is to detect the presence, measure the size, and characterize the shape of gross fabrication flaws in ceramic components and discard those components before they are incorporated into housing assemblies. Furthermore, a method must be established to detect the onset and monitor the progression of spalling induced by cyclic pressurization of the ceramic component so that components containing fatigue cracks extending past the metallic end rings may be replaced.

NRaD considers cracks, and voids or inclusions with diameters greater than 0.050 inch to be gross defects. This size is chosen based on tests performed on components containing defects up to this size which did not lead to catastrophic failure under compressive loading. Figure 9 shows a defect measuring 0.045 inch in diameter discovered in a 94-percent alumina-ceramic cylinder with wall thickness equal to 0.412. This void did not initiate cracking even when the nominal hoop stress in the cylinder reached 300,000 psi (reference 13). More information on the tolerability of defects will become available as a result of testing done on cylinders of various ceramic compositions under the program described in reference 1.

AVAILABLE NDE METHODS

ND inspection methods may be divided into two major categories: inspection methods using

electromagnetic waves and inspection methods using *acoustic waves.* Methods falling along the electromagnetic wave spectrum include X-ray inspection, florescent dye-penetrant inspection, visual inspection, and infrared inspection. Many variations on acoustic methods are available; they vary by setup, frequency, and type of transducer.

Surface defects may be detected best with the aid of a dye penetrant, which accentuates the presence of surface porosity and cracks. Residual stress measurements may be obtained by neutron diffraction or X-ray diffraction. Internal defects may best be detected by ultrasonic or radiographic methods.

This report deals solely with the detection of internal defects, and the methods investigated include radiographic and ultrasonic methods only. The evaluation of methods for detecting residual stresses in components is beyond the scope of this study, but is considered important and should be closely investigated in the future.

SELECTION OF NDE METHOD

Before one selects an NDE method for inspecting alumina-ceramic components for deep submergence application, one must first answer a few questions:

What type of inspection is to be performed?

The ND inspection of ceramic components may be divided into two types: *pre-service* and *in-service.* Pre-service inspection is performed before the ceramic component becomes part of the complete housing assembly. It is important to reject those components which have gross fabrication flaws before integrating them with other components into the housing assembly. The failure of just one component may lead to the catastrophic failure of all the other components. In-service inspection determines whether the component has been damaged during its operational use.

What type of defects are you looking for?

The types of defects which may occur in alumina-ceramic components have already been discussed. As will be demonstrated soon, most NDE methods are only effective in the detection and/or characterization of certain types of defects. The type of defect being sought, therefore, influences the type of NDE method that should be used to detect that defect.

At what stage of fabrication is the inspection to be performed?

As is shown in figure 3, the typical fabrication sequence for a large hemispherical or cylindrical alumina-ceramic component includes powder preparation, isostatic pressing, green machining, firing, rough grinding, and final grinding. Figure 3 also expresses on a percentage basis how much of the component cost has been expended by the time the component is through that fabrication step. Obviously, more money can be saved the earlier a component can be evaluated and identified as a reject. NRaD has not had the opportunity to investigate NDE methods applicable to components prior to firing. NDE prior to firing may not be effective as defects may still be introduced into the component as a result of firing (see discussion above: **Defect types and their causes**). Inspection of the powder for contaminants may be beneficial in the prevention of defects, but that is a quality-assurance issue rather than an ND inspection issue.

As figure 3 indicates, approximately 55 percent of the component cost may be saved if the component is inspected prior to final grinding. Grinding accounts for hours of labor and machine time.

Component cost is not the only variable that must be considered when deciding at what stage of fabrication one should perform the NDE. The performance of each NDE method depends on the stage of fabrication as defect detectability may vary depending on the fabrication stage. Equipment scheduling also must be considered. While it may be desirable to inspect the component prior to grinding, this may not be possible when machine time for grinding must be scheduled. One may, instead, decide to get the grinding of the component done while a machine is available to do the work.

What defect characteristics are sought?

Defect characteristics may be classed into various levels. The lowest level of inspection would identify the presence of a defect. Higher levels of inspection would determine the exact location of the defect in two or three dimensions. Even higher levels of NDE would indicate the defect size and shape. This type of information is considered superfluous, however, if one cannot adequately interpret its meaning. For example, figure 10 shows the shape of a void found in a ceramic cylinder. Knowing the shape of this void still does not answer whether the component is safe to use.

What can you afford to spend?

The amount of funding budgeted for ND inspection of the ceramic components also will be an issue in the selection of the method. There are some very comprehensive NDE methods available, but they may be prohibitively expensive and may provide information that you are not willing to pay for. Furthermore, some of the methods require the preparation of a witness standard. If a method requiring such a standard is chosen, one must be sure that enough money and time is budgeted for the fabrication of this specimen.

What risks are you willing to subject the component to?

The final item to consider before selecting the NDE method and vendor is the amount of risk that you are willing to subject the component to. Cost and schedule are always at risk when a component has to be shipped out to an NDE vendor. Components may be damaged during shipping or during inspection by the vendor. One may consider bringing the NDE into the manufacturing plant. This way, shipping would not be required and fixtures for handling the components would be on hand.

Once all of these questions have been answered, the choice for the NDE method will become clearer.

OBJECTIVE

The objective of this study is to evaluate several NDE methods for *pre-service* and *in-service* inspection capabilities. The minimum acceptable goal is detection of internal defects measuring larger than 0.030 inch. The methods that are evaluated include: film radiography, digitization and enhancement of film radiography, digital radiography, computed tomography, full-immersion pulse-echo ultrasonic inspection, waterjet through-transmission ultrasonic inspection, and scanning acoustic microscopy.

These methods are evaluated to determine their ability to: detect the presence of flaws (level one), determine the location of flaws (level two), determine the size of flaws (level three), and determine the shape of flaws (level four).

The final goal of the study is to make a recommendation for the NDE of large alumina-ceramic components used in deep submergence housings.

APPROACH

METHODS FOR PRE-SERVICE INSPECTION

NRaD evaluated various NDE methods by having 96-percent alumina-ceramic specimens or tiles fabricated with predictable defects in them. A total of thirty two tiles were fabricated by Wesgo, Inc. and delivered to NRaD. The tiles included two sets of eight curved tiles and two sets of eight flat tiles. One set each of curved and flat specimens had as-fired surfaces, the other set was finish ground. Each tile contained twenty-five defects of one type, occupying half the tile at approximately mid thickness. The defects were placed roughly in a five-by-five matrix pattern.

Figure 11 shows the engineering drawing for these tiles. The curved tiles measured 3 inches high by 6 inches long by 1 inch thick. The radius of curvature was 12.5 inches. Each set of eight tiles was labeled A1 through H1 for finish ground tiles and A2 through H2 for as-fired tiles. Table 1 shows the predicted dimensions of the defects and the materials used to create the defect. The eight curved, as-fired tiles were mounted onto aluminum rings (figure 12) to form the ring assembly shown in

figures 13 and 14. This ring assembly simulated a three-inch-wide "slice" of a twenty-five inch diameter alumina-ceramic cylinder. The twenty-five inch-diameter was chosen because of work performed concurrently on a twenty-five inch O.D. pressure housing (references 2 and 4).

The assembled ring was forwarded to the following vendors of NDE techniques

- Scientific Measurement Systems, Inc. (Austin, TX) performed the digital radiography and computed tomography.
- Sonic Testing and Engineering, Inc. (South Gate, CA) performed the full-immersion pulse-echo ultrasonic inspection.
- Martin Marietta Laboratories (Baltimore, MD) performed the waterjet through-transmission ultrasonic inspection and scanning acoustic microscopy.
- N. Lane and Associates (Chiloquin, OR) performed the film radiography and computer digitization and enhancement which was done on the flat tile specimens rather than the curved specimens in the interest of getting results back quickly.

METHODS FOR IN-SERVICE INSPECTION

As a second part to the study, an alumina-ceramic cylinder having internal cracks caused by cyclic fatigue was inspected using digital radiography, computed tomography, and the full-immersion pulse-echo technique. These services were provided by Scientific Measurement Systems, Inc. and Sonic Testing and Engineering, Inc., respectively.

RESULTS

RADIOGRAPHIC METHODS

Film Radiography

The physical principle behind X-ray film radiography is called Lambert's law of absorption. It states that regions of equal material thickness and density will absorb equal amounts of radiation passing through them.

The application to NDE lies in the detection of areas which absorb more or less radiation than the component does on average, thereby revealing a nonuniformity in the specimen.

Figure 15 shows the setup for taking a film radiograph of a cylindrical component. The area of the wall being inspected is placed between a plate of photographic film and source of radiation. The radiation source illuminates the exposure area, and the rays passing through the wall expose the film proportionately to the intensity of radiation which has passed through the object. Thus, the film represents a map of the amount of radiation that has passed through the object. The less exposed regions of the film represent regions where less radiation was allowed to pass; these would be areas containing denser materials or more material thickness.

The detection of voids and inclusions is achieved because voids represent missing material in the wall and, thus, would allow more radiation to pass through. Inclusions represent differences in density: Inclusions of higher density allow less radiation to pass through, those of lower density allow more radiation to pass through.

Cracks can only be detected if they are open and if their direction of propagation is in line with the path of the X-ray. Cracks perpendicular to the path of radiation would be difficult, if not impossible, to detect, as they do not represent a difference in material density or material thickness, even if they are open.

The contrast provided by film radiography is limited to resolving differences in density down to approximately 1 or 2 percent, at best. This means that in order to detect a defect in a one-inch-thick specimen, the defect size must be greater than 0.020 inch in depth.

As the setup in figure 15 shows, the inspection of a single cylinder requires more than one exposure to cover the entire object and also requires access to the inside of the component. X-ray shots could be taken through the entire object, but this reduces resolution and makes it difficult to determine the location of the defect as the two-dimensional projection onto film would not differentiate between

the front and back wall of the component. Access to the center of the component may be especially difficult when the component being inspected is a hemisphere. Due to shielding and energy requirements, film radiography is not readily portable, but thanks to widespread medical applications many facilities are available and inspection is relatively inexpensive. Industrial facilities capable of handling the largest of our components are available.

Inspection Setup. Eight as-fired flat tiles and eight finish-ground flat tiles were taken to a veterinary clinic to be X-rayed. The equipment used was manufactured by Bennet, Inc., Model P425-AT. Settings were 102 kV at 400 milliamps. Exposure time was 26.5 milliseconds.

Results. Examination of X-ray shots taken of the as-fired flat alumina tiles showed that pore defects less than, or equal to, 0.030 inch in diameter were not visible at all. One-inch long by 0.030-inch diameter rods (specimen D2), 0.052-inch diameter pores (specimen E2), and 0.105-inch diameter pores (specimen F2) were easily visible, as shown in figures 16, 17, and 18. Furthermore, the defects are shown true size. Planar defects in sample G2 were not visible at all, while the larger planar defects in sample H2 were only barely visible, and, therefore, they are not reproduced in this report.

Inspection of X-ray shots taken of finish-ground ceramic specimens showed that defects in specimens D1, E1, and F1 were more visible due to improved contrast provided by the smoother surface finish. Planar defects in specimen G1 still were not visible, and defects in specimen H1 became only slightly more visible.

Based on these results, it may be concluded that film radiography provides true-size two-dimensional representations of defects having diameters equal to, or larger than, 0.050 inches in 1-inch-thick alumina-ceramic components. Thin planar defects are virtually undetectable using film radiography. Finish ground surfaces only slightly improve the detectability of thin planar defects.

X-ray film radiography is recommended as an inexpensive method to determine the size, in two dimensions, of defects which are greater than 0.050 inch and which already have been detected by some other method. X-ray film radiography should not be used as a level-one or level-two inspection technique as it neither provides a high rate of defect detection, nor does it provide accurate three-dimensional location information.

Computer Digitization and Enhancement of Film Radiographs

Computer digitization of film radiographs is achieved by viewing the illuminated X-ray film through a CCD (charge-coupled device) camera. The camera "sees" the image through thousands of pixels which assign a numerical value to the intensity with which they are illuminated. This digitized information then may be re-displayed on a computer screen. Enhancement is the manipulation of the data to make the defects more apparent to the user.

Inspection Setup. Since digitization and enhancement are just extensions of film radiography, the comments regarding setup apply equally to the current discussion. The ability of digitization and enhancement to detect defects is limited to the film radiograph from which the image is taken. Digitization and enhancement simply helps the user identify defects not easily visible on the film.

Results. Digitized images viewed on a VGA monitor provide enhanced contrast because the image is displayed on a linear grey scale, while the human eye responds logarithmically to the grey scale (reference 7). Figure 19 shows the difference between how the human eye responds to the contrast and how the computer screen displays it. All figures shown are taken from reference 7.

Digitized images of film radiographs examined previously are shown in figures 20, 21, and 22. The only improvement was that defects in sample H2 (figure 23) became more visible. However, the improvement was approximately equal to that provided by grinding specimens prior to X-raying them (figure 24).

Contrast enhancement was applied to specimen C2 and results show that the 0.030-inch spherical defects became barely visible. Figures 25 and 26

show magnified, expanded grey-scale images of defects taken from as-fired flat tiles D2, E2, F2, and G2. The left side represents enhanced images and the right side represents embossed images. It is important to note that although these methods permit characterization of the defects they do not improve detectability.

In summary, digitization of film images improves image contrast because the computer displays the image on a linear grey scale, while the human eye responds logarithmically to the film image, thereby increasing the visibility of defects. Enhancement processes do not add to the detectability, but can be useful in the characterization of the defect. Digitization is limited to the quality of the image obtained from film radiography and, therefore, is recommended only for the same purpose as film radiography: Characterization of defect size in two dimensions once they have been detected by some other means.

Digital Radiography (DR)

The physical principle behind digital radiography is the same as for film radiography, except that the method of detecting the amount of radiation passing through the specimen is different. Figure 27 shows the inspection setups for digital radiography and computed tomography. The specimen is placed between a movable source of highly collimated radiation and a movable linear array of radiation detectors called scintillators. The source and detector array are moved in increments vertically between exposures to build a complete image of the specimen. The advantage to this method lies in the high sensitivity of the radiation detectors. This makes much higher contrast resolution possible over a wide range of illumination.

The method is not portable, and the number of facilities capable of providing the service is limited. Furthermore, the size of the object to be inspected is limited by the size of the machine, although the machine used to inspect our twenty-five-inch diameter ring is capable of inspecting components up to five feet in diameter and six feet tall. Access to the center of the component is not possible, and, therefore, DR images will always be superpositions of the front and back wall of the component being inspected. Therefore, multiple DR shots should be taken so that it may be determined on which side of the cylinder an indication may exist.

Inspection Setup. The digital radiographic inspection of the ring assembly was performed by Scientific Measurement Systems, Inc. using an SMS Model 201 scanner equipped with a 420 kV X-ray source. Four shots were taken to image the eight as-fired tiles, two at a time. The scanning parameters were as follows (reference 8):

Source:	420 kV, 3mA
Filtration:	1mm brass
Aperture:	1mm x 1mm
Ray spacing:	0.55mm
Integration time:	0.2 seconds
Height:	75.4mm
Duration:	7 minutes

The radiation source may be interchanged. In this case, X-rays were used, but gamma ray sources of varying energy levels also may be used. The energy level chosen depends on how much penetration is required. Filtration is used to reduce the beam-hardening effect. The aperture refers to the amount of radiation that is allowed to pass to the scintillators, analagous to the F-stop on a camera. A smaller aperture, combined with smaller incremental steps (ray spacing) between exposures, will result in higher spatial resolution, but will increase the amount of time required per exposure as well as the number of incremental steps required to build one complete image. The required exposure time (integration time) increases inversely with the square of the aperture, increasing with it the machine time required to build the entire image. All figures shown are taken from reference 8.

Results. Figures 28 and 29 show the four digital radiographs taken of the ring assembly. Each radiograph represents images of two specimens that were superposed on each other because the digital radiograph was taken through the entire ring assembly. For example, Figure 28a shows

specimens A2 and E2 because they were opposite each other in the ring assembly.

The 0.052-inch inclusions in tile E2 are clearly shown. However, not all five columns of defects are shown in this image. Figure 28b shows tiles B2 and F2. This image reveals only the 0.105-inch-diameter spherical inclusions of tile F2. The 0.015-inch-diameter spherical defects of tile B2 are not visible. Figure 29a shows the image of tiles C2 and G2. A few of the 0.030-inch defects are barely visible and the 0.105-inch-square by 0.005-inch-thick planar defects are visible. Figure 29b shows the image of tiles D2 and H2. The rod-shaped defects of tile D2 are easily visible and some of the 0.210-inch square by 0.005-inch planar defects are visible.

As is the case with film radiography, those spherical defects which are larger than 0.030 inch in diameter are most easily detectable as are the 0.030-inch-diameter rod-shaped defects. Planar defects are not easily visible using this method, but are much more visible than on film radiographs.

DR provides accurate two-dimensional sizing of defects greater than, or equal to, 0.030 inch in diameter in a 1-inch thickness of alumina ceramic. DR, however, does not provide the user adequate defect detection, nor does it give adequate defect location. Therefore, it is not recommended as a screening method for ceramic components. Instead, DR is recommended as a method for characterizing two-dimensional defect size and shape once the defect has already been detected by some other method. DR is not recommended for the detection of cracks of any width if the cracks lie perpendicular to the ray path, nor is it recommended for the detection of cracks parallel to the ray path if the crack opening is smaller than 0.030 inch.

Computed Tomography (CT)

CT is an extension of DR. Instead of building a two-dimensional projection of a three-dimensional object, CT provides the user with cross-sectional slices of the specimen being inspected. By stacking these slices, three-dimensional information may be obtained. CT slices are obtained by taking DR shots of the specimen from hundreds of directions. The computer then uses the data taken from all these shots to construct a density map of a slice of the specimen. The method is costly as it requires a great amount of data acquisition and processing time.

Inspection Setup. A series of nineteen slices was taken from an area of the ring assembly. The CT was performed on the same machine that performed the DR. The source, aperture, and ray spacing were the same as used in the DR. The number of views was 1,000, and plane spacing was 1.0 mm. All figures shown are taken from reference 8.

Results. Figures 30 through 36 represent the nineteen slices taken of curved specimens C2 through H2. Each set represents the highest to the lowest CT slices ordered top to bottom and left to right. Figure 31 shows the non-enhanced CT slices of specimen D2, while figure 32 shows the enhanced slices of specimen D2. Defects were visible in all of the specimens except for A2 and B2. A2 did not have any defects, and B2 contained 0.015-inch equi-axed pores. These tomographs are not shown.

Planar defects in specimen G2 and H2 were visible. It is not evident, however, that the defects in specimen G2 are planar (figure 35). Planar defects in specimen H2 appear planar, but much thicker than they actually are (figure 36). Note that the defect orientation varies from defect to defect.

CT provides the user with the most complete information of any of the NDE methods investigated by NRaD under this effort. It provides three-dimensional location information and a fairly accurate representation of defect size and shape. Due to its expense, this method is not recommended for the detection of defects, but is, instead, highly recommended for a level-four characterization of the defect once its location is known. The smallest defects detected in this study were 0.030-inch defects in a 1-inch wall thickness. Scientific Measurement Systems, Inc. reports that smaller inclusions can be imaged at the expense of more time.

A 12-inch-OD by 14.6-inch-long 94-percent alumina-ceramic cylinder which had been cycled five hundred times to 10,000 psi external pressure (reference 8) exhibited extensive spalling (figure 45). The cylinder was forwarded to Scientific Measurement Systems, Inc. for DR and CT inspection and none of the internal cracks were detected. Therefore, these two methods should not be relied upon for in-service inspections.

ULTRASONIC INSPECTION METHODS

Two ultrasonic inspection methods were investigated in this study: full-immersion pulse-echo and waterjet through-transmission.

Figure 37 shows diagrammatically how these methods work. A high-frequency sound wave is propagated into the material. The signal is monitored to determine characteristics about the specimen. After the signal has been propagated into the material, it may be monitored in one of two ways; on the opposite side of the material being inspected, as is the case with through-transmission, or on the same side of the material from which the signal was sent, as is the case with the pulse-echo technique. In the first case, the amplitude of the transmitted signal is monitored, and, in the second case, the amplitude of the return echo is monitored.

Sound is not easily propagated into a material through air, therefore, a medium must be provided to carry the sound wave from the transducer to the specimen. Water is an effective medium and is readily available. The specimen and transducer may either be fully immersed in a tank of water, or the water may be supplied locally in the form of a waterjet aimed at the area being inspected. The methods can be mixed, one also can have waterjet pulse-echo or full-immersion through-transmission inspections.

There are a number of other variables to ultrasonic inspection techniques. One is the choice of sound frequency to be used. Higher frequencies have smaller wavelengths and are capable of detecting smaller defects, however, they do not carry as well through material as do longer wavelengths.

Several transducer types may be used. Planar transducers propagate parallel sound waves only. These transducers suffer less from the effects of diffraction, but have a larger spot size, effectively reducing spatial resolution. Focused transducers have a smaller spot size in their focal plane, but have diverging spot size away from the focal plane. This results in like defects located at different depths being represented differently on the C-scan.

Sound waves may be propagated into the material normal to the surface (longitudinal wave) or at an angle (shear wave).

Full-Immersion Pulse-Echo

In the full-immersion pulse-echo technique, the transducer sends a signal into the material and then "listens" for the return signal. The return signal is displayed on an oscilloscope as return-signal amplitude versus time. This is known as an A-scan. Generally, two characteristics are always present: A strong front-wall echo and a strong back-wall echo. The region between these two echoes represents the wall thickness and is marked by what is called the "gate". If there is a detectable defect in the material being inspected, there will be an echo originating from that defect. It will be seen on the oscilloscope, or A-scan, as a spike between front- and back-wall echo. This is called a "finding". The depth of the finding in the material can be found as a function of the time at which the echo occurs.

A C-scan is a two-dimensional representation of the specimen surface that is being scanned. It maps the return signal amplitude for each point scanned on the specimen's surface and is represented by shades of grey on a black-and-white C-scan or color on a color C-scan. The return signal amplitude may be interpreted as representing the defect size and/or shape.

The size of the object to be inspected is limited by the size of the water tank and the facility's handling capabilities. This method is not readily portable, but the system is relatively low tech and may be installed at the manufacturing facility.

Inspection Setup. The full-immersion pulse-echo inspection was performed by Sonic Testing and

Engineering, Inc. using a Cal-Data System. The setup shown in figure 37 is a representation of the test setup used to inspect the ring assembly. Sonic Testing and Engineering utilized a 3.0-inch focal length, 3/8-inch diameter, 10-MHz longitudinal transducer fully immersed in a tank of water. The C-scans shown were taken in 0.030-inch incremental steps.

Prior to inspecting the curved specimens, Sonic Testing and Engineering adjusted the system gain so that defects in specimen C2 had a return signal amplitude of 80-percent.

Results. Figures 38 through 44 show color C-scans of the as-fired curved ceramic specimens. Examination of the C-scans reveals that the pulse-echo method was able to detect even the smallest defects, although not all twenty-five defects were found in every specimen. Figure 38 shows the 0.015-inch defects. Notice that they are represented much larger than actual size on the C-scan. The C-scan representation is not meant to represent defect size, the return signal amplitude must be compared against a witness specimen containing defects of known sizes. Even then, the return signal amplitude varies with the depth of the defect inside the specimen. This is most clearly shown in figure 40 which is a C-scan of the specimen containing 1-inch-long by 0.030-inch-diameter rod-shaped defects. Notice that the signal returned by the rods is not uniform along the length of the rods, especially those shown in the lower-left-hand side of the figure.

The number of defects detected per sample increases with increasing defect size, although some of the large planar defects in sample G2 (figure 43) are still not totally visible. However, the detectability for a large variety of defects is much better than that provided by radiographic methods.

Figure 46 is a C-scan taken at 0.025-inch increments of a 1.25-inch-thick tile containing 0.030-, 0.053-, and 0.079-inch-diameter defects at various depths inside the specimen. This C-scan is meant to demonstrate how the return signal amplitude of a defect varies with depth. Defect number 1 in column 1 is closer to the tile's upper surface than defect numbers 4 through 5. These five defects are all the same size (0.030 inch). The defect farthest away from the upper surface (number 5) appears largest on the C-scan because it is intercepted by the widest part of the divergent sound beam passing over it. At the same time, however, the signal amplitude returned by this defect is lower (approximately 20 percent) than that returned by defect number 2, which has 100-percent reflection at its center. Notice how defect numbers 4, 8, 12, 17, 22, and 26 appear to be roughly the same size. They are, however, defects of varying sizes lying at roughly the same depth, 0.750 inch deep. Their return signal amplitude varies, however, with the largest defects returning the strongest signal. The depth effect may be compensated for by generating and applying a depth amplitude-correction curve. This curve compensates for the depth effect by changing the signal amplitude of the return signal. One final item worth noting about figure 46 is the missing defects which are supposed to be located next to defect number 1 and above defect numbers 6, 10, 15, and 20. These defects are either too close to the surface of the tile to be detected by the 0.025-inch incremental passes made over them, or they are hidden by a "blinding" effect caused by the strong echo from the front surface of the tile.

The full-immersion pulse-echo technique is a good and relatively inexpensive method of detecting defects inside ceramic materials. It provides the exact location of defects in three dimension and has been shown to be able to detect defects down to 0.015-inch in diameter in a one-inch-thick sample with the inspection performed at 0.030-inch increments. Furthermore, it was capable of detecting all of the defect types represented by the NRaD specimens. Characterization of defects using the pulse-echo technique is more difficult as the C-scan representation is not a good indication of defect size or shape. At best, the size of the inclusion may be bracketed by comparing it with a carefully prepared witness standard containing flat bottom-drilled holes of known size located at various distances from the surface. Matters are further complicated by the fact that shape, depth, and orientation of the defect will influence the return signal. For these reasons, it is recommended that

it be full-immersion pulse-echo ultrasonic C-scan be used primarily for the screening of component defects (level-one inspection), and for locating defects (level-two inspection). This method should be supplemented with other methods to characterize the defect, if required. The method is inexpensive enough that it is advisable to perform multiple scans of the same component to increase the ability to detect defects. It is recommended that the longitudinal wave scan be supplemented by ±45-degree-angle shear wave scans. Inspection of a zirconia-toughened alumina-ceramic cylinder (reference 10) showed that an internal axially-radially oriented crack barely visible on the longitudinal scan became very apparent on the shear wave scan. The pulse-echo inspection method should not be relied upon for the detection of near surface defects. A way of getting around this problem is to either rely on shear wave C-scans or the scan parts in their as-fired or rough ground state. By doing this, the "blinding" effect takes place in a region of the part that is of no interest anyway as it will be ground away for the finished part.

Detection of spalls. A 12-inch-OD by 14.6-inch-long 94-percent alumina-ceramic cylinder, having internal spalls, was taken to Sonic Testing and Engineering, Inc. for a pulse-echo inspection to determine the extent of spalling inside the cylinder wall. The C-scan shown in figure 45 is the result of this inspection. The C-scan was obtained by scanning the cylinder using a 3.0-inch focal length, 10-MHz transducer. Inspection was performed at 0.050-inch intervals. Internal circumferential cracking is clearly shown in the figure. This is an excellent method for determining the extent of internal cracking in cylinders. One drawback is that if two or more cracks run parallel to each other in the wall, the one closer to the front surface will hide the one behind it. This is not a problem at NRaD because we are only concerned with whether internal cracking has progressed past the metallic end ring. Once such a crack exists, it is irrelevent whether there is another crack behind it. The inspection was performed with the titanium end ring removed from the cylinder. A method of determining the extent of internal cracking through the titanium end ring would be even more desirable, but this was not possible.

In a search for more portable methods of detecting spalling, NRaD has shown that commercially available thickness detectors are good indicators of spalling. Commercially available thickness detectors measure the thickness of a part using a pulse-echo technique. The time required for the signal to return from the back wall is divided by the speed of sound in that material to determine thickness. Thickness detectors have been shown to detect the interface at an internal crack. The detector shows a different thickness than the actual part thickness when passing over a spalled region. Not just any thickness detector will work. It is important to check the inspection frequency of the detector so that the sound will be adequately propagated in the alumina-ceramic medium. NRaD used a thickness detector manufactured by Panasonics, Inc. The inspection frequency used was 10 MHz. Thickness detectors use contact transducers. Using these in conjunction with a contact gel results in good coupling between the transducer and the material.

Waterjet Through-Transmission

The test setup for the through-transmission ultrasonic inspection is similar to that for pulse-echo inspection, as shown in figure 37. However, for a through-transmission inspection, access is required to both sides of the material being inspected as one transducer sends the signal and the other receives the signal. The C-scan output represents the strength of the signal that emerges from the other side of the material. Signal attenuation greater than that of the average background indicates a "finding."

Through-transmission ultrasonic inspection has some advantages over the pulse-echo technique. First, the sound wave traveling through the material being inspected must travel through the material thickness only once. In the pulse-echo technique, the sound must travel twice the distance of the material thickness. The use of a planar transducer in the ultrasonic inspection has the advantage of minimizing the depth-amplitude effect. The use of waterjets helps reduce the effective sound aperture, making possible a higher spatial resolution.

Some disadvantages to the waterjet through-transmission ultrasonic inspection include the noise which may be caused by the quality of the material surface being inspected. Rougher surfaces create more background noise which could "hide" some of the smaller defects. Through-transmission also does not give the defect depth in the material because it does not use an echo and, therefore, cannot measure the time of the signal.

The waterjet through-transmission ultrasonic inspection method can be portable and has the advantage of not requiring a large water tank. It can be set up temporarily in the ceramic manufacturing plant. However, access to both sides of the material is required. This may be difficult in the case of a hemisphere.

Inspection Setup. The through-transmission ultrasonic inspection of the ring assembly containing as-fired samples was performed by Martin Marietta Laboratories. LUP™ waterjet probes 1/16-inch in diameter were used. The transducer was a 10-MHz planar transducer. The test index was 0.020 inch. All figures shown are taken from reference 11.

Results. The through-transmission C-scans for as-fired curved specimens A2 through H2 are shown in figures 47 through 54. The grey background appearance of the C-scans may be attributed to noise created by the as-fired surface roughness. Martin Marietta Laboratories claims that this noise would be reduced if the surface finish of the specimens were smoother. The 0.015-inch defects in specimen B2 are not visible on the C-scan. The 0.030-inch spherical defects in specimen C2 are clearly visible, although not all twenty-five defects are apparent. Figure 50 shows specimen D2. Note how the fibers are visible in their entirety; visibility does not appear to be depth dependent. Defects in all the other specimens are clearly visible and are shown uniformly, again, as a result of not being depth dependent. Comparison with pulse-echo results show how nonuniform the representation of the defects is in the pulse-echo technique. As is the case with pulse-echo, the through-transmission C-scans do not give an accurate representation of the defect size. Martin Marietta Laboratories claims that a correction factor must be applied to the C-scan because of the test nozzle's diameter. The correction is to subtract 0.120 inch from the apparent dimension, a correction based on the waterjet nozzel diameter. This correction does not seem to apply to planar defects.

Waterjet through-transmission C-scans are effective in detecting defects equal to, or larger than, 0.030 inch in a 1-inch-thick alumina material specimen. The rate of detectability rises with increasing sizes of defects. Advantages of the method are that uniformly sized defects are represented uniformly on the C-scan, even though they may not appear true to size. The detectability of defects does not vary with depth or defect orientation as it does in the pulse-echo method. Furthermore, this method does not have the "skin effect" of the pulse-echo method, making even defects that are very close to the surface detectable. The disadvantages of this method are that the quality of the scan seems to be affected by the quality of the component's surface finish, therefore, making it less suitable for inspection when ceramic components are in the as-fired state, although the results on the 1-inch-thick as-fired specimens are very good. Furthermore, through-transmission does not provide the user with information on the depth of the defect within the specimen.

Waterjet through-transmission ultrasonic inspection is recommended for a level-one inspection of large alumina-ceramic components only. Determination of defect size and depth within the wall must be made by another method. The method is not recommended for the detection of defects smaller than 0.030 inch if the component is to be examined in its as-fired state. Waterjet through-transmission is a good method to consider for inspection of parts in the manufacturing plant because it does not require a large tank and may be set up on a temporary basis.

Scanning Acoustic Microscopy

Knowing that accurate sizing and depth information is not given by their waterjet through-transmission method, Martin Marietta Laboratories complements its inspection of parts with scanning acoustic microscopy. Scanning acoustic

microscopy (SAM) is a full-immersion pulse-echo technique in which scanning is performed in very small increments, giving detailed images of defects.

Inspection Setup. Martin Marietta Laboratories used SAM to look at as-fired specimens B2, D2, F2, G2, and H2. Inspection frequencies were 5 and 10 MHz. All figures shown are taken from reference 11.

Results. The results of the SAM are shown in figures 55 through 60. Inspection of specimen B2 actually revealed the 0.015-inch defects in the first row only. Martin Marietta Laboratories admits that these defects would not have been found had their presence not been known. Figure 56 shows the ability of SAM to magnify defects. Only the regions with high signal-return echoes can be used for sizing, however. Figure 57 shows a magnified view of the rod-shaped defects in specimen D2. The shape of the rod appears distorted because the shape passes through various depths within the tile. SAM is limited to examining only a narrow plane of depth within the sample at one time. Figures 58 through 61 show scans of specimens F2, G2, and H2. Sizing defects is not readily possible because of diffraction effects.

SAM is not recommended for defect detection in ceramic components. NRaD would not even recommend it for the determination of flaw shape or size, especially when there are other less costly, and more accurate, methods available to complete these tasks.

CONCLUSIONS

The following conclusions were made based on the nondestructive evaluation performed on the specially prepared 1-inch-thick alumina-ceramic specimens:

1. X-ray film radiography was capable of detecting non-planar defects equal to, or larger than, 0.052 inch. Planar defects could only barely be detected in finish-ground specimens.
2. Digitization and enhancement of film radiographs make defects slightly more visible by enhancing contrast. The detectability of defects is limited to the film radiograph from which the image is digitized. Enhancement is useful for the characterization of defects.
3. Digital radiography was able to detect non-planar defects equal to, and larger than, 0.030 inch as well as planar defects as thin as 0.005 inch. DR was not able to detect internal circumferential cracks in a cylinder known to have these cracks.
4. Computed tomography was able to detect non-planar defects equal to, or larger than, 0.030 inch as well as planar defects as thin as 0.005 inch. CT was not able to detect closed internal circumferential cracks in a cylinder known to have these cracks. CT gives the user a good three-dimensional indication of defect size, shape, and location.
5. Both ultrasonic methods examined were able to detect all of the defect types represented in the specimens, except for the 0.015-inch defects which the waterjet through-transmission method was not able to detect.
6. While the full-immersion pulse-echo technique did detect the smallest of defects, it did not detect all of them in one scan. Furthermore, its sensitivity to defects seems to depend on the depth of the defect, as does the C-scan representation of defect shape and size. These shortcomings may be compensated for by making multiple scans of the component and using a depth-amplitude correction curve arrived at with a well-prepared witness standard. The pulse-echo technique has a "blinding" effect at the wall boundaries and may not be able to detect defects near the surface. This problem may be mitigated either by inspecting the ceramic component before it is finish ground, or by supplementing the longitudinal wave C-scan with shear wave C-scans. The pulse-echo technique was an excellent method for detecting and characterizing internal circumferential cracks in ceramic cylinders.
7. The waterjet through-transmission inspection method was not able to detect the 0.015-inch defects. Its advantages are that the C-scan

representations of similar defects do not vary with the depth of the defect in the wall thickness, nor does the sensitivity to defects vary with depth. Furthermore, this method does not have trouble detecting defects near the skin of the component wall. This method may be easier to set up in a ceramics manufacturing plant for on-the-spot inspection of components. However, it will not provide the user with the depth of the defect within the wall.

8. While both of the ultrasonic inspection methods evaluated by NRaD were excellent detectors of defects equal to and larger than 0.030 inch, they are not good for the characterization of defect shape and size. At best, the size of a defect may be bracketed by comparison with a carefully prepared witness standard.

9. Scanning acoustic microscopy was able to detect all of the defect types represented, although the smallest of defects were found only because their presence was known. SAM is effective in magnifying defects, but is limited because the representation of the image depends on the width of the gate. In order for the entire defect to be imaged, it must lie in one narrow plane of depth. SAM is not effective for scanning components for defects, nor is it effective for the characterization of defects.

10. The best methods for scanning components for defects are ultrasonic techniques. Pulse-echo and through-transmission will cost approximately the same for like components. DR shots taken from several directions also may be an effective screening method and will cost the same as the ultrasonic techniques. X-ray film radiography would be the least expensive method of screening components, but this method is unlikely to detect planar defects and non-planar defects smaller than 0.052 inch.

11. Defect characterization may be best achieved by CT, DR, or X-ray film radiography. CT will cost approximately an order of magnitude more than film radiography, but will provide the user with three-dimensional shape, size, and location information while DR and film radiography will provide only two-dimensional shape, size, and location information.

12. The NDE methods most effective for inspection of rough-ground or as-fired parts are full-immersion pulse-echo technique and CT. Film radiography, DR, and waterjet through-transmission ultrasonic scan will be affected by surface roughness.

13. None of the industrial inspection techniques evaluated by NRaD in this effort were able to reliably detect defects smaller than 0.015 inch.

Table 2 is a summary of the NDE methods.

RECOMMENDATIONS

Based on the above findings, NRaD makes the following recommendations for the nondestructive evaluation of alumina-ceramic components having wall thicknesses up to 1 inch thick. These recommendations are based on a requirement for detection of defects larger than 0.030 inch and characterization of defects larger than 0.050 inch.

1. Pre-service inspection should be performed as early as possible during component fabrication since there is a potential of saving up to 55% of component cost if a part is found to be a reject before it is ground.

2. Pre-service inspection should include a screening phase and a characterization phase. Component screening (level-one/level-two inspection) may be performed using either the full-immersion pulse-echo technique or waterjet through-transmission. The full-immersion pulse-echo technique is recommended if the part is in as-fired condition, waterjet through-transmission if the part is already finish ground. The inspection setup recommended for both methods uses 10 MHz transducers and 0.010-inch step increments. In the case of the full-immersion pulse-echo technique, it is recommended that longitudinal scans be complemented by +45-degree and –45-degree shear-wave scans.

3. The ultrasonic inspection methods should use a well-prepared standard specimen fabricated from the same material composition as the component to be inspected. The standard should contain multiple flat-bottom drillled holes at various depths, preferably at 1/4, 1/2, and 3/4 of thickness. Hole diameters should bracket defect dimensions of interest. NRaD uses 1/32-, 1/16-, and 1/8-inch-diameter drilled holes.
4. Inspection equipment should be calibrated using the standard specimen to show defect sizes of interest. In general, NRaD seeks to detect defects larger than 0.030 inch and characterize defects larger than 0.050 inch.
5. Once defects have been detected, those of interest should be examined with any of the radiographic methods available. In order of lowest cost to highest cost, these are film radiography (possibly combined with digitization and enhancement), DR, and CT. Film radiography will probably be the most readily available.
6. SAM is not recommended for screening or characterizing defects.
7. Before choosing the inspection facility, it is recommended that prospective facilities be visited and examined for handling capabilities, size of water tank (when applicable), size of turntable (where applicable), availability of overhead cranes and their capacity and clearance over the side of the water tank (where applicable), and general component traffic in the area where inspection of the ceramic components is being performed. Furthermore, the vendor should be asked to provide a C-scan of the standard specimen to demonstrate ability to detect defects.
8. It is recommended that someone from the ceramic manufacturing or engineering group be present while handling components in the inspection facilities at least for the first time such a component is being inspected at the facility.

The methods and procedures recommended should apply to any homogeneous ceramic composition as long as calibration is performed using a standard made from the same composition.

RECOMMENDATIONS FOR FURTHER RESEARCH

The following areas in the NDE of ceramic material require further attention:

1. Performance of NDE on nonhomogeneous ceramic compositions such as metal-reinforced ceramics (cermets).
2. Cost effective methods for nondestructively determining the residual stresses existing in large ceramic components.

REFERENCES

1. Kurkchubasche, R. R., R. P. Johnson, and J. D. Stachiw. 1993. "Application of Ceramic to Large Housings for Underwater Vehicles: Program Outline," NRaD TD 2585 (Oct). Naval Command, Control and Ocean Surveillance Center, RDT&E Division, San Diego, CA.

2. Johnson, R. P., R. R. Kurkchubasche, and J. D. Stachiw. 1993. "Design and Structural Analysis of Alumina Ceramic Housings for Deep Submerged Service: Fifth Generation Housings," NRaD TR 1583 (Mar). Naval Command, Control and Ocean Surveillance Center, RDT&E Division, San Diego, CA.

3. Stachiw, J. D., R. P. Johnson, and R. R. Kurkchubasche. 1993. "Evaluation of Scale-Model Ceramic Housing for Deep Submergence Service: Fifth Generation Housings," NRaD TR 1582. Naval Command, Control and Ocean Surveillance Center, RDT&E Division, San Diego, CA.

4. Johnson, R. P., R. R. Kurkchubasche, and J. D. Stachiw. 1993. "Evaluation of Alumina Ceramic Housings for Deep Submergence Service: Fifth Generation Housings—Part 1," NRaD TR 1584. Naval Command, Control and Ocean Surveillance Center, RDT&E Division, San Diego, CA.

5. Johnson, R. P., and R. R. Kurkchubasche. 1993. "Evaluation of Alumina Ceramic Housings for Deep Submergence Service: Fifth Generation Housings—Part 2," NRaD TR 1585. (Dec) Naval Command, Control and Ocean Surveillance Center, RDT&E Division, San Diego, CA.

6. Pasto, A. E., B. L. Cox, M. K. Ferber, C. R. Hubbard, M. L. Santella, W. A. Simpson, Jr., and T. R. Watkins. 1993. "Effect of Surface Condition on Strength and Fatigue Behavior of Alumina," NRaD TD 2584. Contractor Report, Oak Ridge National Laboratory, Oak Ridge, TN.

7. Lane, N. W. 1993. "Detection of Flaws in Ceramic Specimens by X-Ray Illumination and Computer Generated Digitization and Enhancement of Filmed Images," Contractor Report performed under contract No. N66001–93–M–0808 (Apr).

8. Scientific Measurement Systems, Inc. 1993. "Digital Radiography and Computed Tomography of Ceramic Test Specimens," Contractor Report performed under contract No. N66001–93–M–0816 (Apr).

9. Scientific Measurement Systems, Inc. 1993. "Ceramic Cylinder Inspection for NCCOSC RDT&E Division," Contractor Report performed under contract No. N66001–93–M–3059 (Aug).

10. Johnson, R. P., and R. R. Kurkchubasche. 1993. "Structural Performance of Cylindrical Pressure Housings of Different Ceramic Compositions Under External Pressure Loading: Part II Zirconia Toughened Alumina Ceramic," NRaD TR 1593. Naval Command, Control and Ocean Surveillance Center, RDT&E Division, San Diego, CA.

11. Djordjevic, B. B., Martin Marietta Laboratories. 1993. "Nondestructive Testing of Ceramic Witness Specimens by Scanning Acoustic Microscopy," Contractor Report performed under contract No. N66001–93–M–0883 (May).

12. Huebel, E. "NDE Standards Fabrication," Contractor Report performed under contract No. N66001–92–M–4682.

13. Stachiw, J. D. 1993. "Exploratory Evaluation of Alumina Ceramic Housings for Deep Submergence Service: Third Generation Housings," NOSC TR 1314 (Sep). Naval Command, Control and Ocean Surveillance Center, RDT&E Division, San Diego, CA.

14. Johnson, R. P., R. R. Kurkchubasche, and J. D. Stachiw. 1993. "Effect of Different Axial Bearing Supports on the Cyclic Fatigue Life of Ceramic Pressure Housings," NRaD TR 1607 (Oct). Naval Command, Control and Ocean Surveillance Center, RDT&E Division, San Diego, CA.

GLOSSARY

CT	computed tomography
DR	digital radiography
ND	nondestructive
NDE	nondestructive evaluation
OD	outside diameter
SAM	scanning acoustic microscopy
W/D	weight-to-displacement

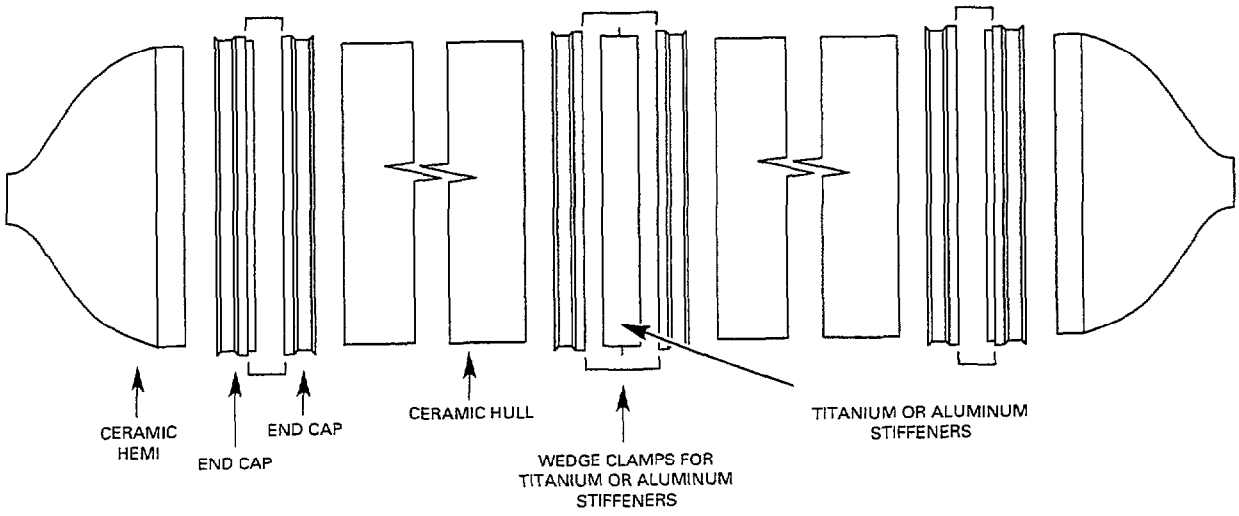

Figure 1. Schematic of typical deep submergence housing assembly designed by NRaD.

Figure 2. Photo of cylindrical hull section of 25-inch-diameter alumina-ceramic housing.

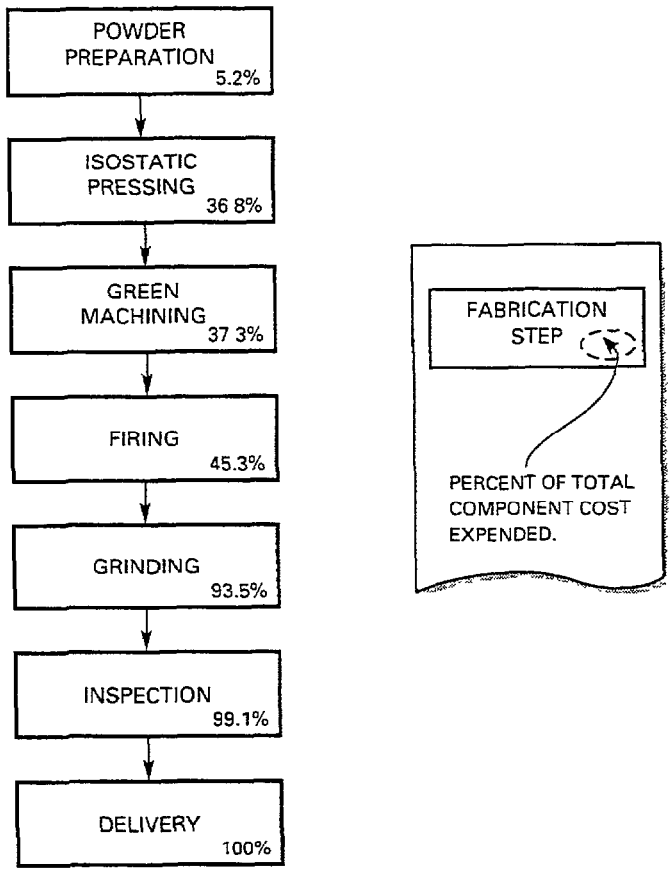

Figure 3. Fabrication process outline for typical alumina-ceramic component.

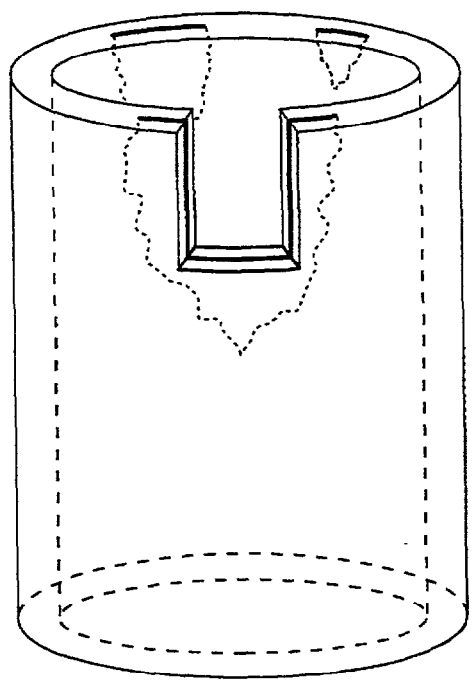

Figure 4. Internal cracking in alumina-ceramic cylinders.

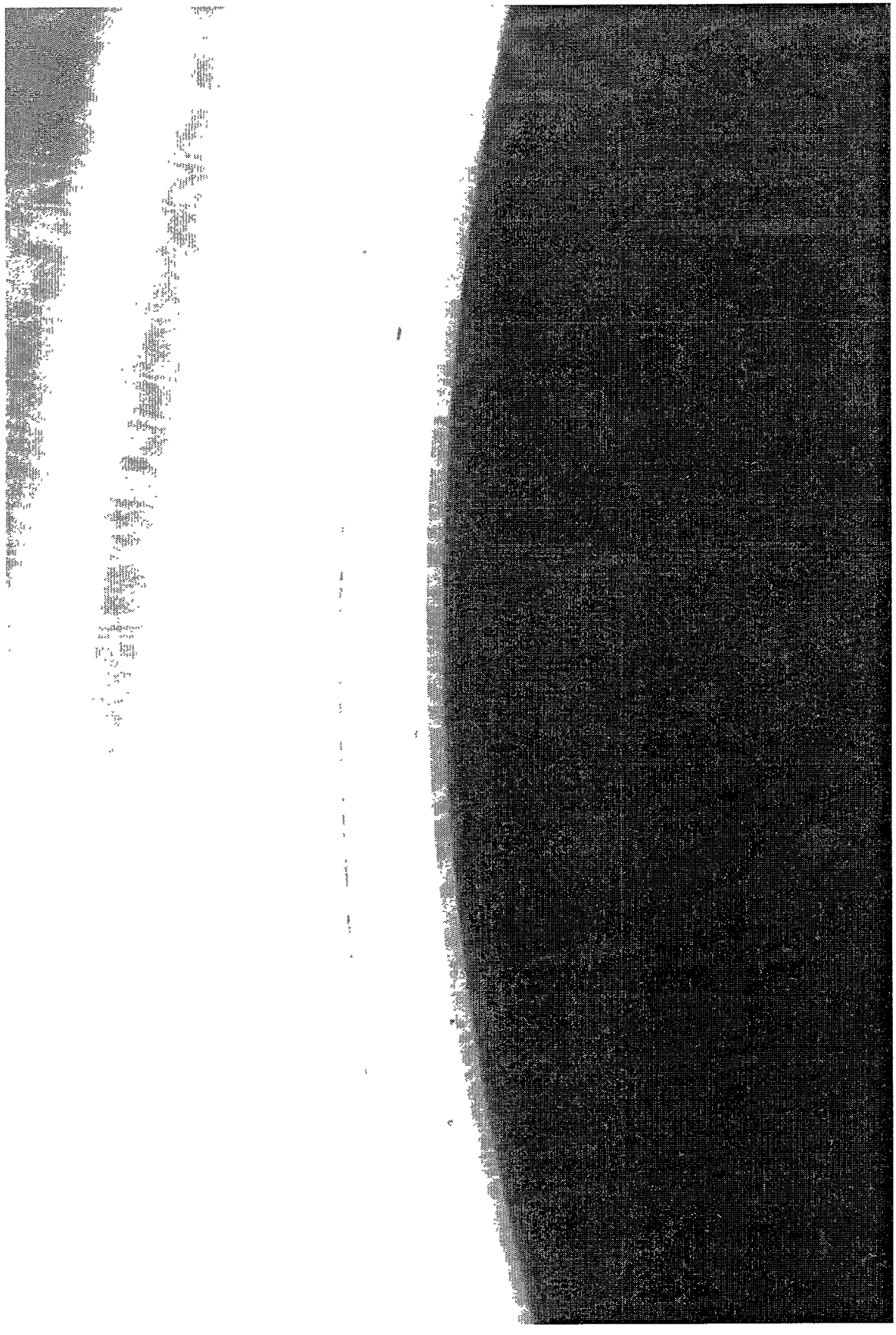

Figure 5 Fatigue crack at ceramic bearing surface.

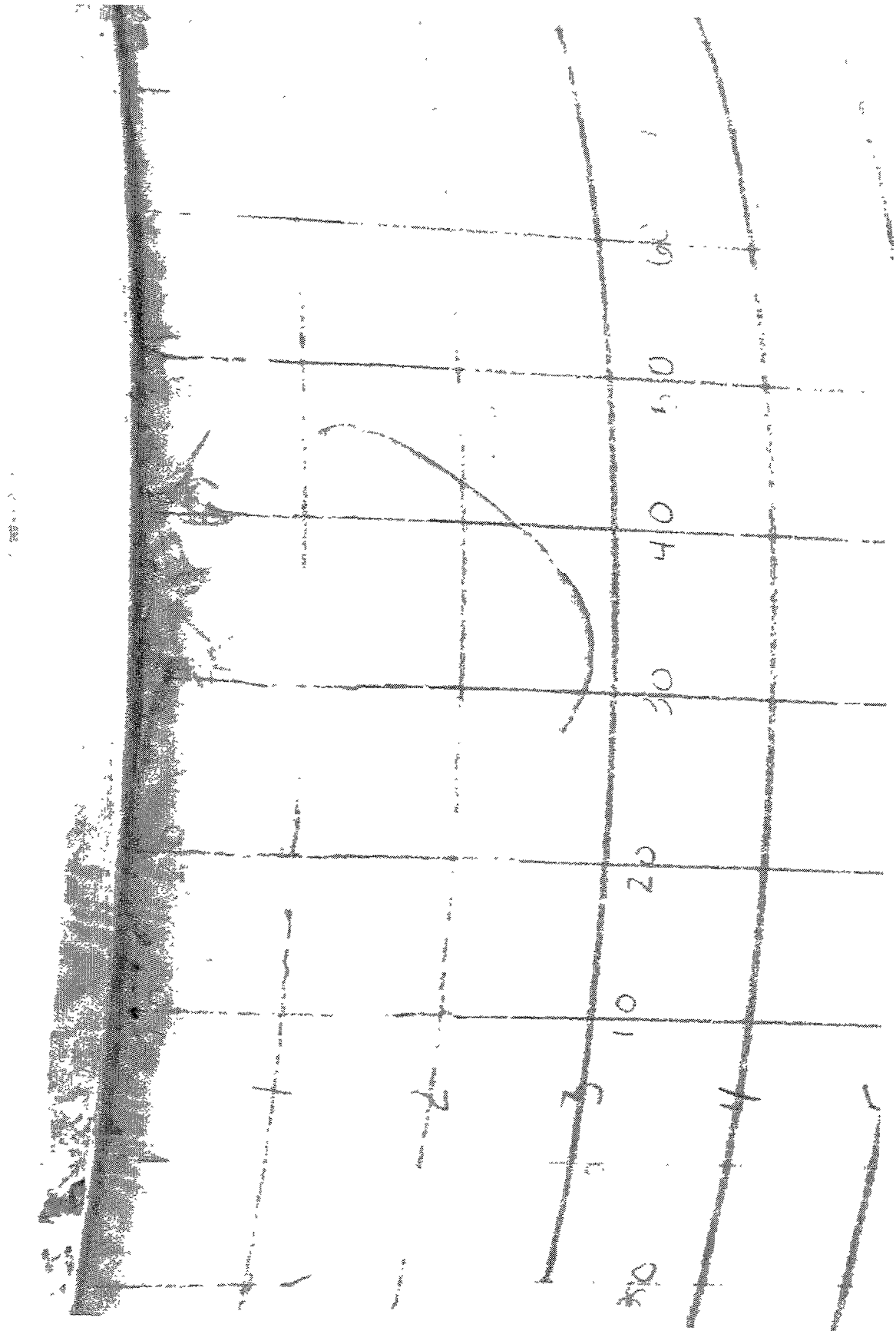

Figure 6. External spalling on alumina-ceramic cylinder (reference 13).

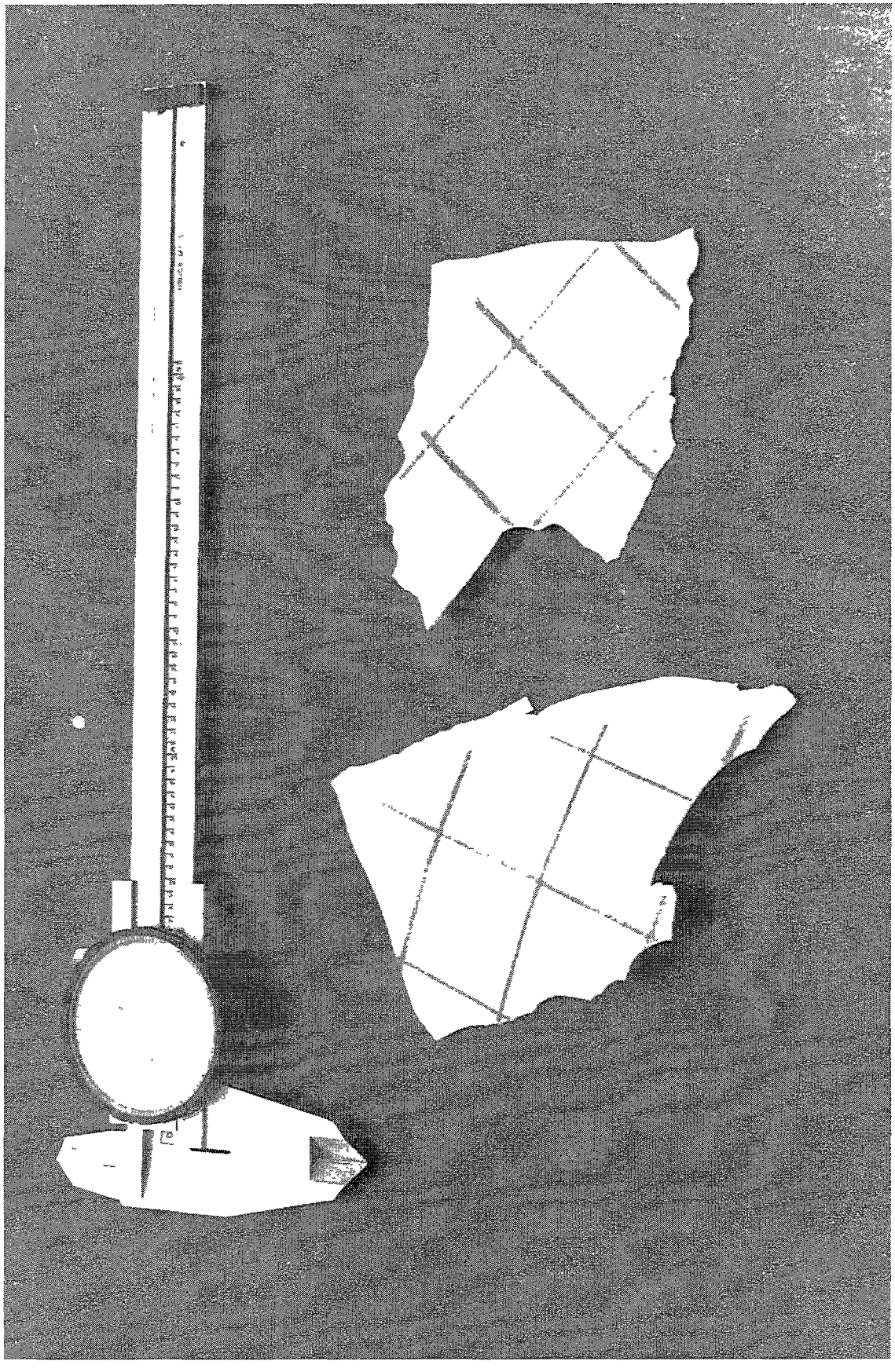

Figure 7. Shards resulting from spalling (reference 13)

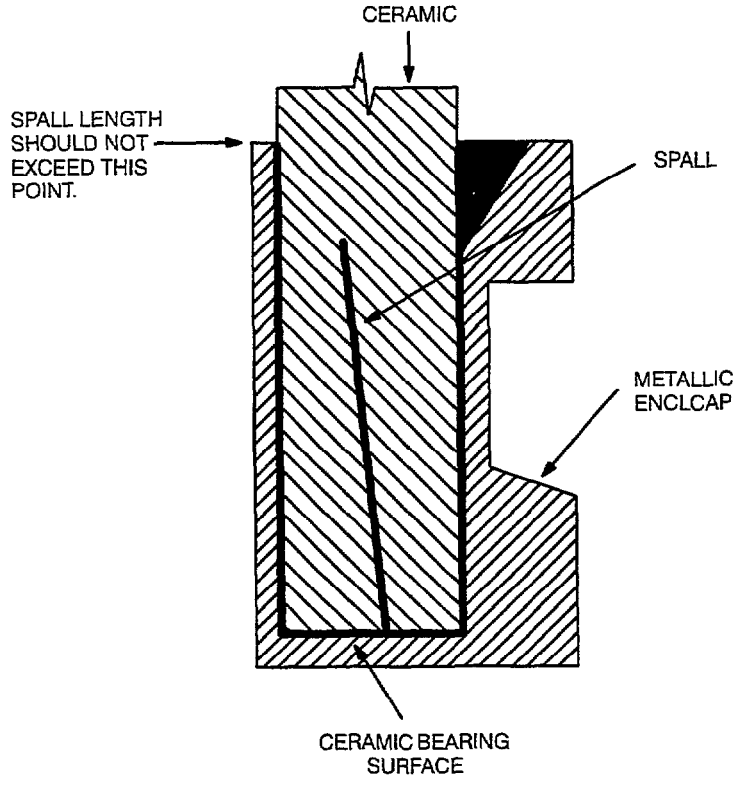

Figure 8. Cross-section of ceramic component end enclosed by U-shaped metallic end ring.

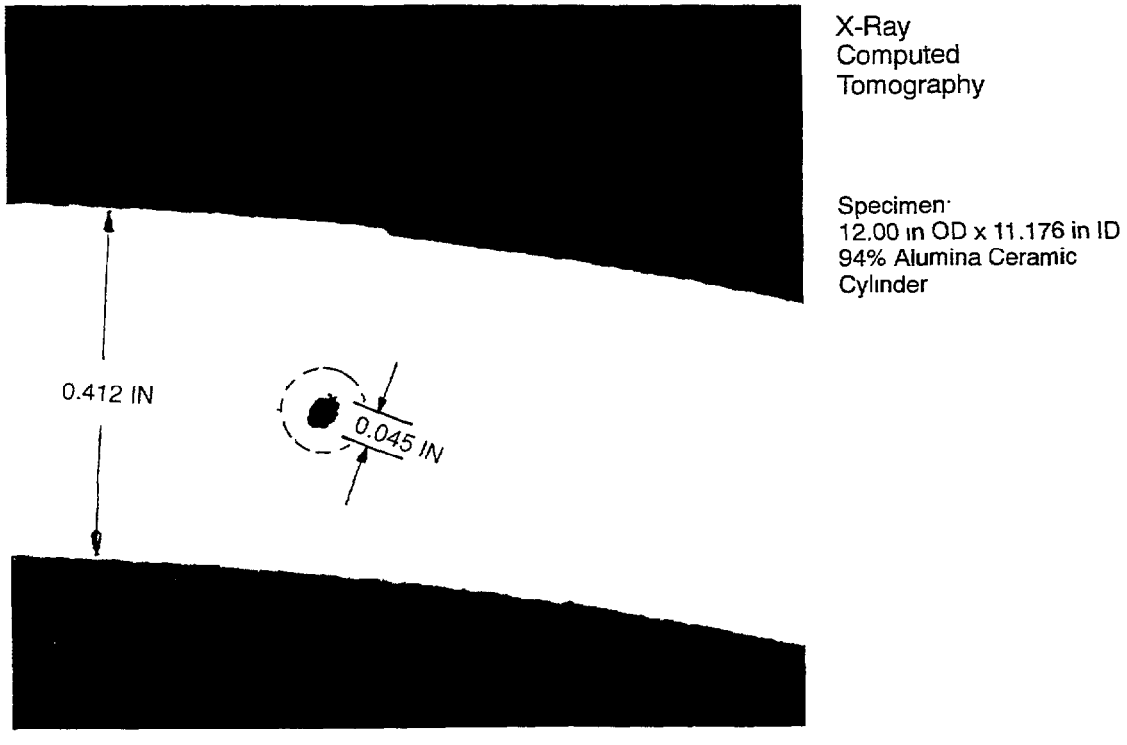

Figure 9. Defect found in wall of 12-inch OD alumina-ceramic cylinder (reference 13).

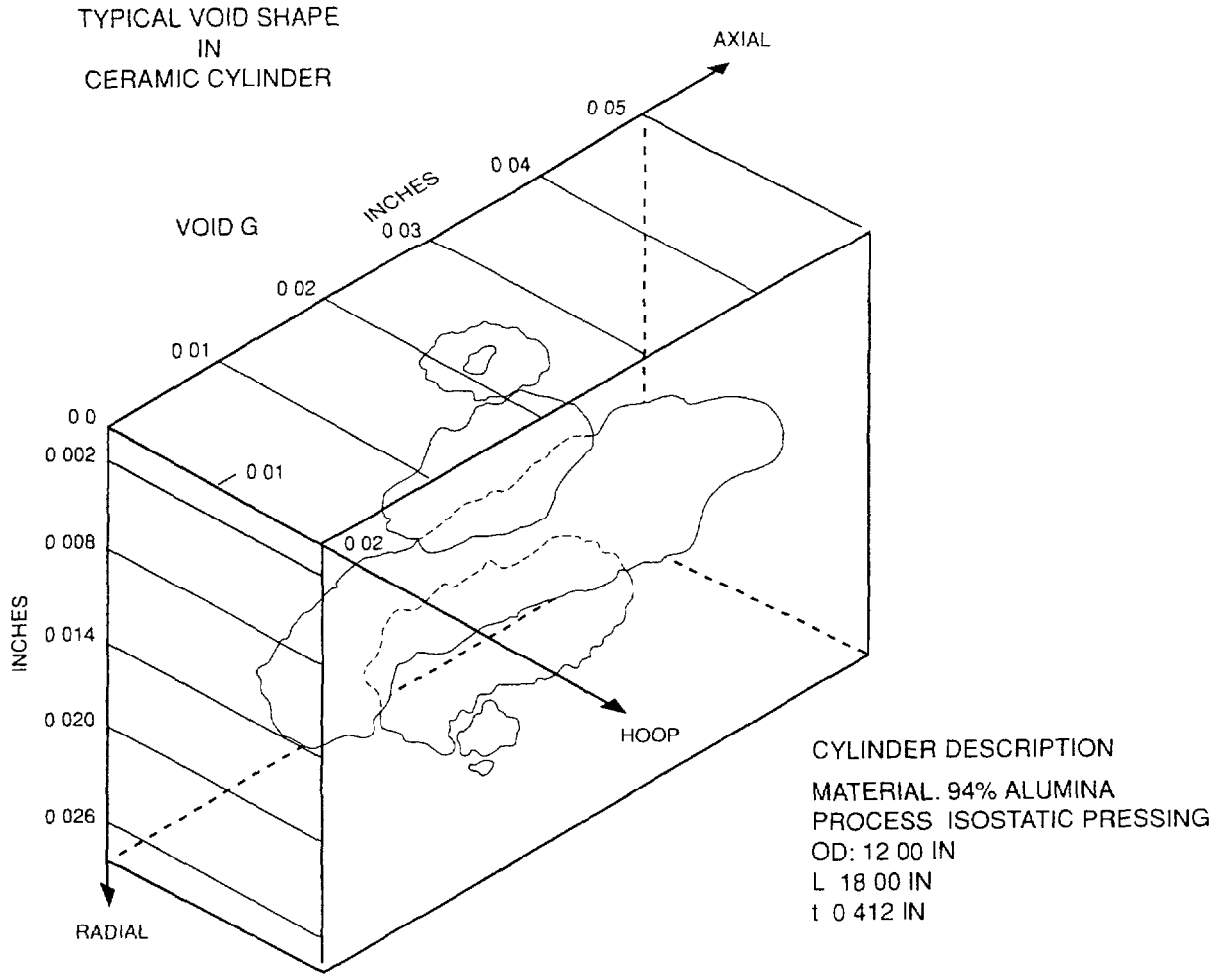

Figure 10. Typical void shape (reference 13)

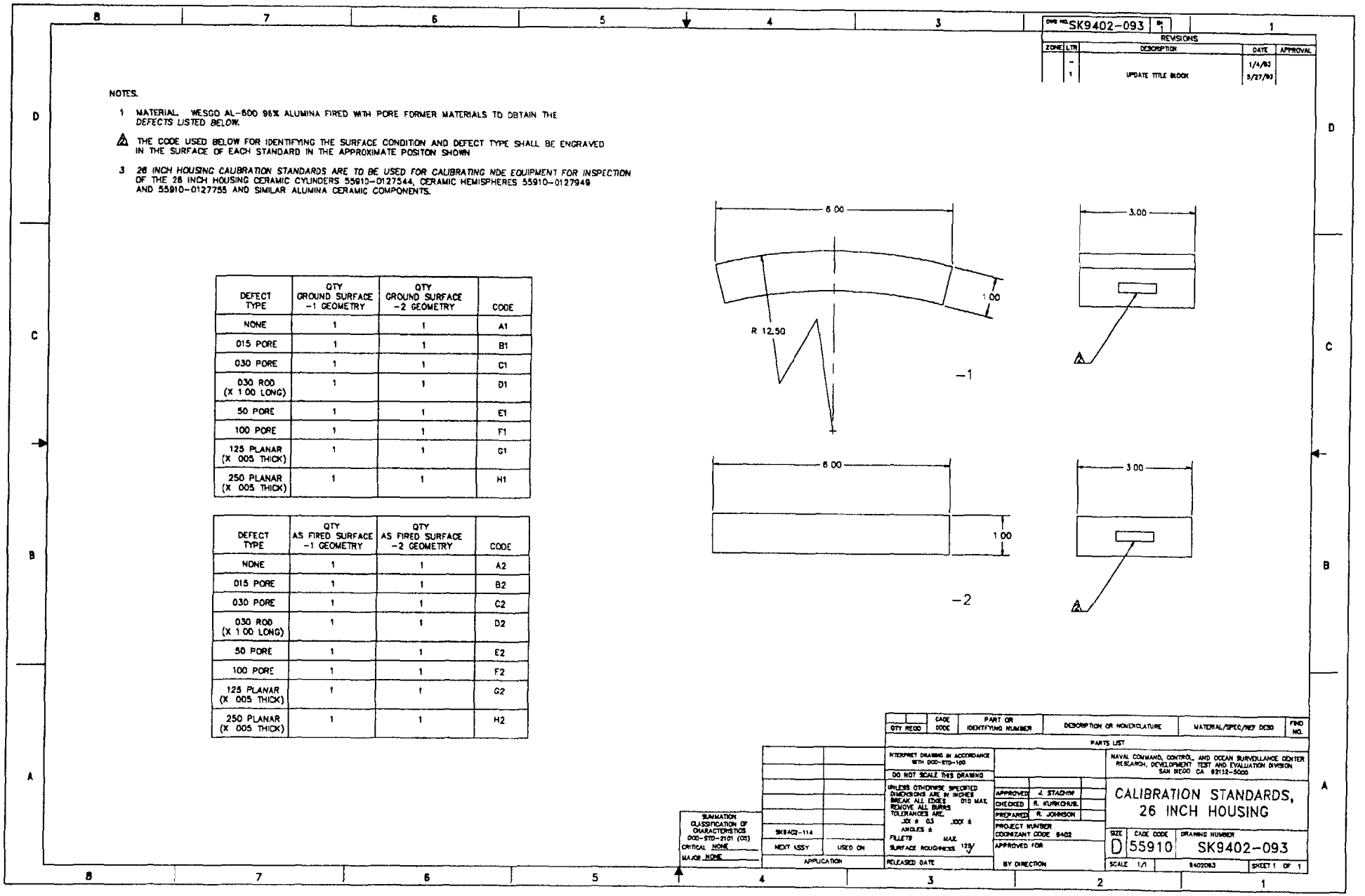

DEFECT TYPE	QTY GROUND SURFACE -1 GEOMETRY	QTY GROUND SURFACE -2 GEOMETRY	CODE
NONE	1	1	A1
015 PORE	1	1	B1
030 PORE	1	1	C1
030 ROD (X 1.00 LONG)	1	1	D1
50 PORE	1	1	E1
100 PORE	1	1	F1
125 PLANAR (X .005 THICK)	1	1	G1
250 PLANAR (X .005 THICK)	1	1	H1

DEFECT TYPE	QTY AS FIRED SURFACE -1 GEOMETRY	QTY AS FIRED SURFACE -2 GEOMETRY	CODE
NONE	1	1	A2
015 PORE	1	1	B2
030 PORE	1	1	C2
030 ROD (X 1.00 LONG)	1	1	D2
50 PORE	1	1	E2
100 PORE	1	1	F2
125 PLANAR (X .005 THICK)	1	1	G2
250 PLANAR (X .005 THICK)	1	1	H2

Figure 11. Engineering drawing for flat and curved calibration standards

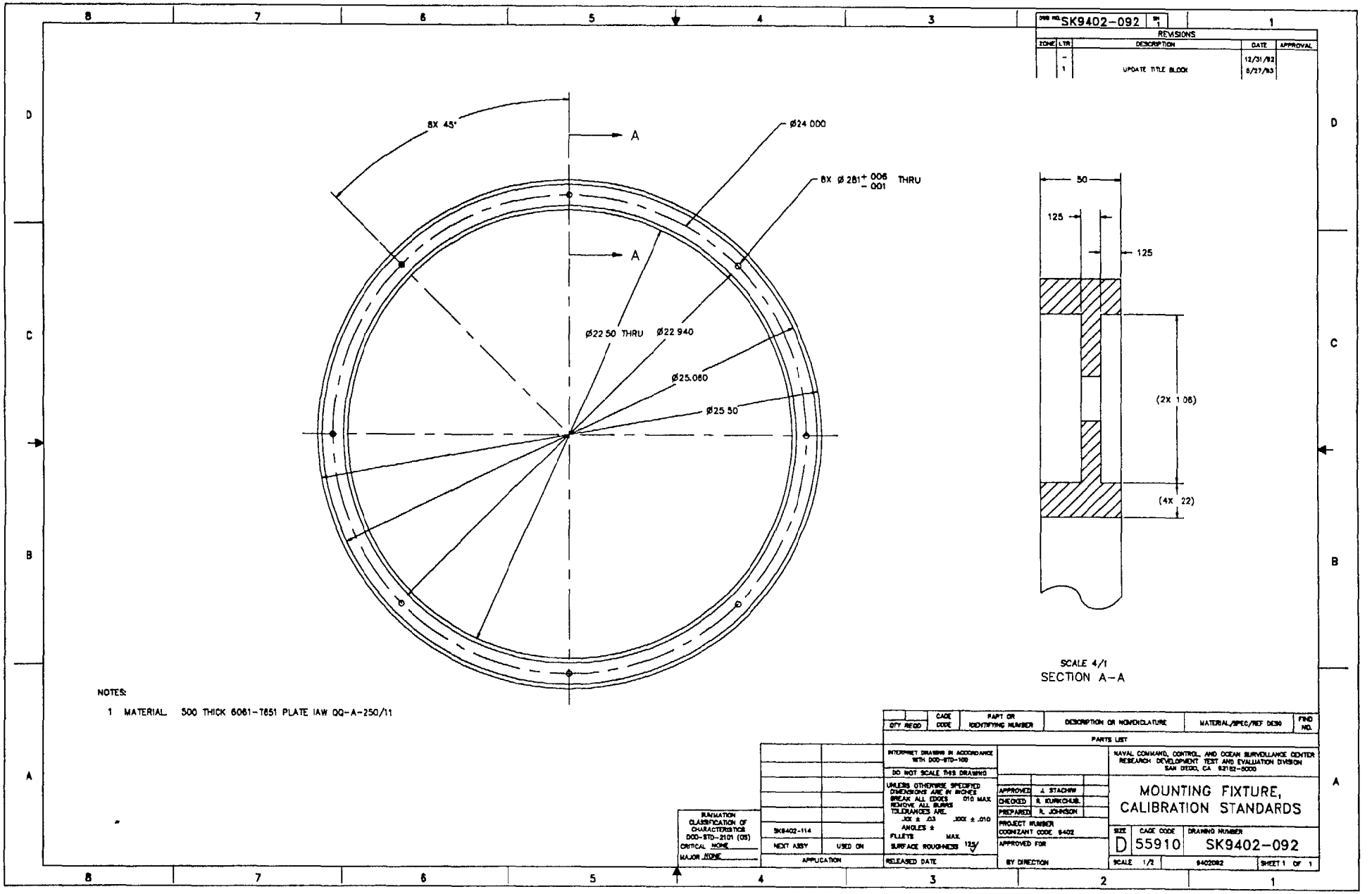

Figure 12. Engineering drawing for 25-inch diameter aluminum rings onto which curved ceramic specimens were mounted

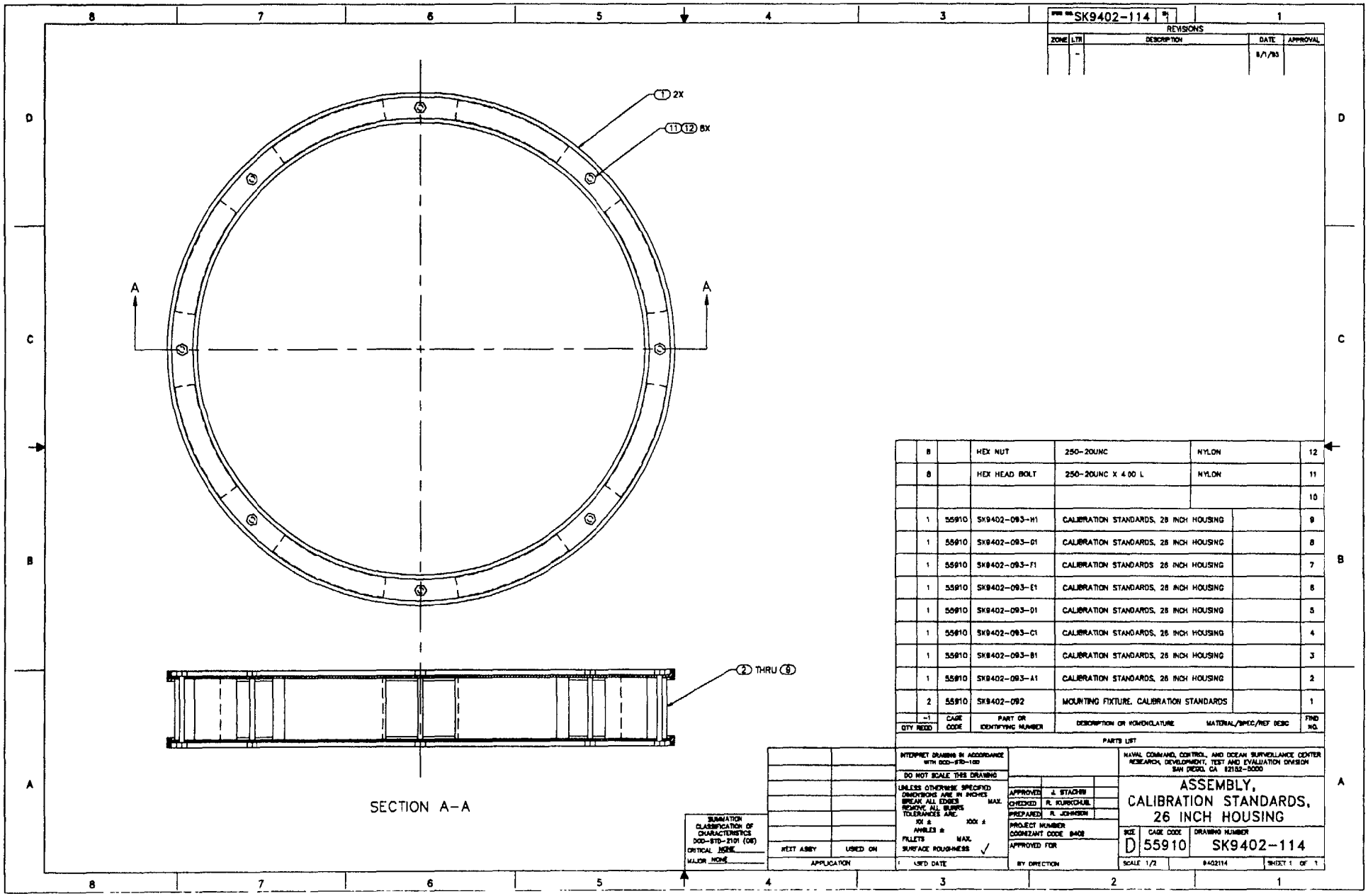

Figure 13 Engineering drawing of assembled ring fixture.

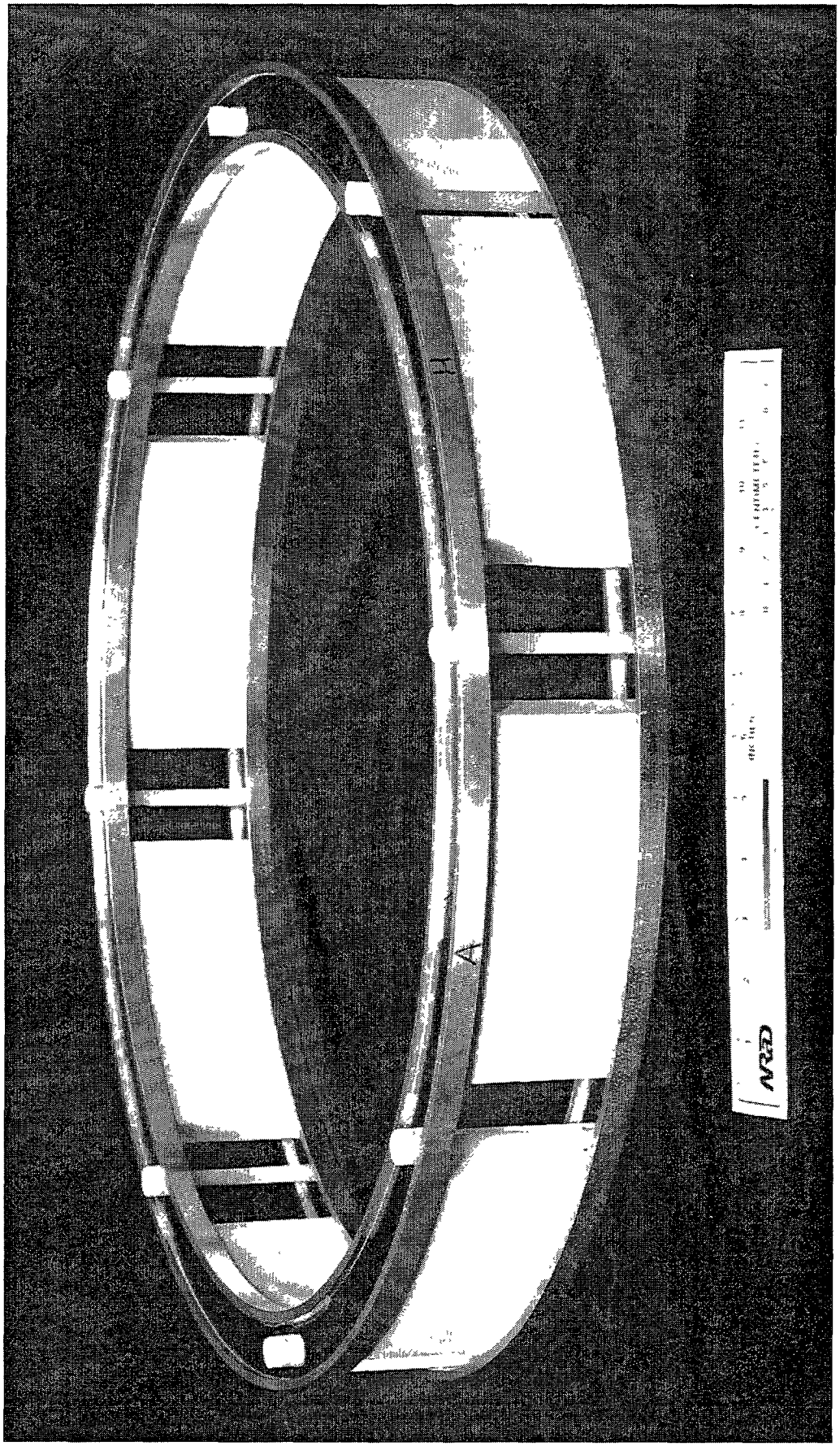

Figure 14 Assembled ring fixture containing as-fired curved ceramic specimens with cast-in defects

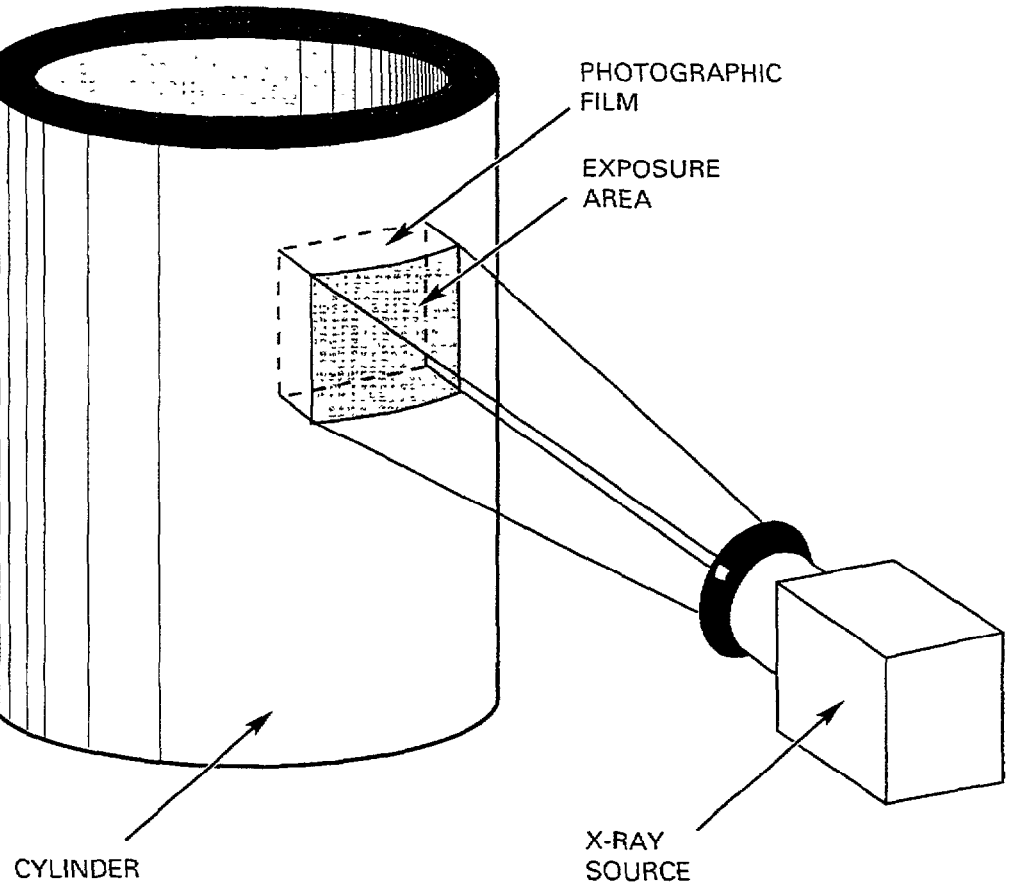

Figure 15. Setup for conventional film radiography of ceramic cylinder.

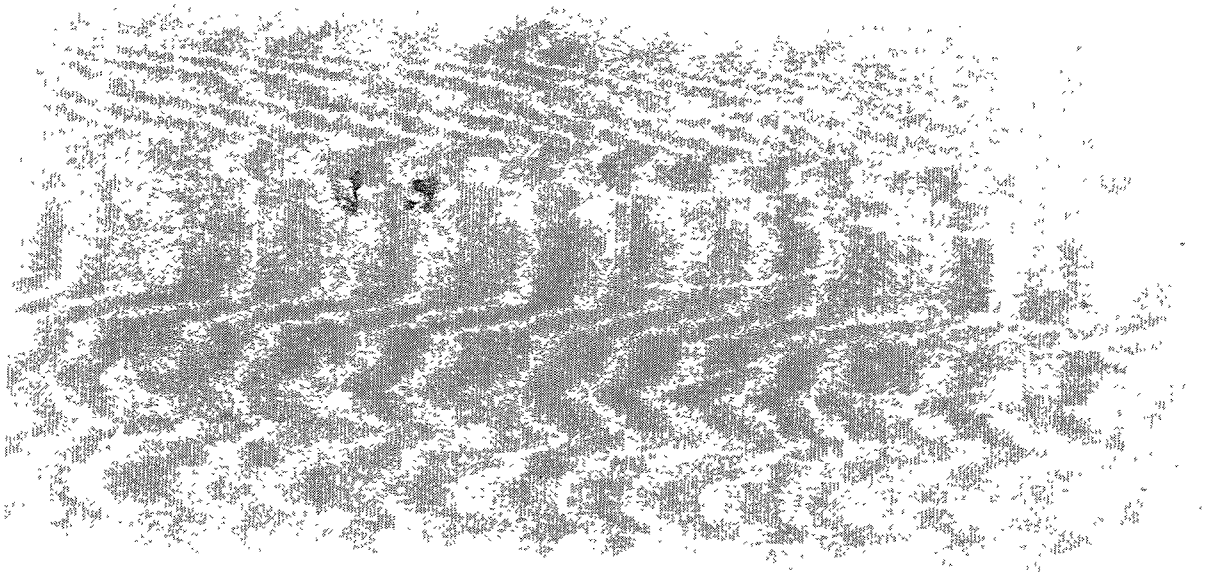

Figure 16. X-ray film radiograph of as-fired flat alumina tile (D2) containing 1-inch-long by 0.028-inch-diameter rod-shaped defects.

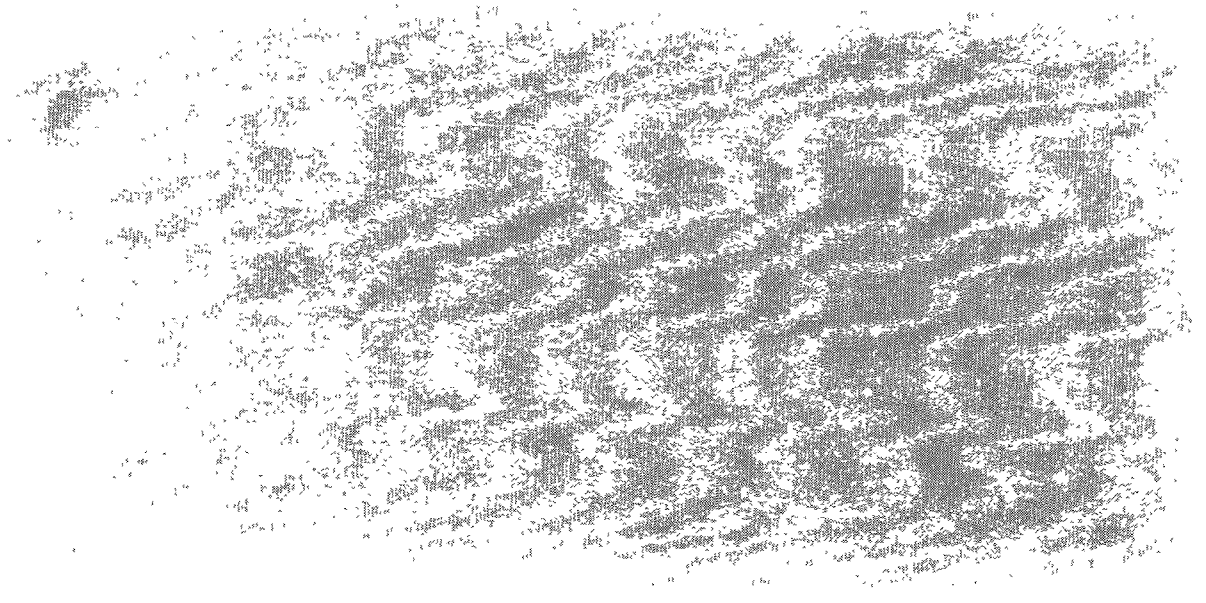

Figure 17. X-ray film radiograph of as-fired flat alumina tile (E2) containing 0.052-inch-diameter spherical defects.

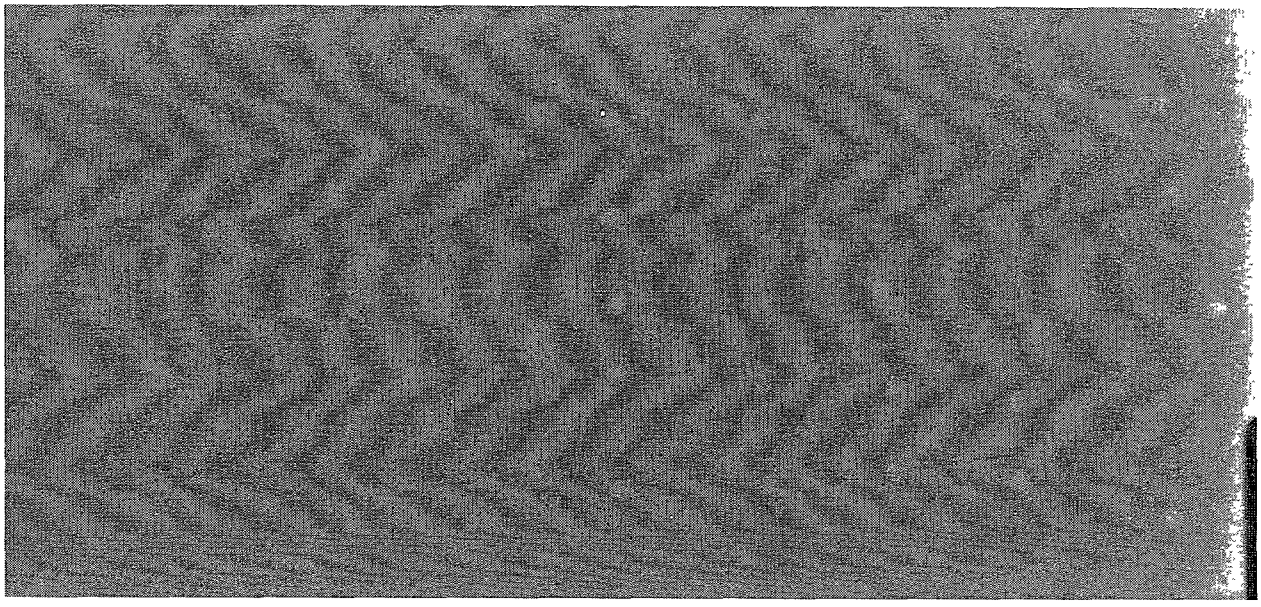

Figure 18. X-ray film radiograph of as-fired flat alumina tile (F2) containing 0.105-inch-diameter spherical defects.

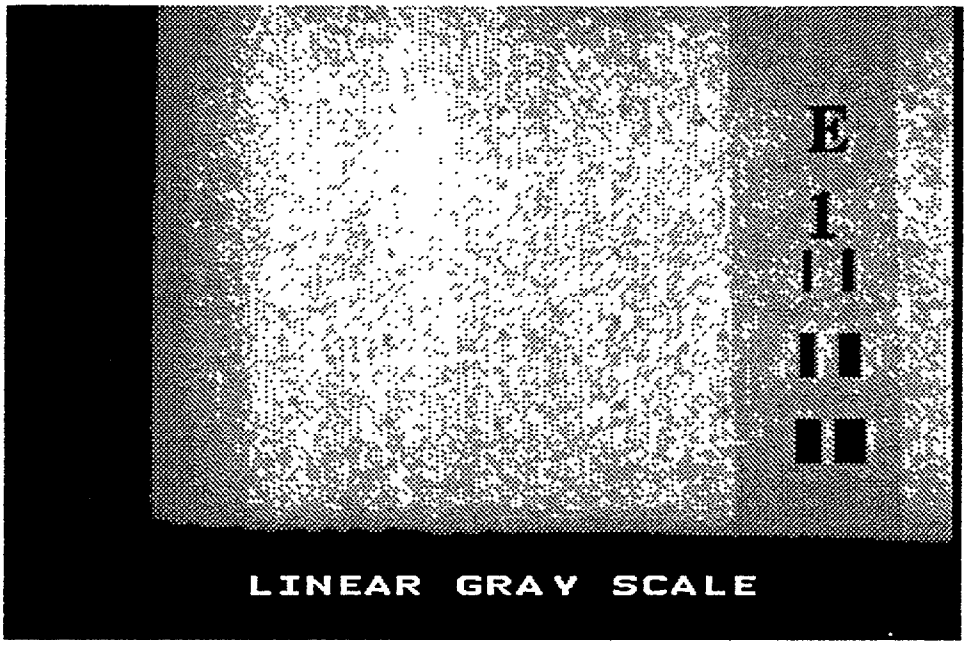

Figure 19a. Digitized image of finish-ground flat tile (E2) as displayed on a computer screen.

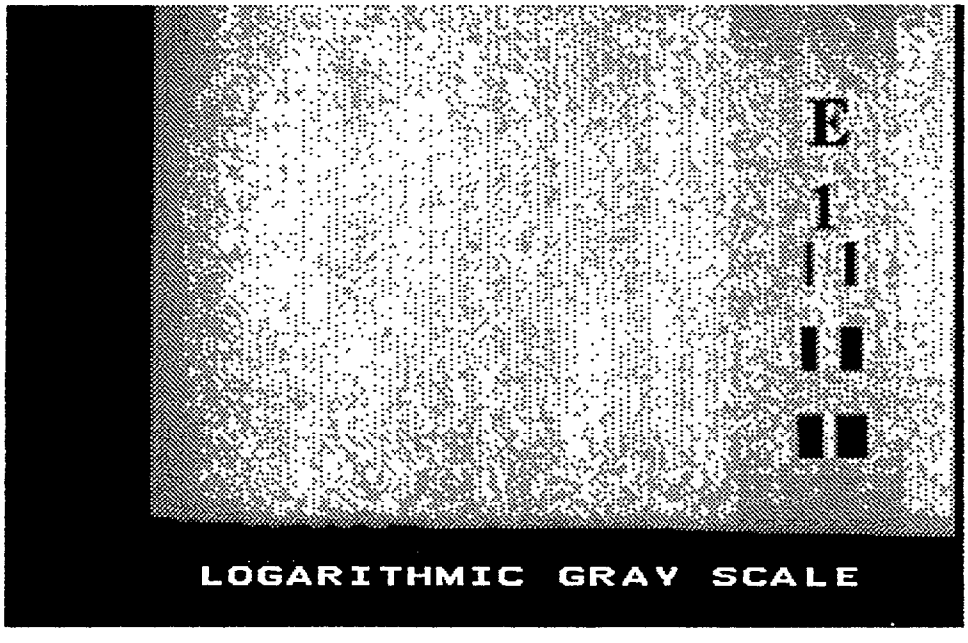

Figure 19b. Digitized image of finish-ground flat tile (E2) displayed via logarithmic grey scale on a computer screen to simulate how the human eye would see it.

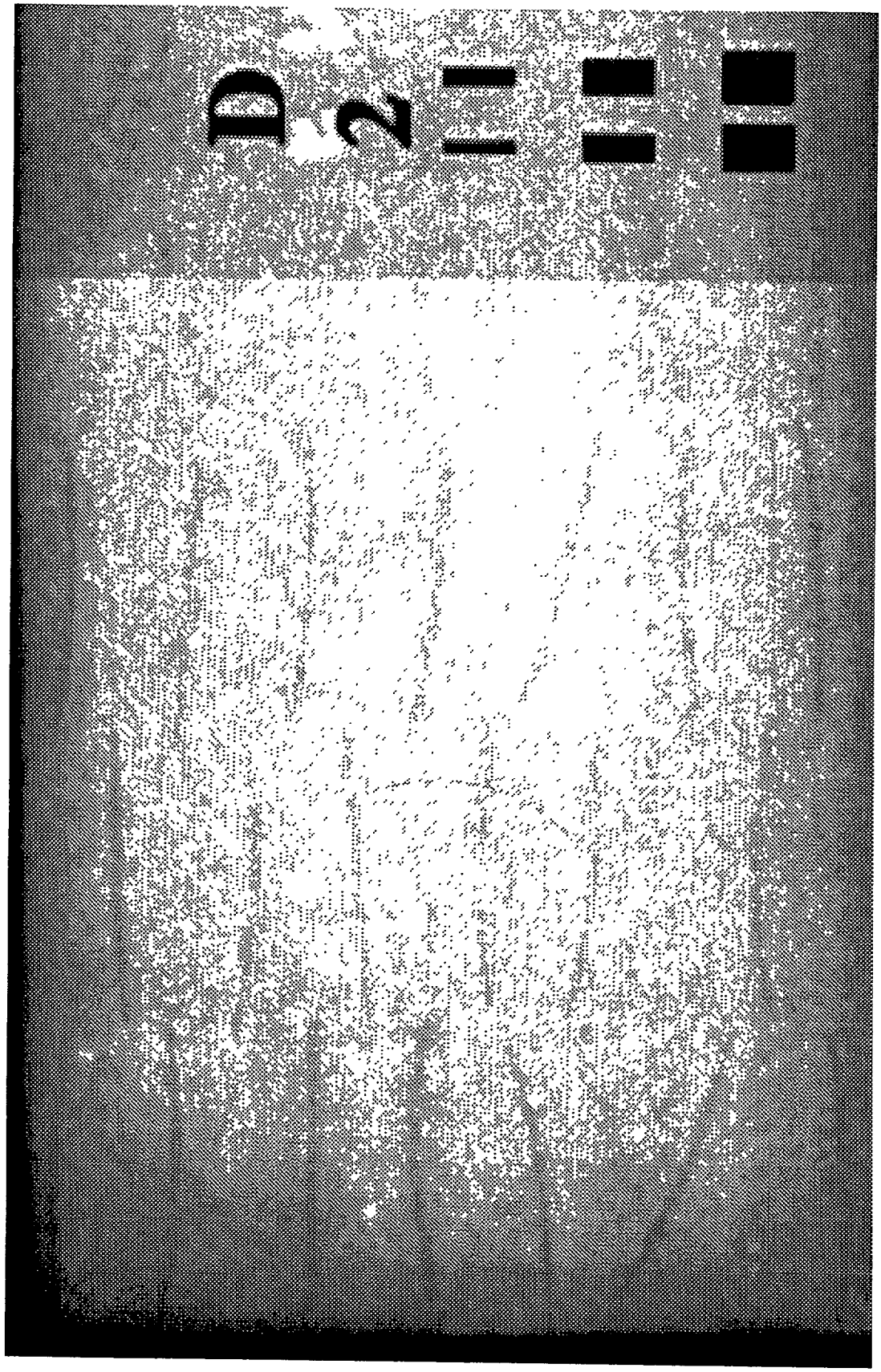

Figure 20. Digitized image of x-ray film radiograph taken of as-fired flat alumina-ceramic tile (D2) containing 1-inch-long by 0 028-inch-diameter rod-shaped defects

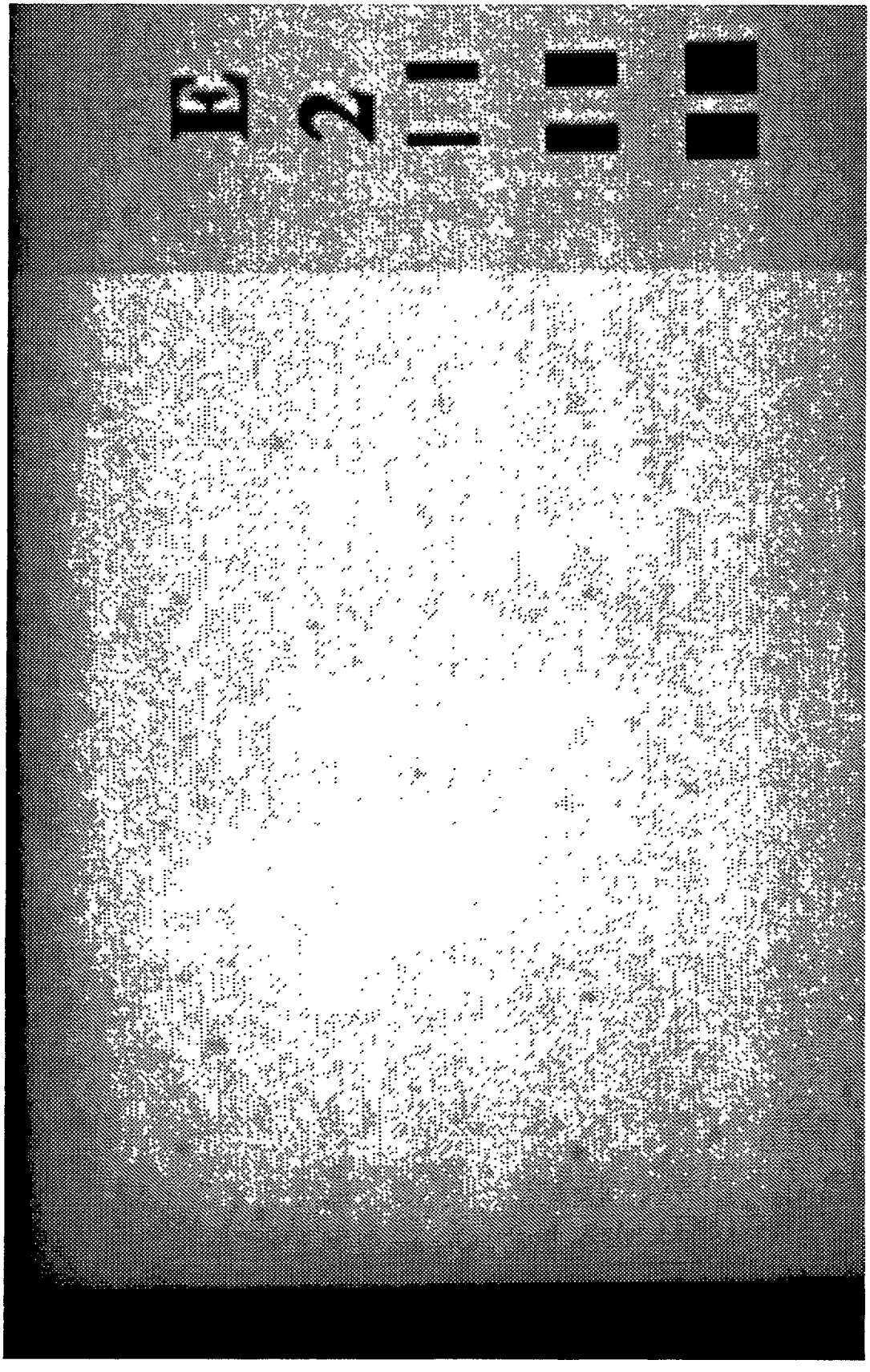

Figure 21. Digitized image of x-ray film radiograph taken of as-fired alumina-ceramic tile (E2) containing 0.052-inch-diameter spherical defects.

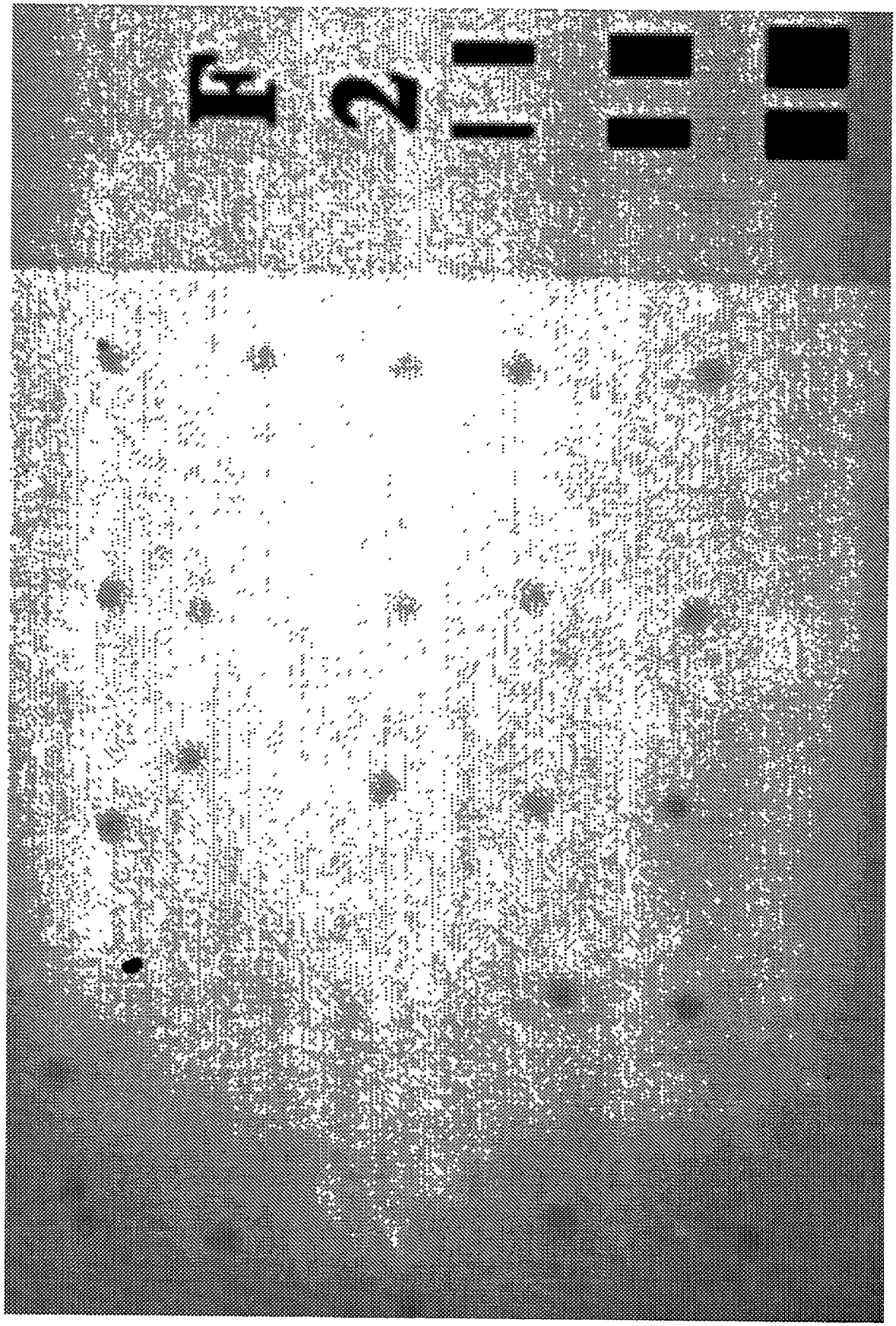

Figure 22 Digitized image of X-ray film radiograph taken of as-fired flat alumina-ceramic tile (F2) containing 0.105-inch-diameter spherical defects.

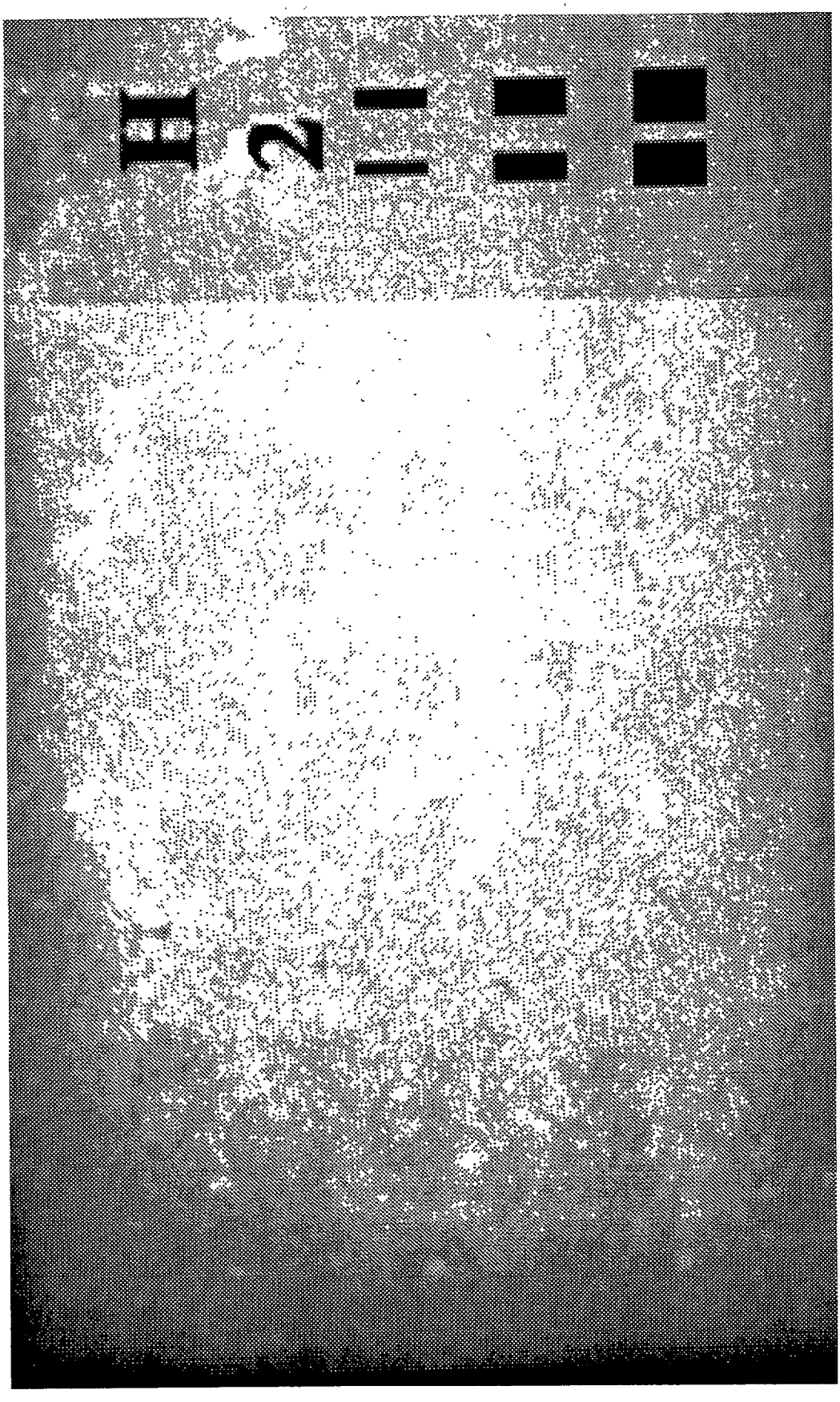

Figure 23. Digitized image of x-ray film radiograph taken of as-fired flat alumina-ceramic tile (H2) containing 0 210-inch-square by 0 005-inch-thick planar defects

Figure 24. Digitized image of x-ray film radiograph taken of finish ground flat alumina-ceramic tile (H1) containing 0.210-inch-square by 0.005-inch-thick planar defects.

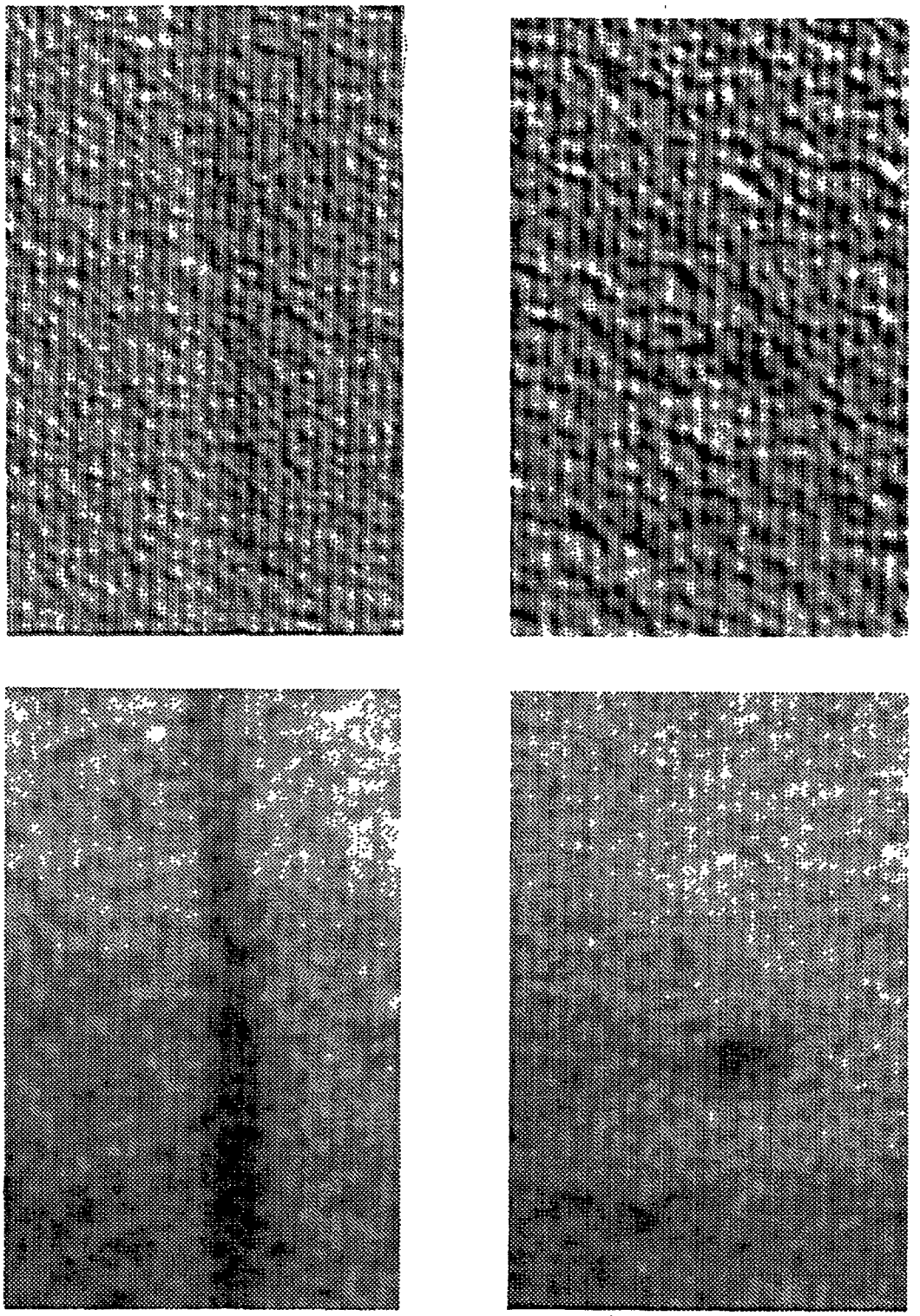

Figure 25. Enhanced and embossed images of defects in as-fired flat alumina-ceramic tiles (a) D2 and (b) E2.

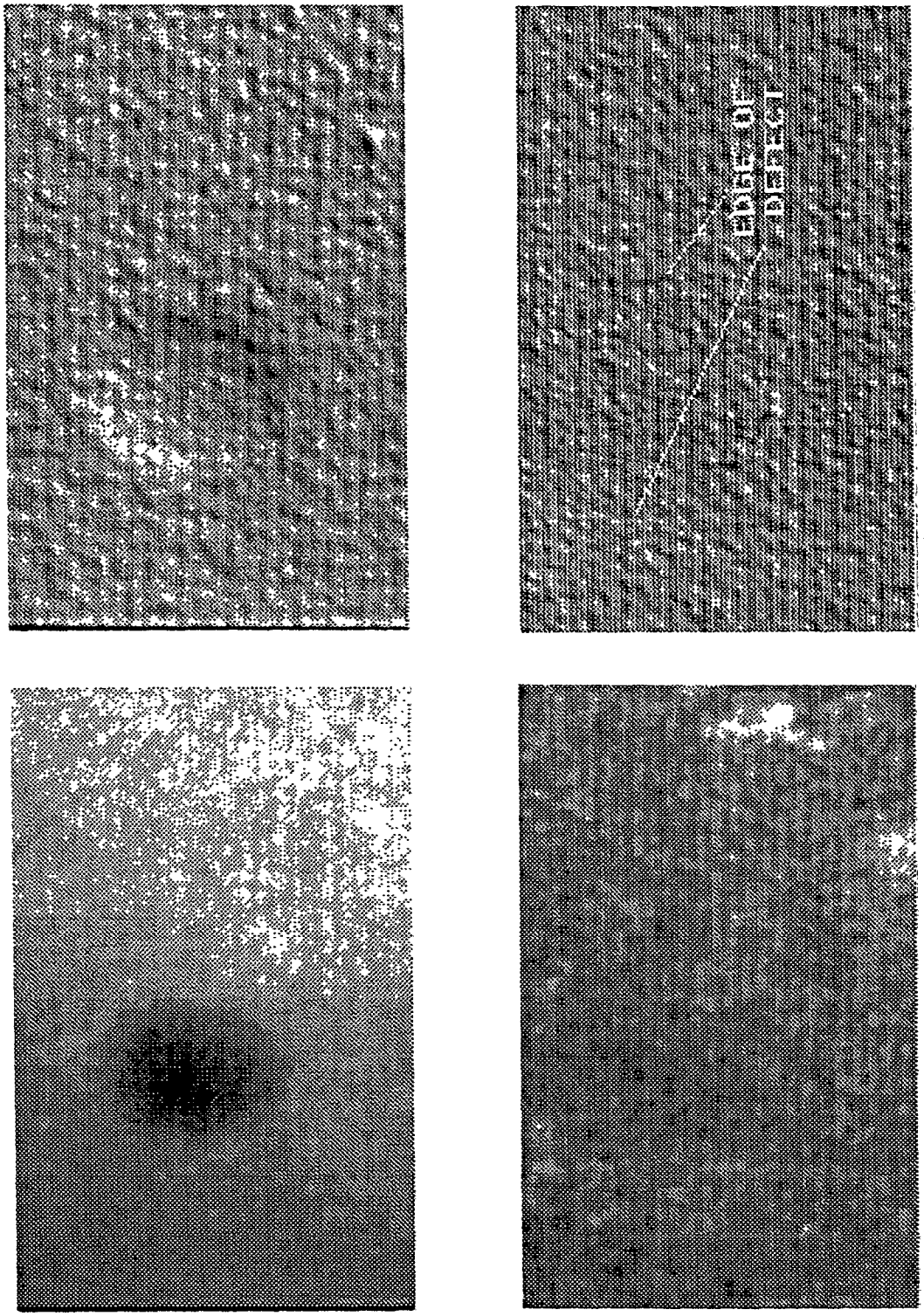

Figure 26. Enhanced and embossed images of defects in as-fired flat alumina-ceramic tiles (a) F2 and (b) G2.

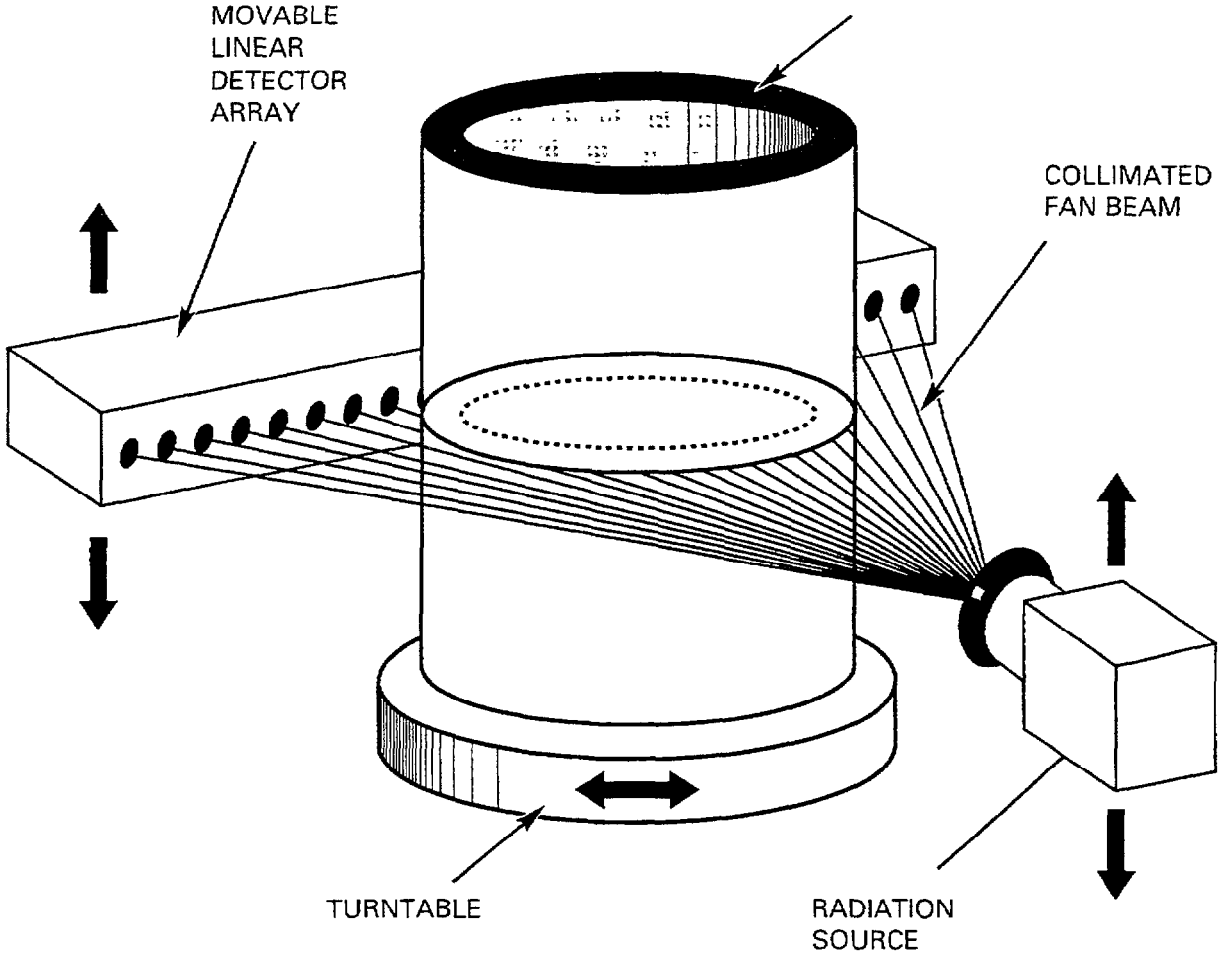

Figure 27 Inspection setup for digital radiography and computed tomography.

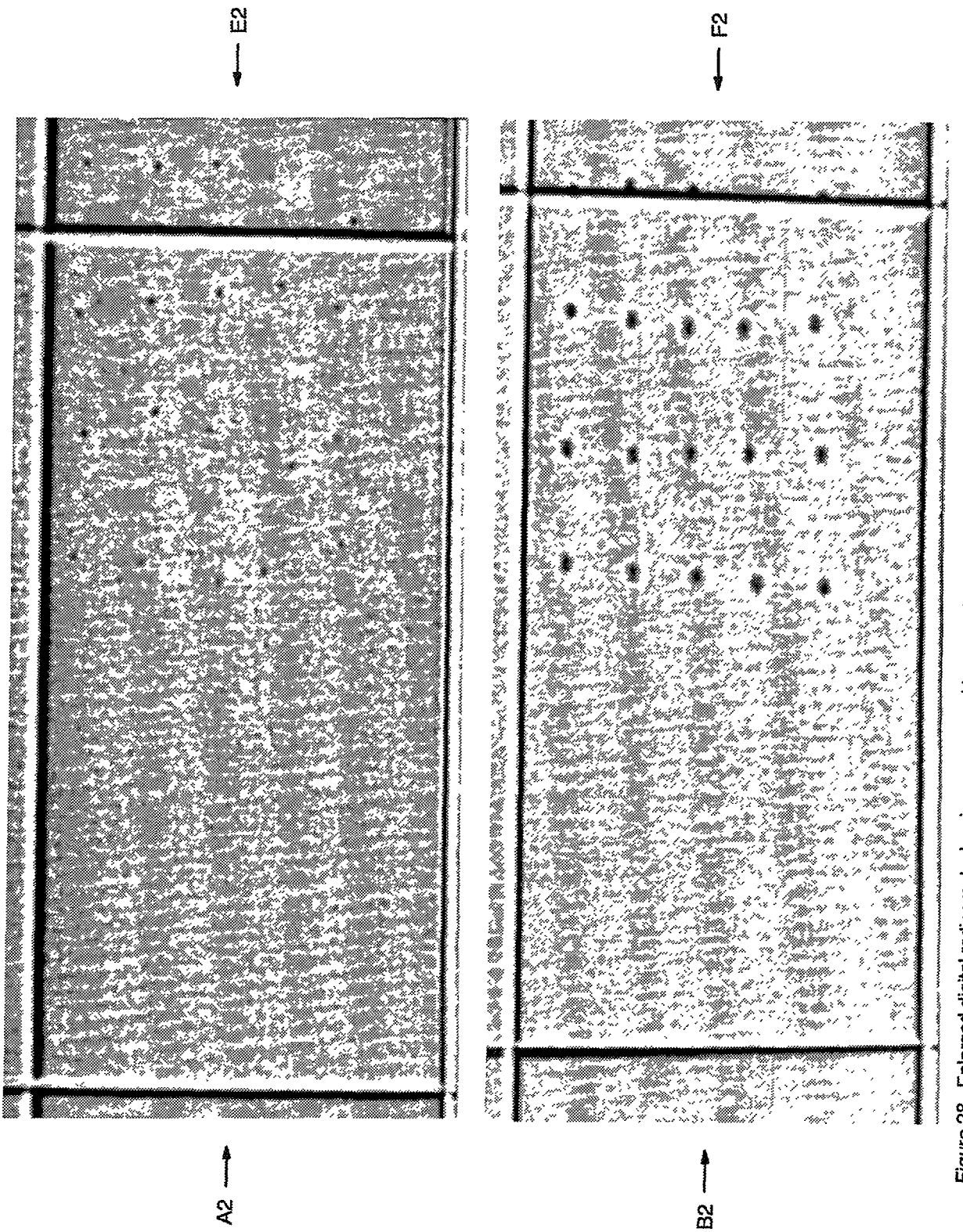

Figure 28. Enlarged digital radiograph showing superposed images of as-fired curved specimens (a) A2 and E2, and (b) B2 and F2.

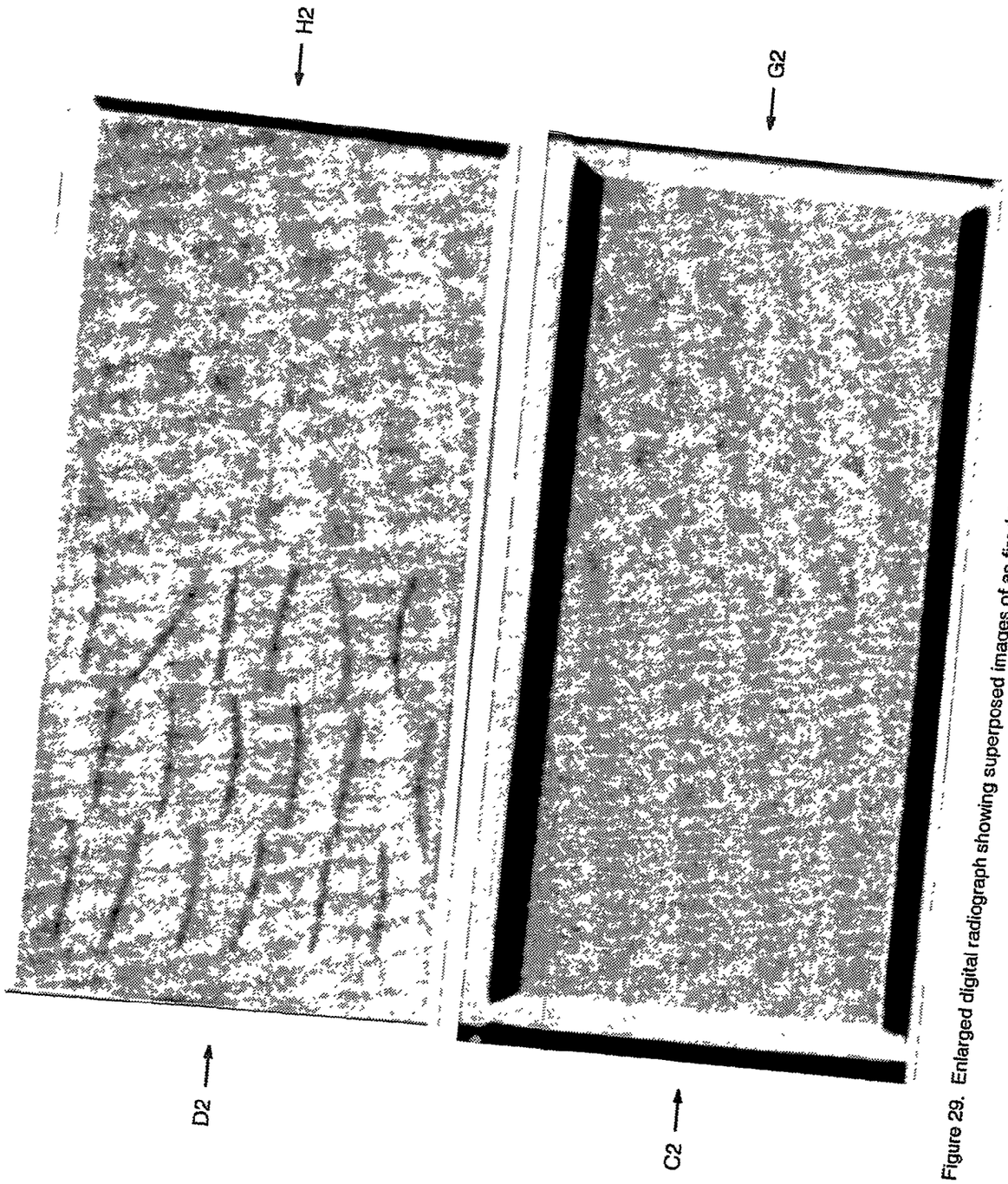

Figure 29. Enlarged digital radiograph showing superposed images of as-fired curved tiles (a) C2 and G2, and (b) D2 and H2.

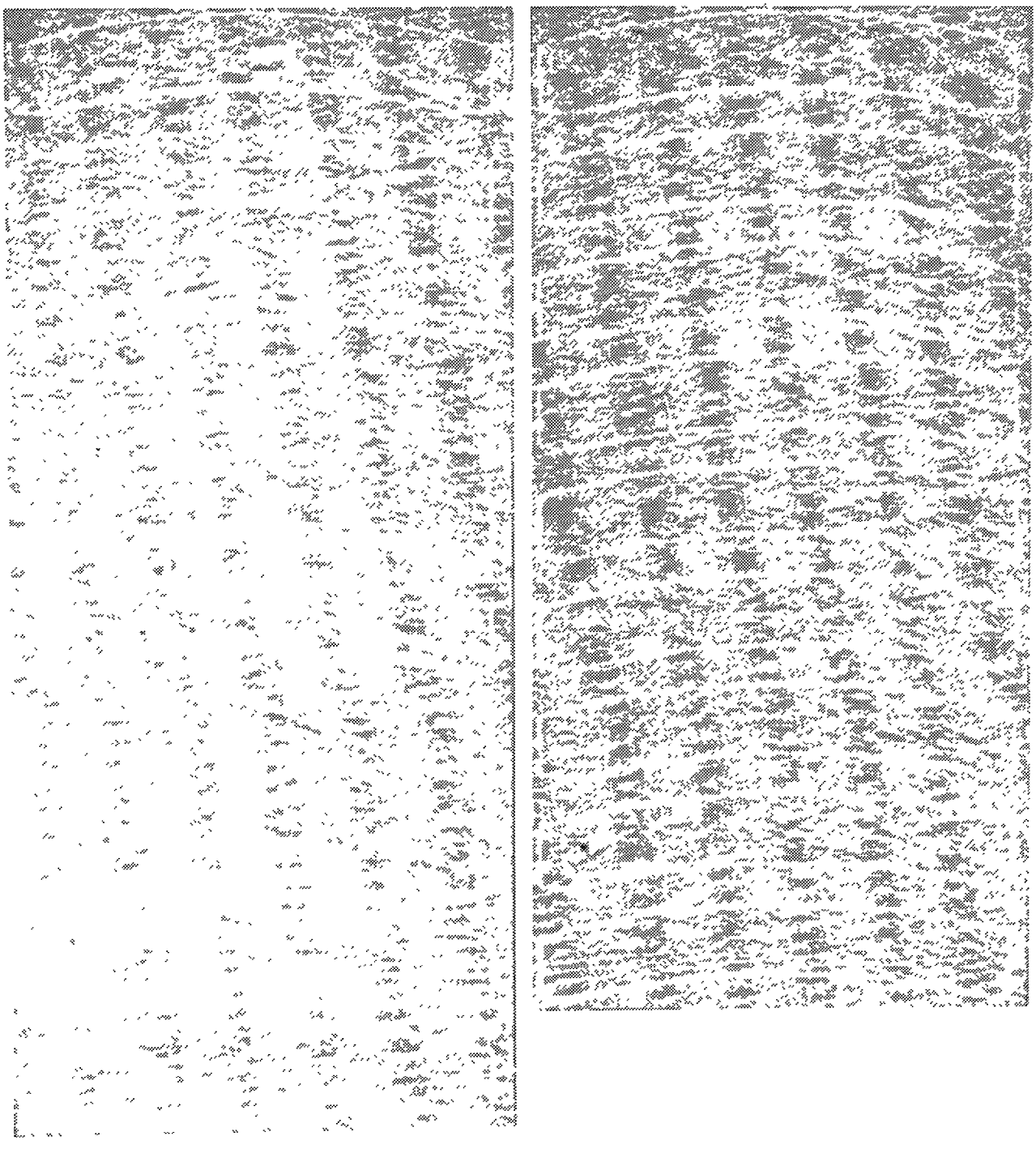

Figure 30. CT slices of as-fired curved specimen (C2) enhanced by subtracting the average of each image from each image.

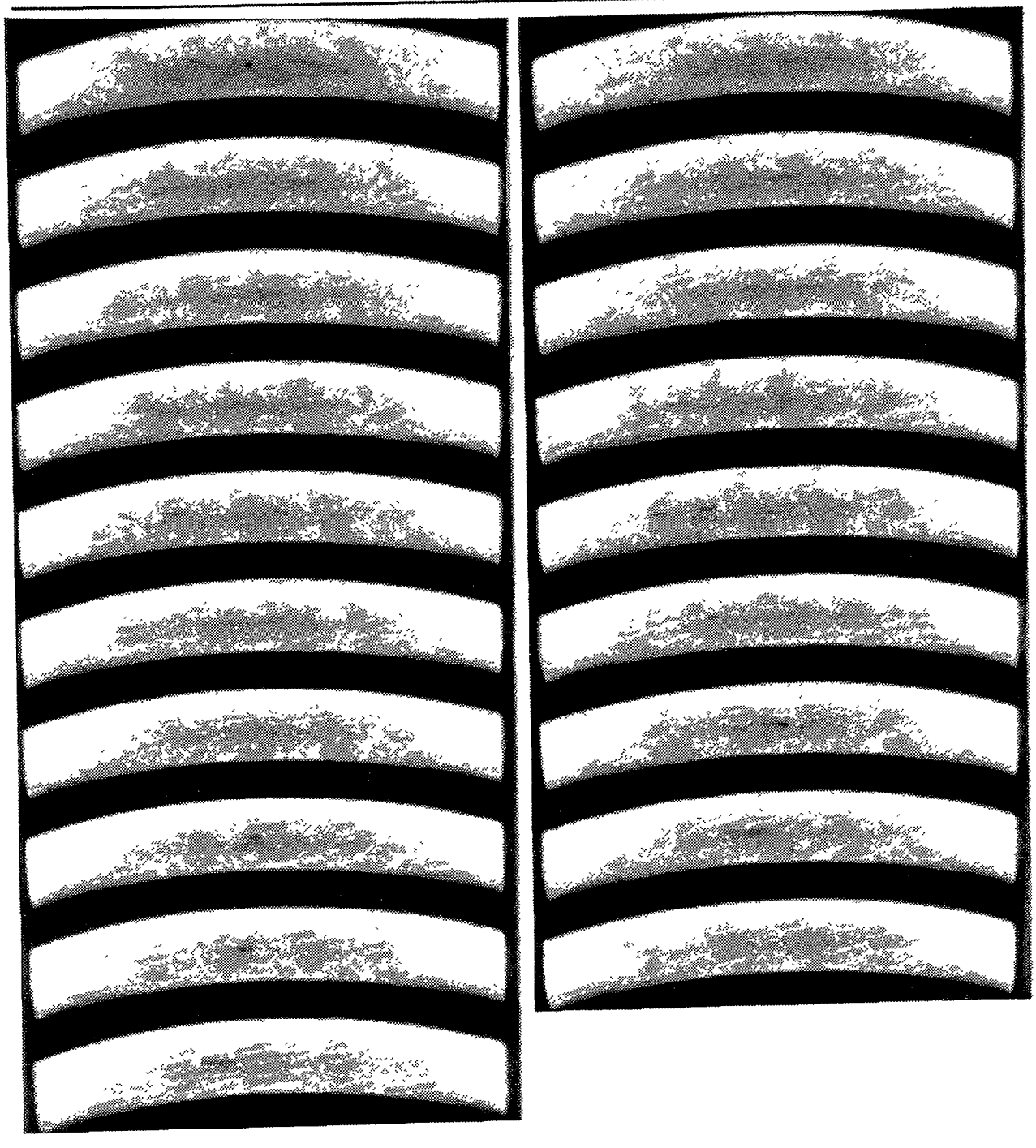

Figure 31. Non-enhanced CT slices of as-fired curved specimen (D2).

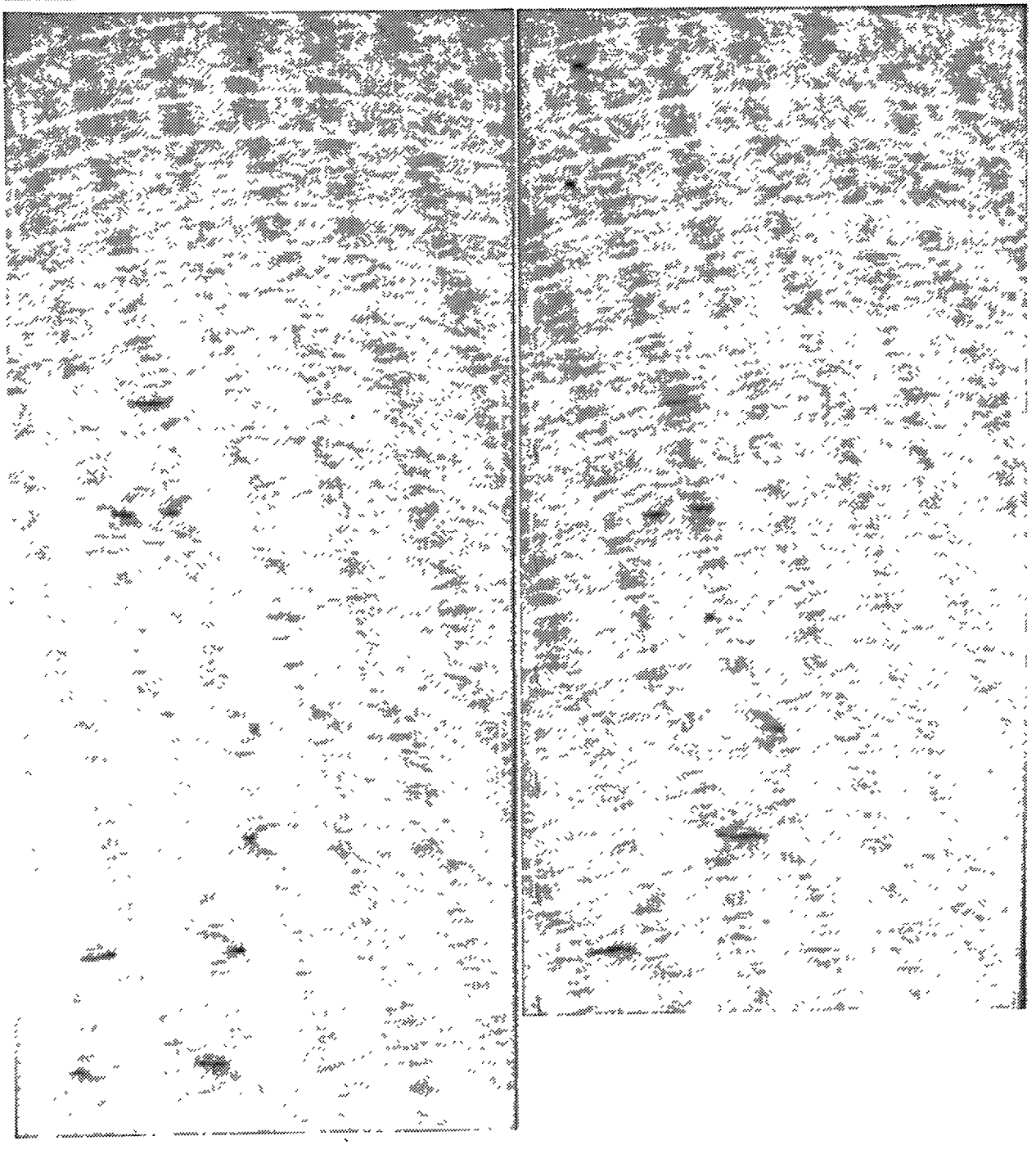

Figure 32. CT slices of as-fired curved specimen (D2) enhanced by subtracting the average of each image from each image.

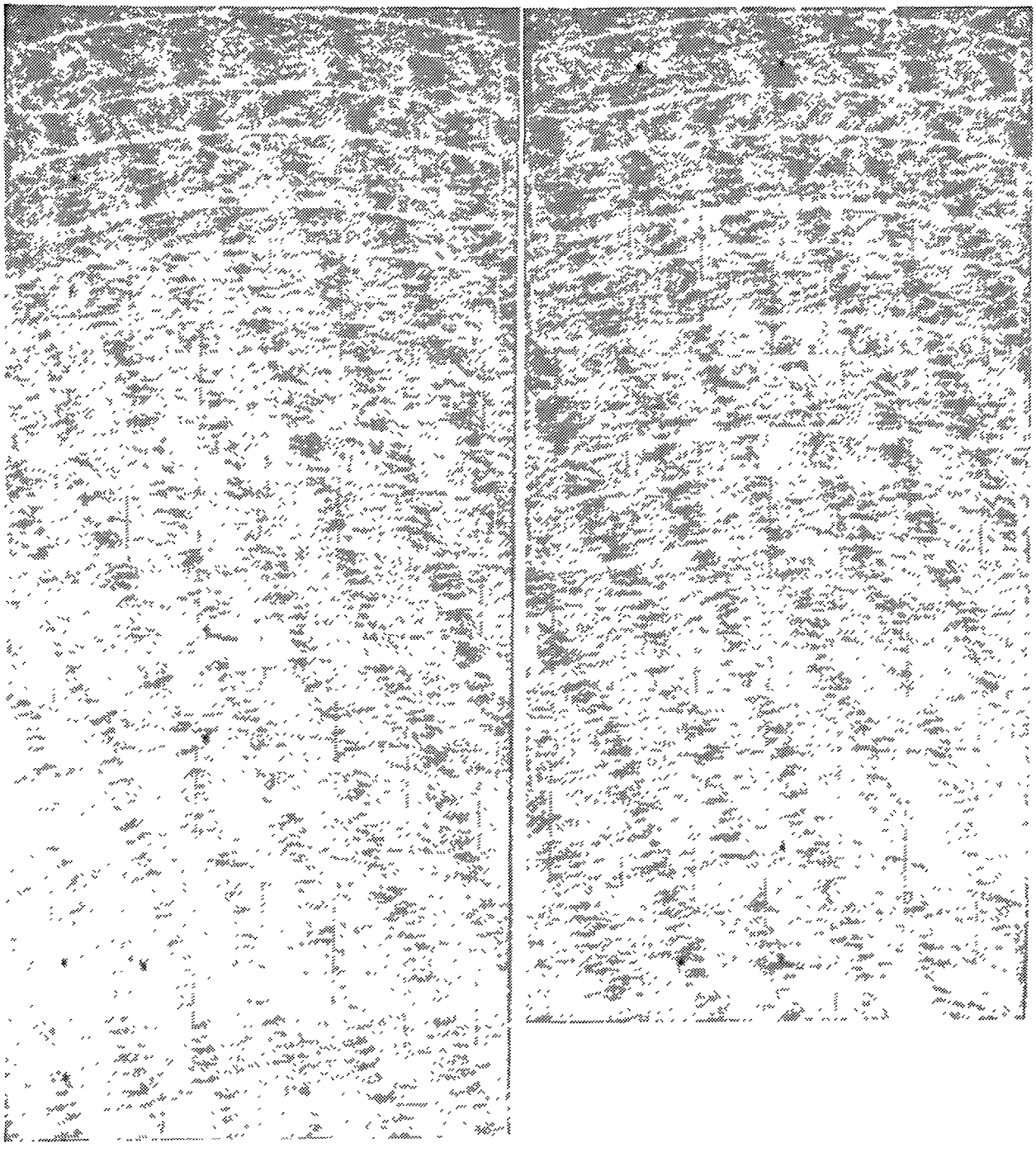

Figure 33. CT slices of as-fired curved specimen (E2) enhanced by subtracting the average of each image from each image.

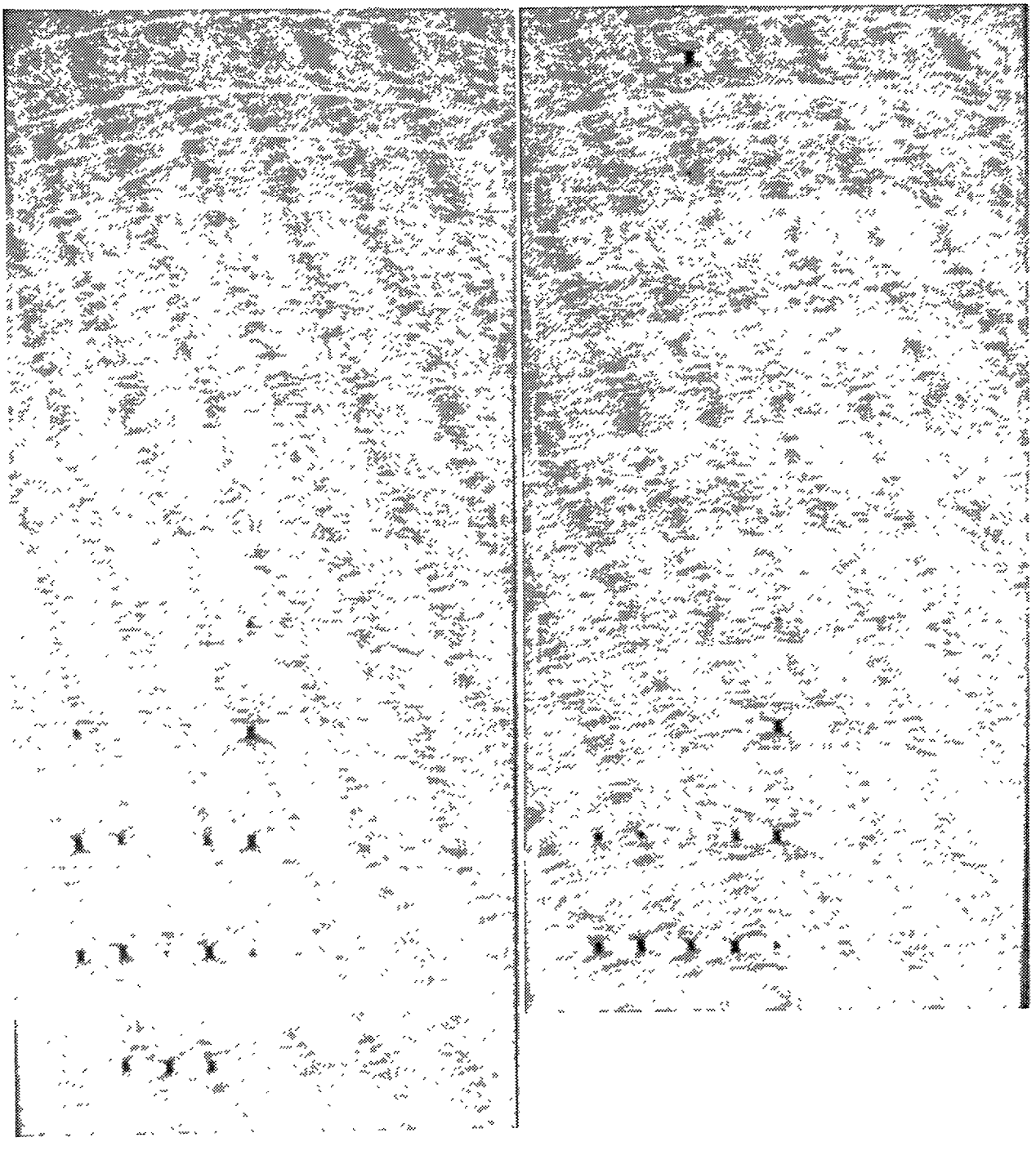

Figure 34. CT slices of as-fired curved specimen (F2) enhanced by subtracting the average of each image from each image.

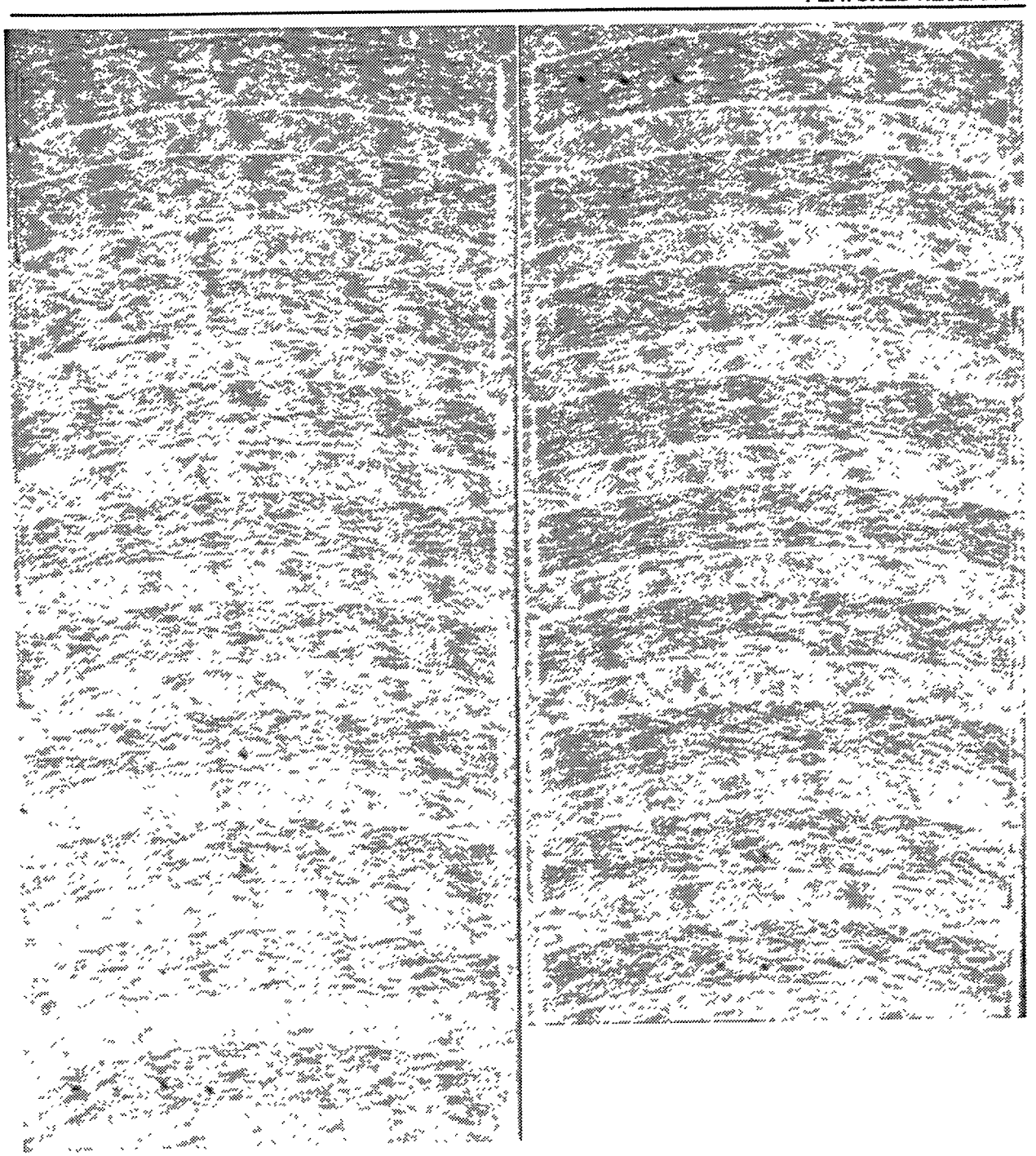

Figure 35. CT slices of as-fired curved specimen (G2) enhanced by subtracting the average of each image from each image.

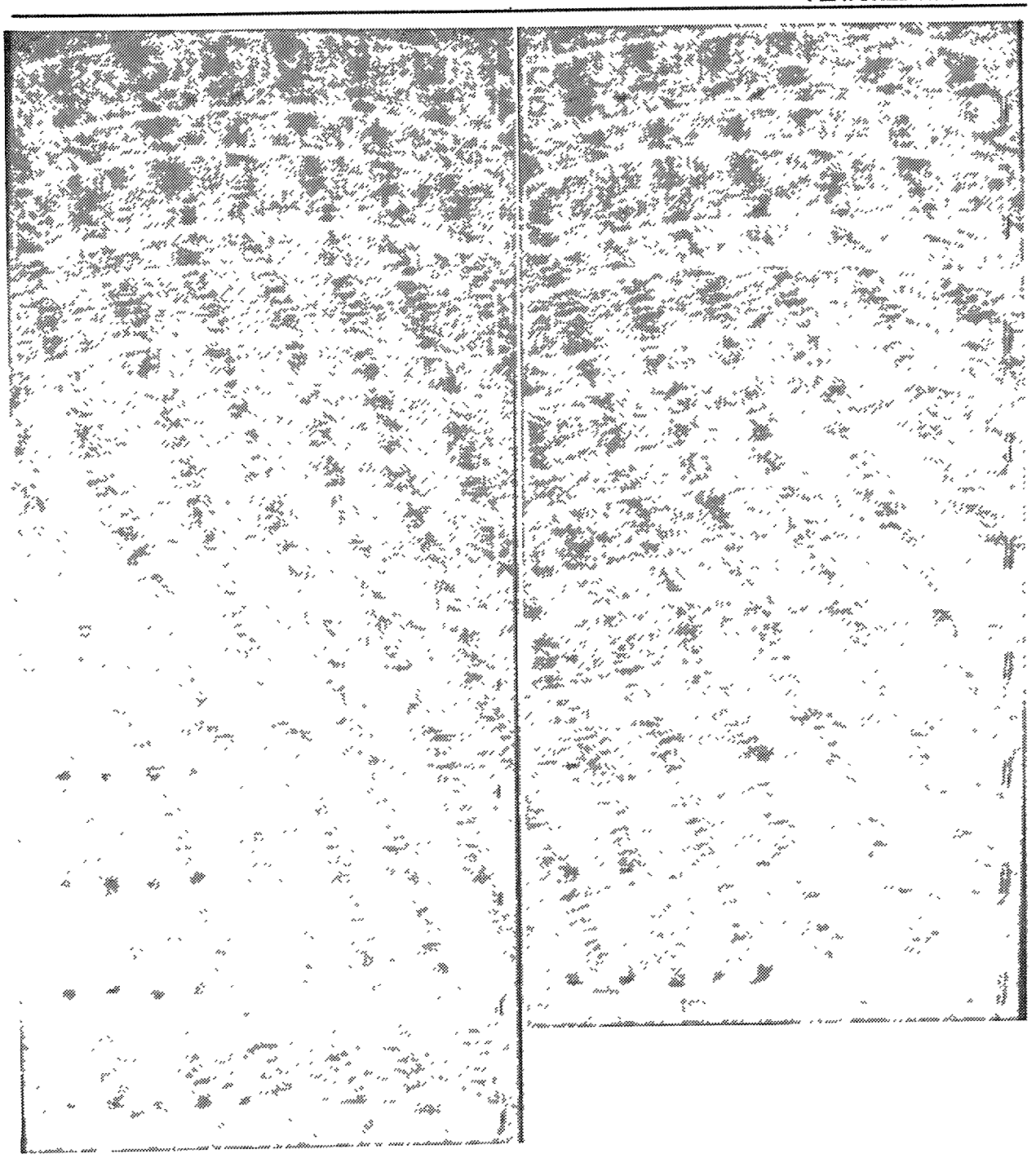

Figure 36. CT slices of as-fired curved specimen (H2) enhanced by subtracting the average of each image from each image.

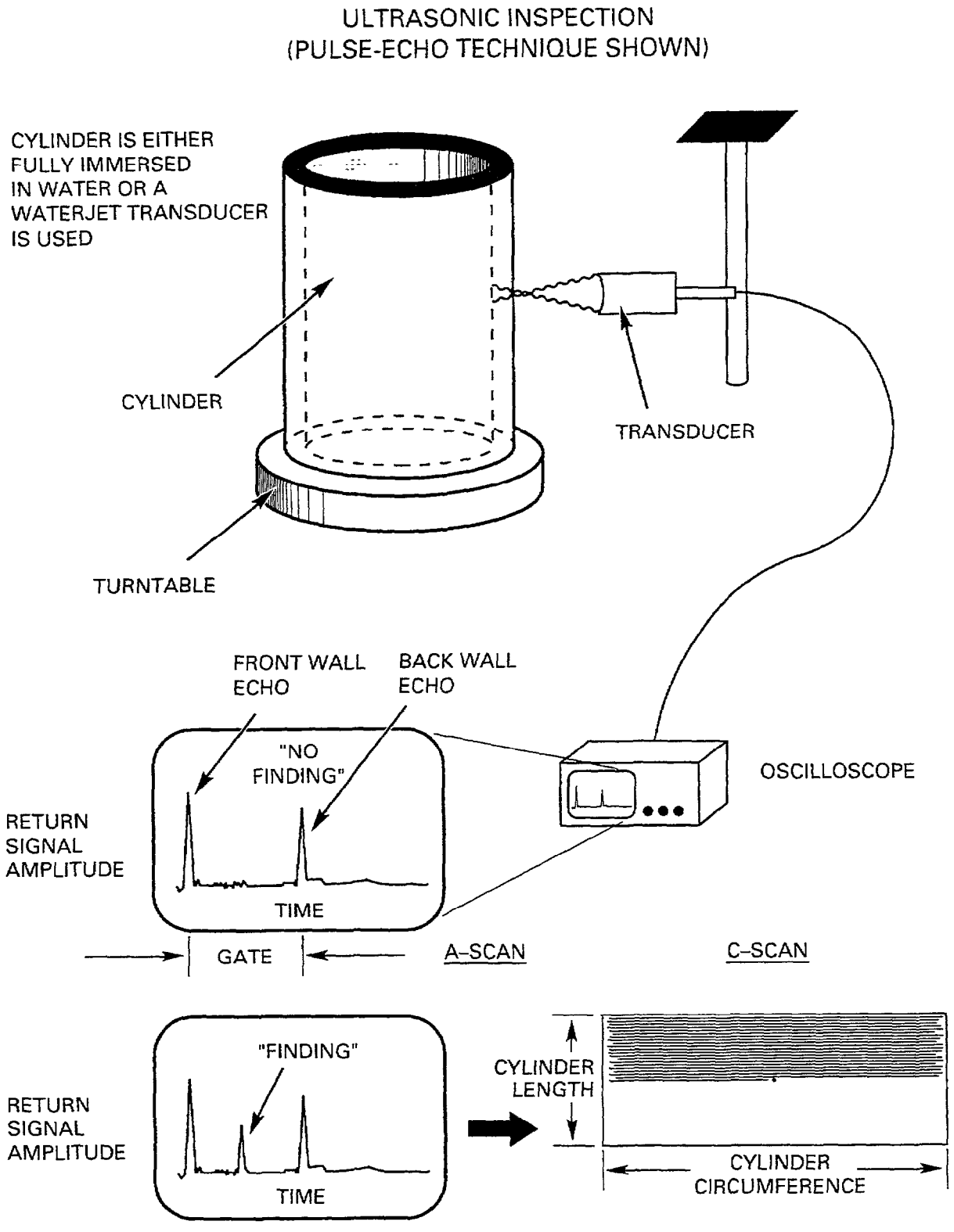

Figure 37. Setup for ultrasonic inspection.

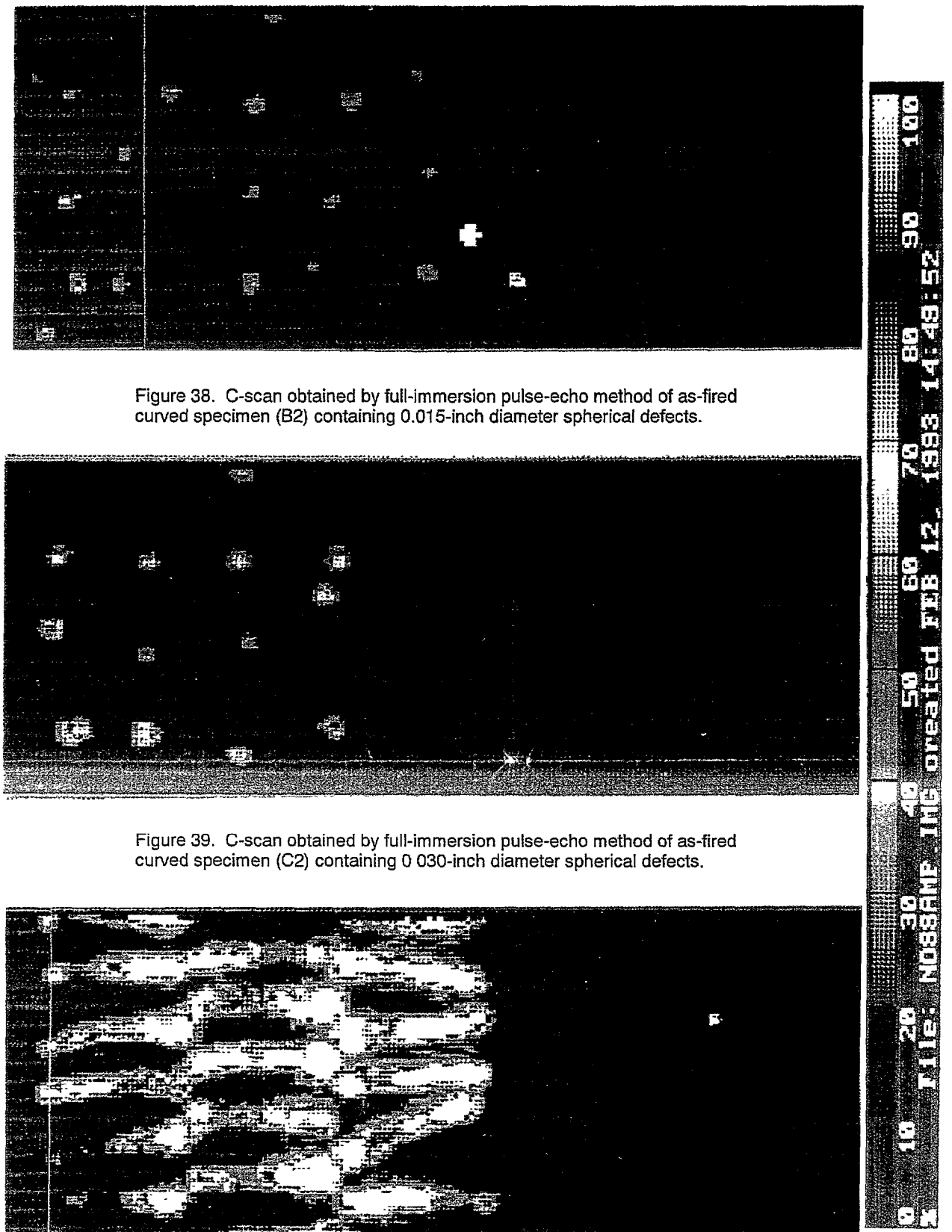

Figure 38. C-scan obtained by full-immersion pulse-echo method of as-fired curved specimen (B2) containing 0.015-inch diameter spherical defects.

Figure 39. C-scan obtained by full-immersion pulse-echo method of as-fired curved specimen (C2) containing 0 030-inch diameter spherical defects.

Figure 40. C-scan obtained by full-immersion pulse-echo method of as-fired curved specimen (D2) containing 1-inch-long by 0.028-inch-diameter rod-shaped defects.

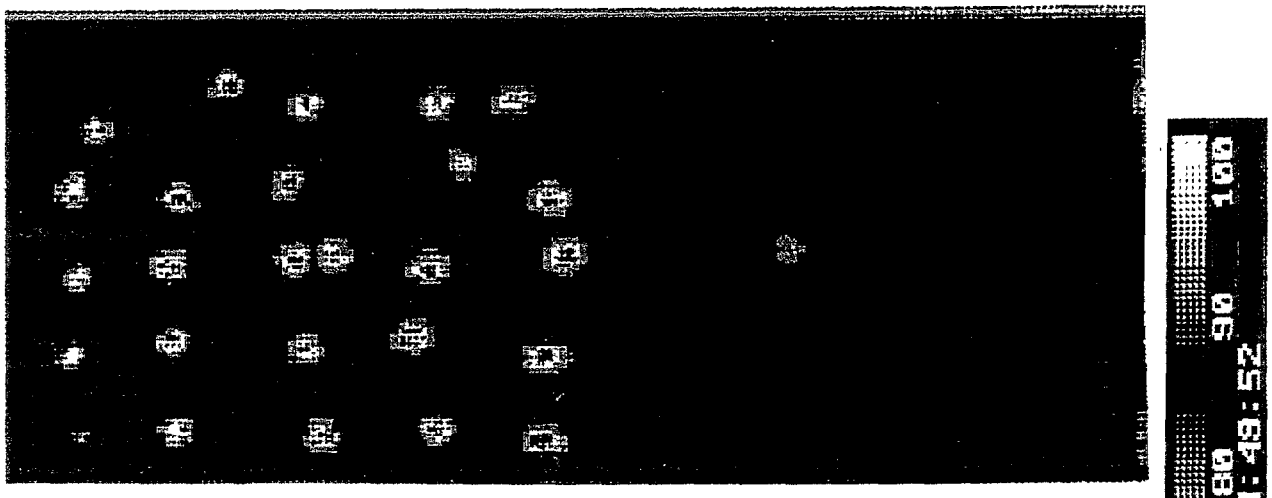

Figure 41. C-scan obtained by full-immersion pulse-echo method of as-fired curved specimen (E2) containing 0.052-inch diameter spherical defects.

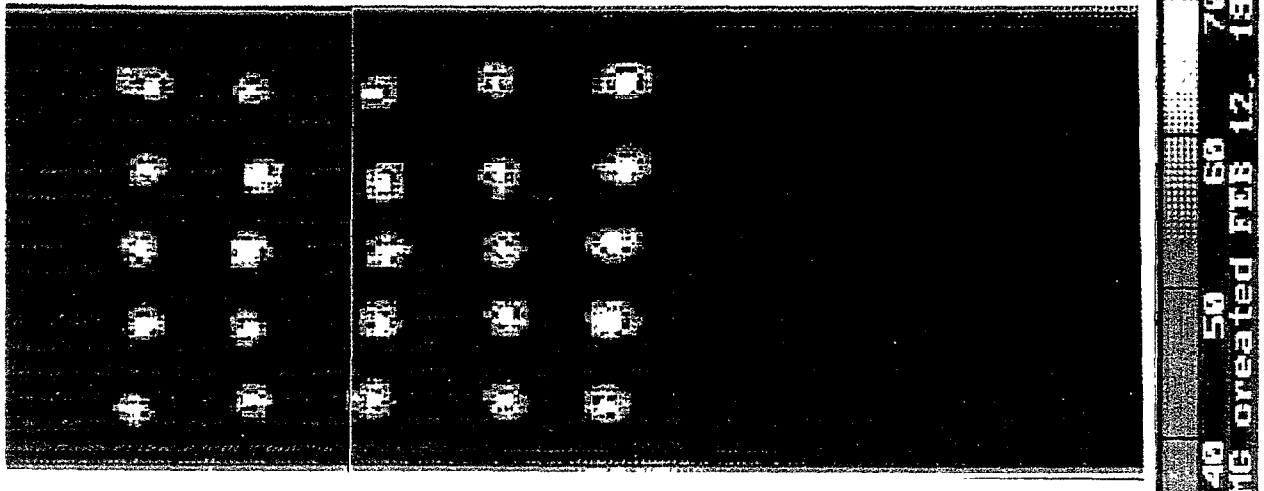

Figure 42. C-scan obtained by full-immersion pulse-echo method of as-fired curved specimen (F2) containing 0.105-inch-diameter spherical defects.

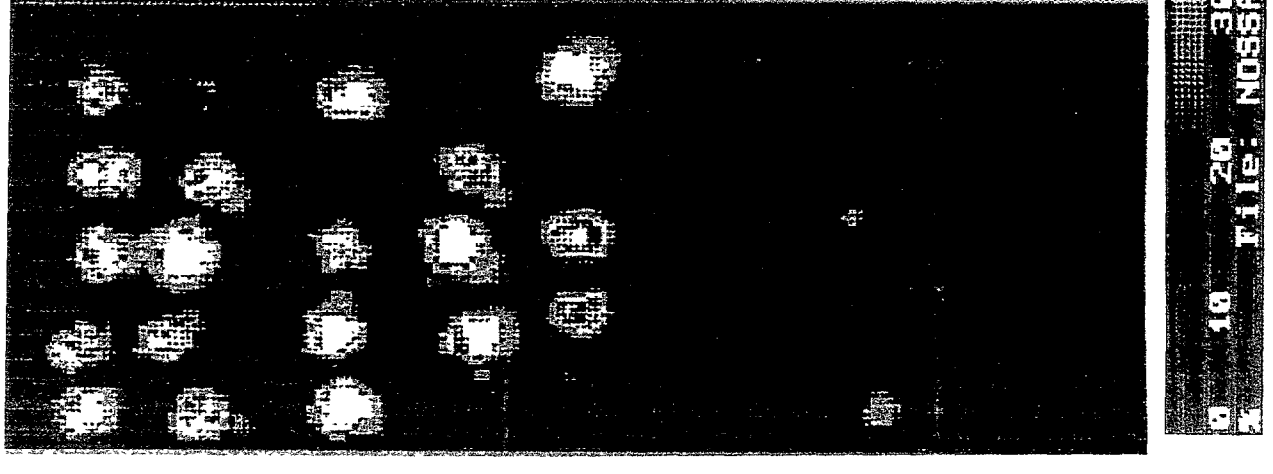

Figure 43. C-scan obtained by full-immersion pulse-echo method of as-fired curved specimen (G2) containing 0.105-inch-square by 0.105-inch-thick planar defects.

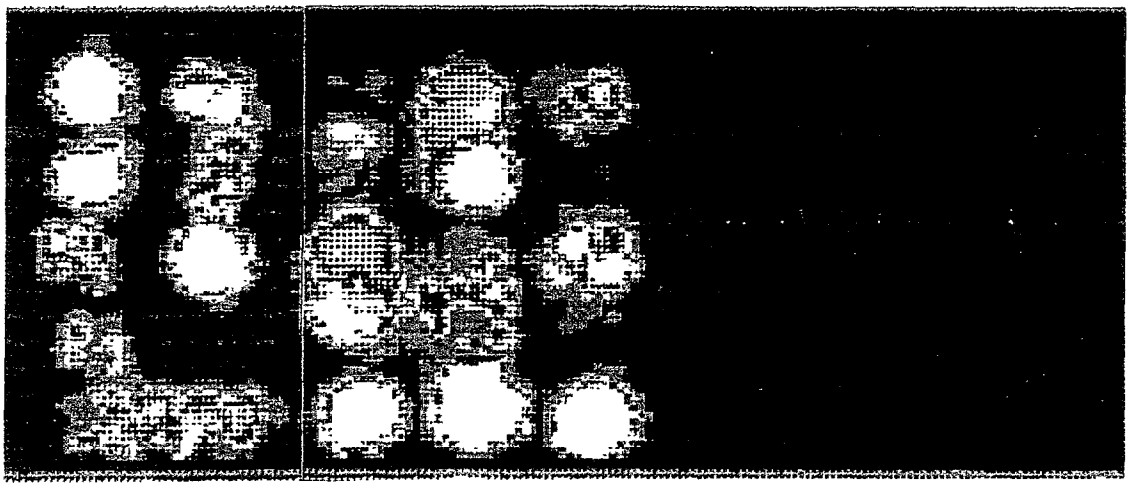

Figure 44. C-scan obtained by full-immersion pulse-echo method of as-fired curved specimen (H2) containing 0.210-inch-square by 0.005-inch-thick planar defects.

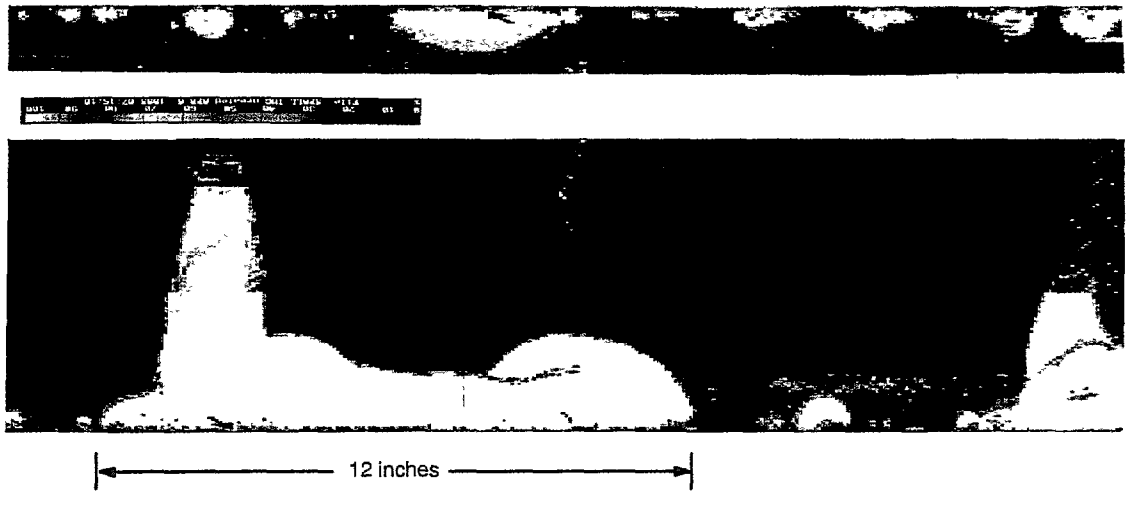

Figure 45. C-scan obtained by full-immersion pulse-echo technique of 12-inch-OD by 14-inch-long alumina-ceramic cylinder having internal circumferential cracks caused by cyclic pressurization (reference 14).

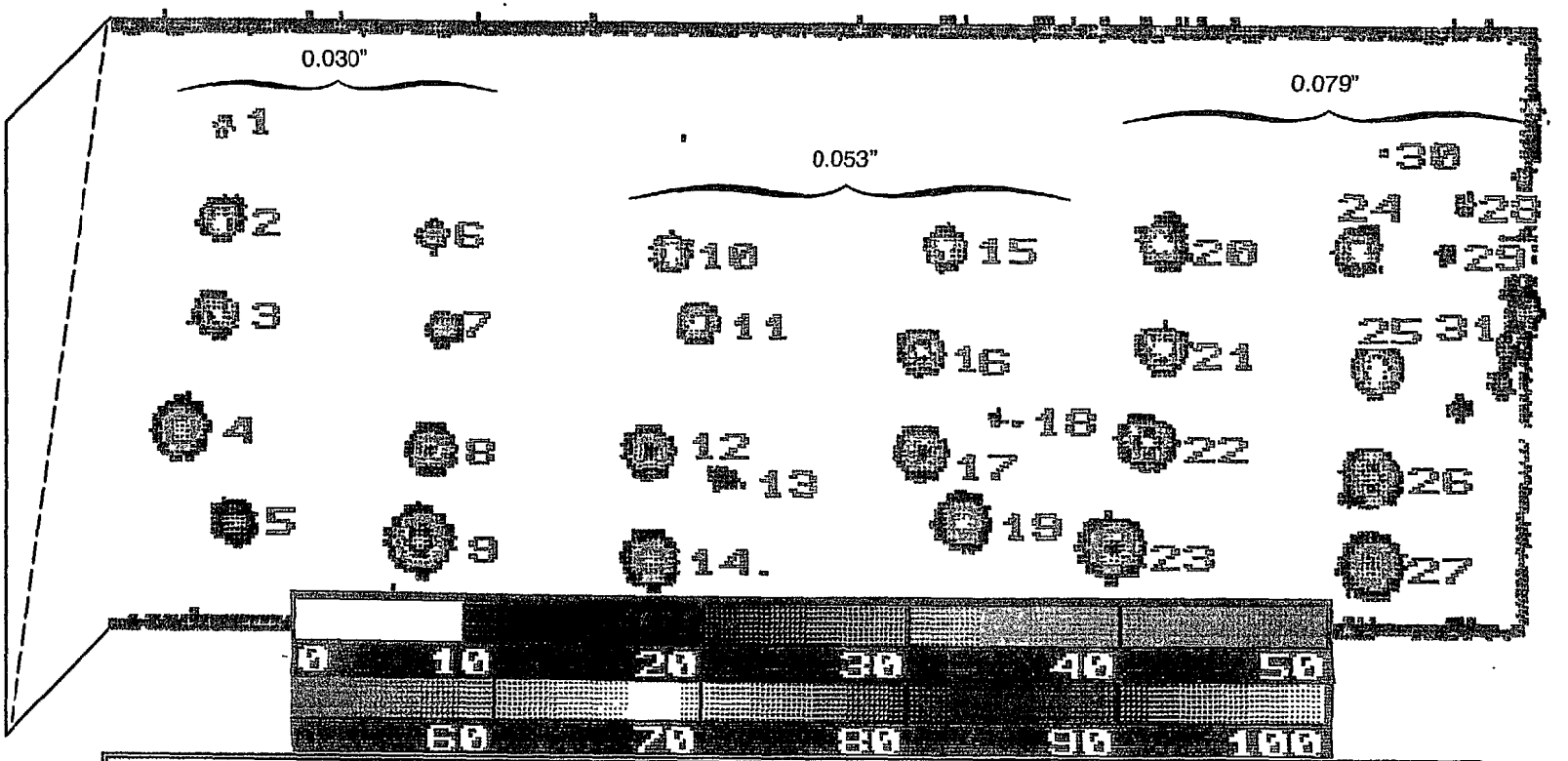

DEPTH OF FINDINGS IN 1.25 INCH THICK ALUMINA TILE "A"

Finding No.	Depth (inches)	Finding No.	Depth (inches)	Finding No.	Depth (inches)	Finding No.	Depth (inches)	Finding No	Depth (inches)	Finding No.	Depth (inches)	Finding No.	Depth (inches)
1	0 125												
2	0.310	6	0 305	10	0.310	15	0.350	20	0.275	24	0.305	28	not resolved
3	0 525	7	0.500	11	0.430	16	0 550	21	0 525	25	0 575	29	0.450
4	0.850	8	0.775	12 13	0.775 0 780	17 18	0.780 0.575	22	0 750	26	0.835	30 31	not resolved
5	1 050	9	1 050	14	1.035	19	0.975	23	1 035	27	1.100	33	not resolved

Figure 46. C-scan obtained by full-immersion pulse-echo method of a 1.25-inch alumina-ceramic tile containing defects at various depths.

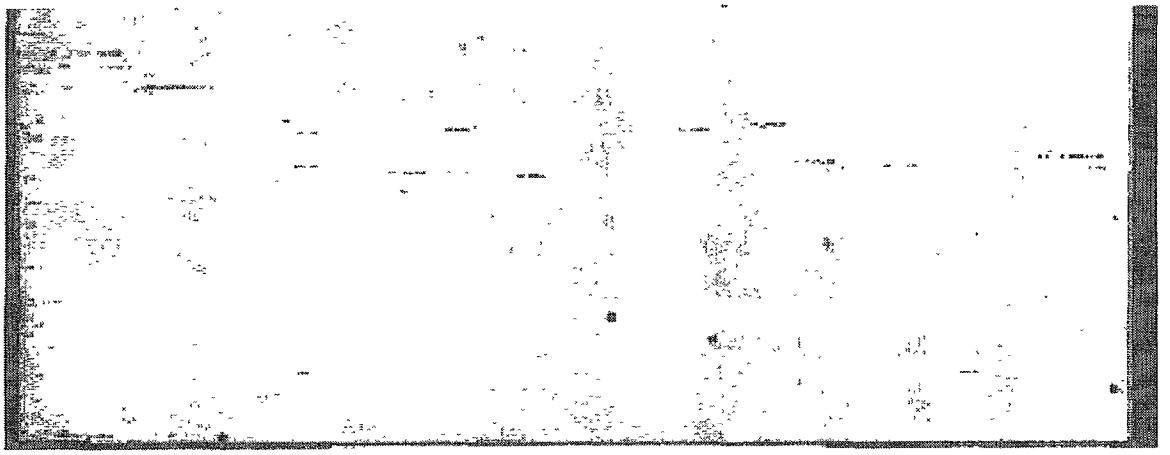

Figure 47. C-scan obtained by waterjet through-transmission method of as-fired curved ceramic specimen (A2) containing no known defects.

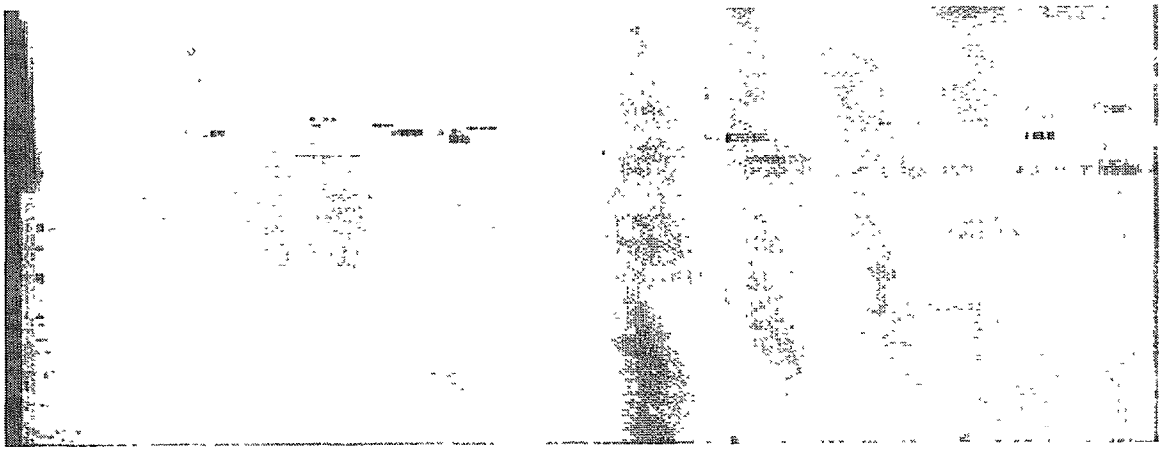

Figure 48. C-scan obtained by waterjet through-transmission method of as-fired curved ceramic specimen (B2) containing 0.015-inch equi-axed defects.

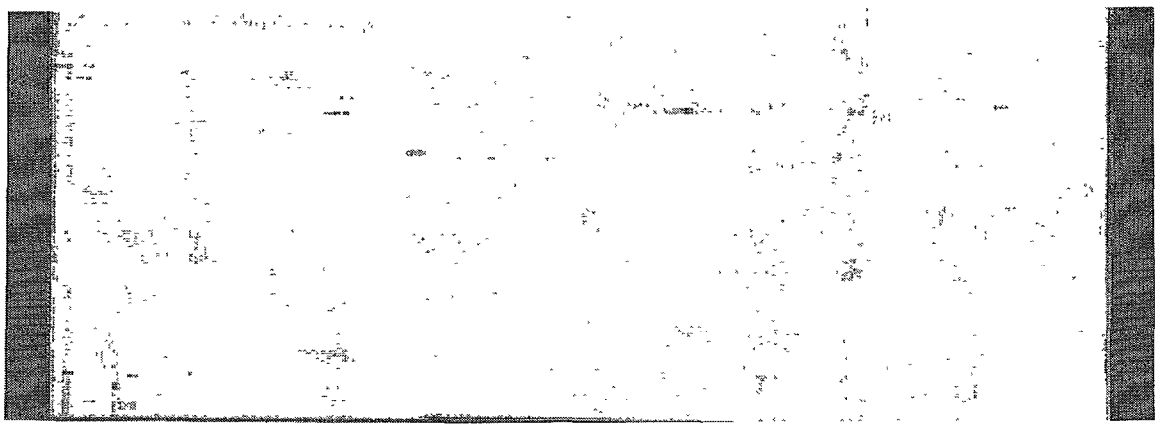

Figure 49. C-scan obtained by waterjet through-transmission method of as-fired curved ceramic specimen (C2) containing 0.030-inch equi-axed defects.

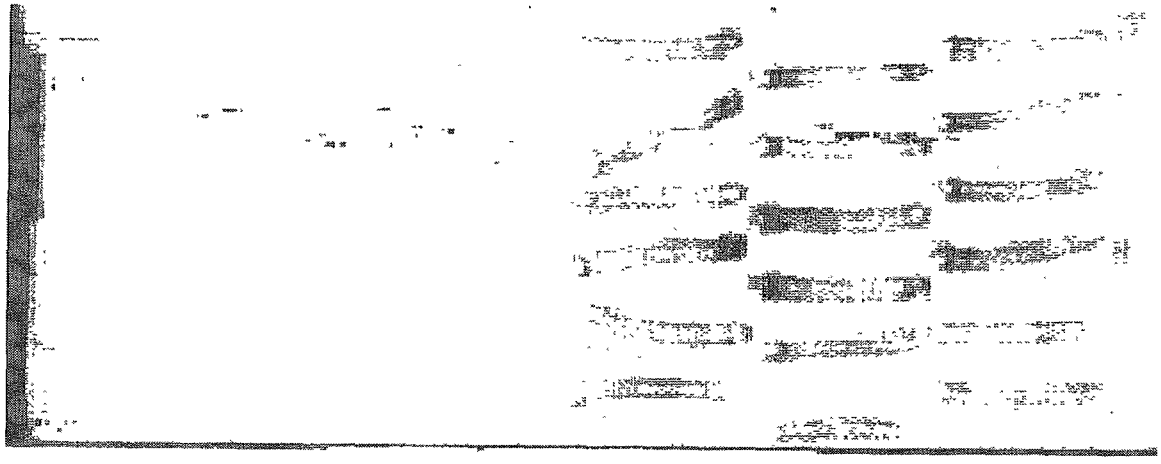

Figure 50. C-scan obtained by waterjet through-transmission method of as-fired curved ceramic specimen (D2) containing 1-inch-long by 0.028-inch-diameter rod-shaped defects.

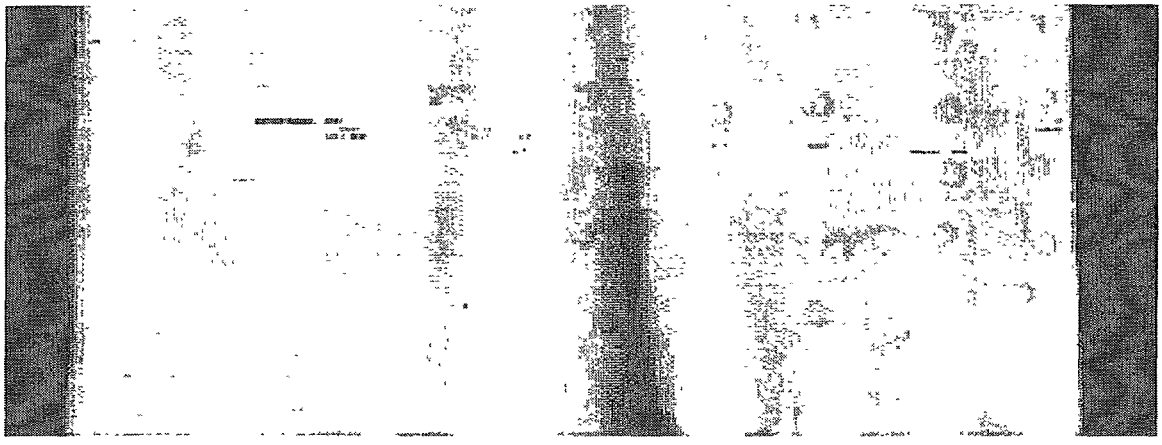

Figure 51. C-scan obtained by waterjet through-transmission method of as-fired curved ceramic specimen (E2) containing 0.052-inch-diameter spherical defects.

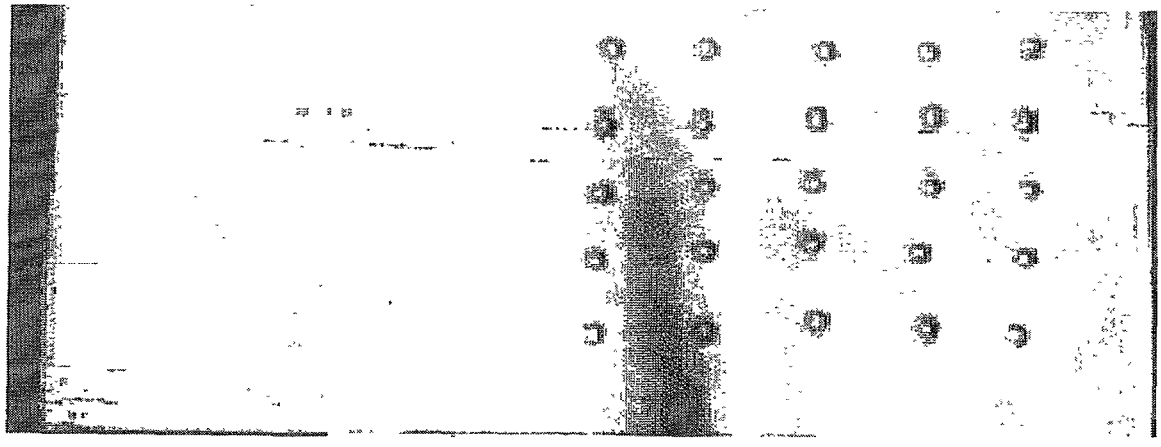

Figure 52. C-scan obtained by waterjet through-transmission method of as-fired curved ceramic specimen (F2) containing 0.105-inch-diameter spherical defects.

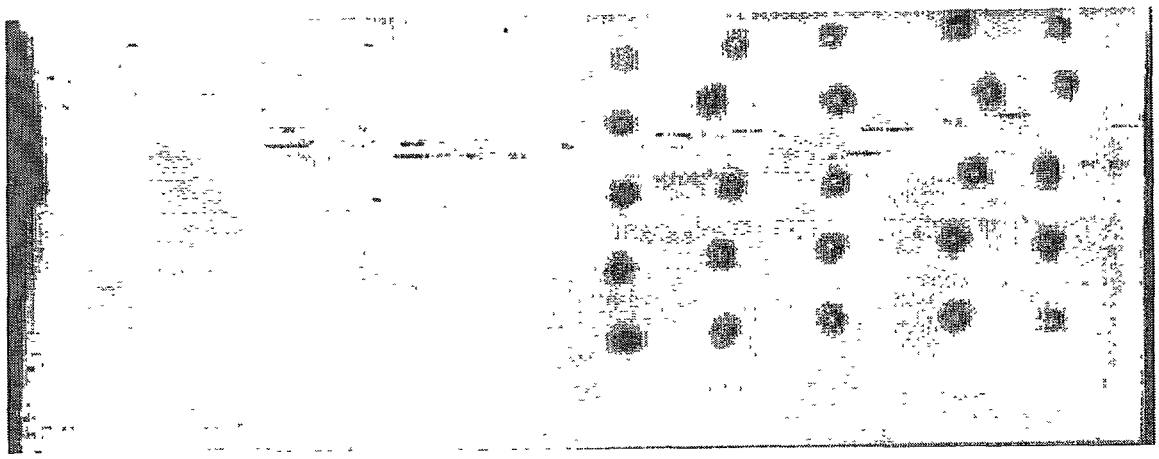

Figure 53. C-scan obtained by waterjet through-transmission method of as-fired curved ceramic specimen (G2) containing 0.105-inch-square by 0.005-inch-thick planar defects.

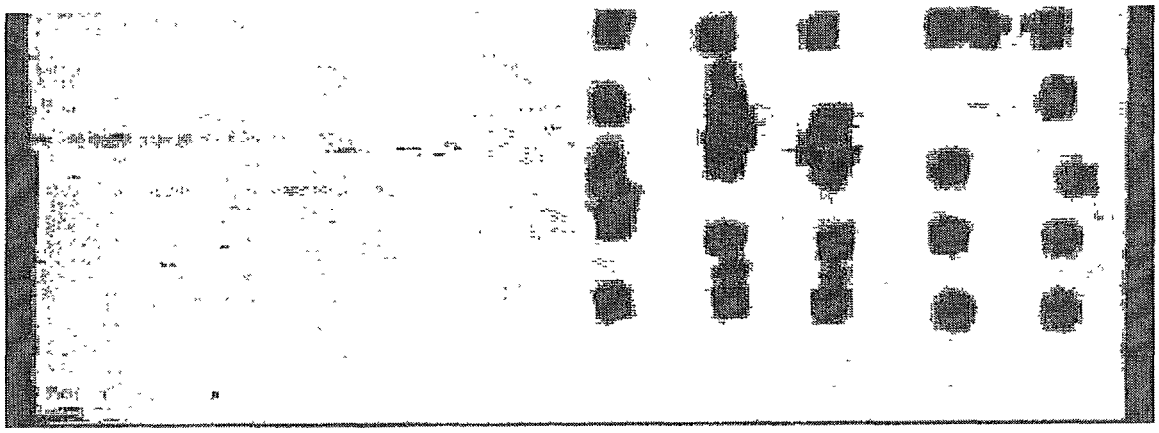

Figure 54. C-scan obtained by waterjet through-transmission method of as-fired curved ceramic specimen (H2) containing 0.210-inch-square by 0.005-inch-thick planar defects.

Figure 55. C-scan obtained by SAM of one column of defects found in as-fired curved ceramic specimen (B2) containing 0.015-inch equi-axed defects. The area shown represents a 0.5-inch by 3-inch area on the specimen, each pixel measures 0.0065 x 0.0065 inch.

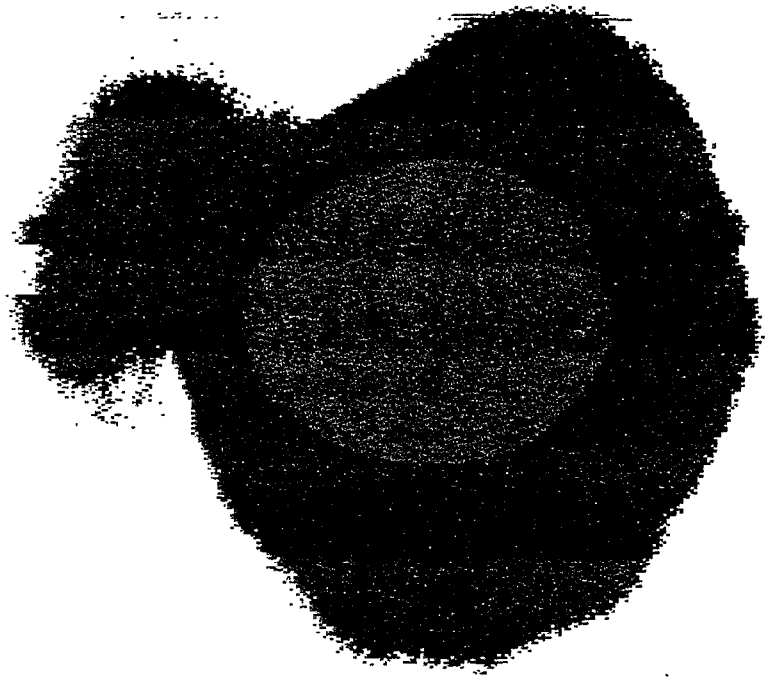

Figure 56. Magnified C-scan obtained by SAM of one defect in as-fired curved ceramic specimen (B2). The area shown measures 0.096 x 0.096 inch, each pixel measures 0.0002 x 0.0002 inch.

Figure 57. C-scan obtained by SAM of one column of defects found in as-fired curved ceramic specimen (D2) containing 1-inch-long by 0.028-inch-diameter rod-shaped defects. The area shown represents a 2.25-inch by 1.5-inch area on the specimen.

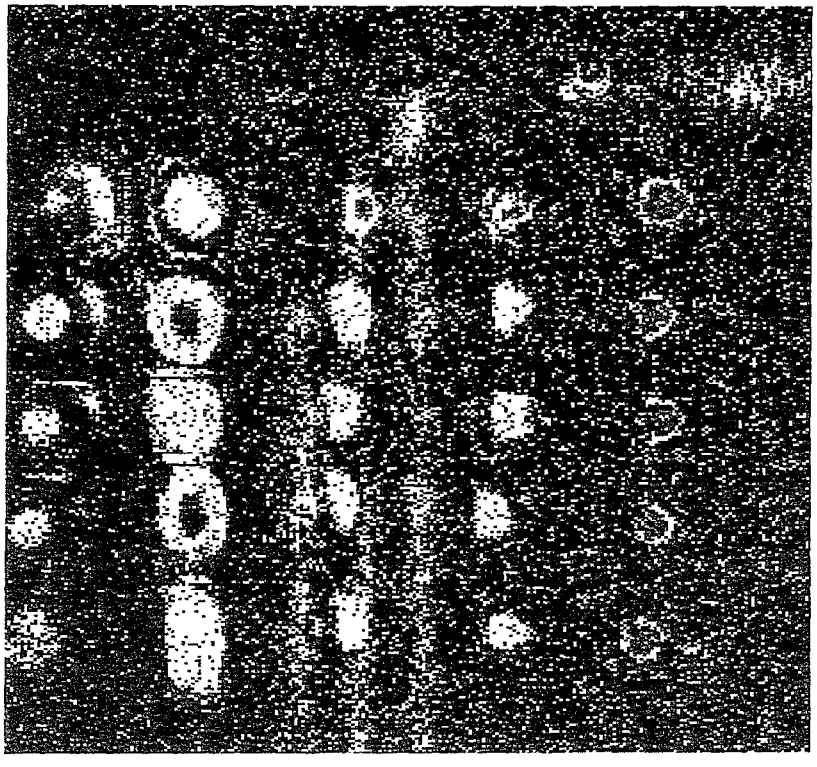

Figure 58. C-scan obtained by SAM of as-fired curved ceramic specimen (F2) containing 0.105-inch-square by 0.005-inch thick planar defects. The area shown measures 3 x 3 inches.

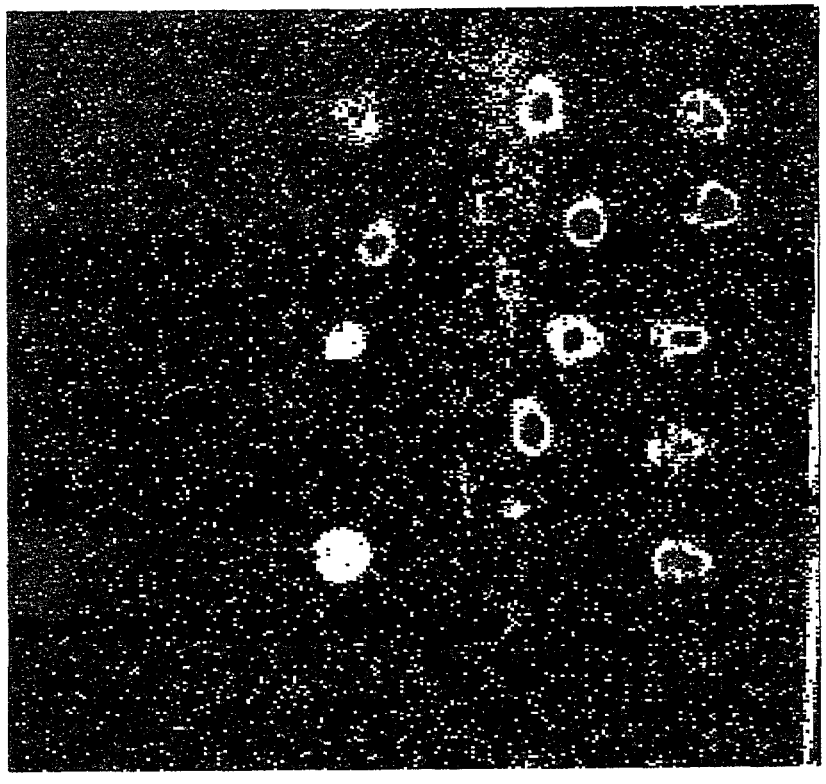

Figure 59. C-scan obtained by SAM of as-fired curved ceramic specimen (G2) containing 0.210-inch-square by 0.005-inch-thick planar defects. The area shown measures 3 x 3 inches.

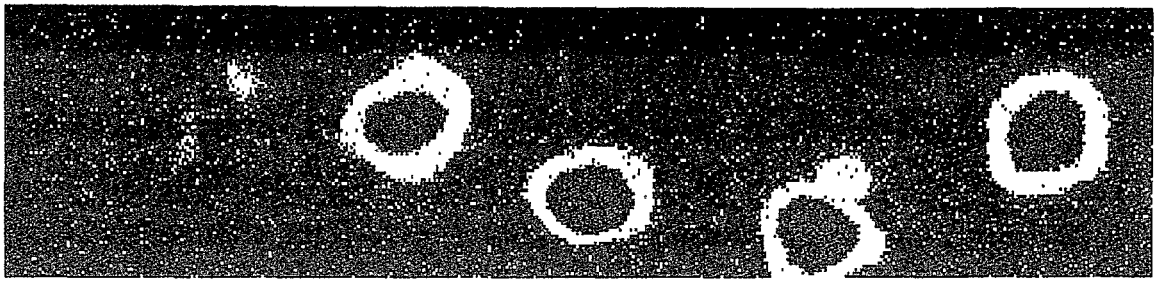

Figure 60. C-scan obtained by SAM of one column of defects found in as-fired curved ceramic specimen (G2) containing 0.105- inch-square by 0.005-inch-thick planar defects. The area shown represents a 0.5-inch by 2.25-inch area on the specimen.

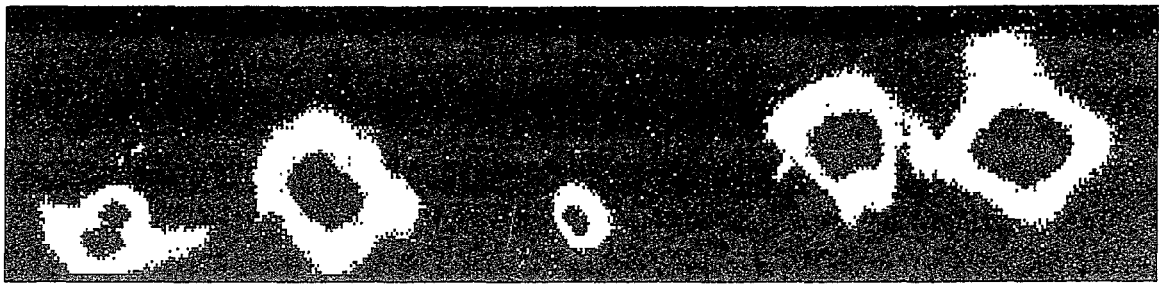

Figure 61. C-scan obtained by SAM of one column of defects found in as-fired curved ceramic specimen (H2) containing 0.210-inch-square by 0.005-inch-thick planar defects. The area shown represents a 0.5-inch by 2.25-inch area on the specimen.

Table 1. Nondestructive evaluation specimen defect code.

CODE	DEFECT SHAPE	MATERIAL USED TO CREATE DEFECT	DIMENSION	PREDICTED DIMENSION
A	None	None.	None	None
B	Equi–axed	Sugar: screened, refined, microscopically hand–selected.	0.018 inch	0.015 inch
C	Equi–Axed	Sugar: crushed and screened crystallized rock. Microscopically hand selected.	0.036 inch	0.030 inch
D	Rod	Nylon: 80-pound test fishing line.	0.034 x 1.2 inch	0.028 x 1 inch
E	Spherical	Nylon: Grade 500P from Industrial Techtonics Inc., Michigan.	0.0625 inch	0.052 inch
F	Spherical	Nylon: Grade 1 from Bal–tec Los Angeles, CA.	0.125 inch	0.105 inch
G	Planar	Polyethylene.	0.125 x 0.125 x 0.006 inch	0.105 x 0.105 x 0.005 inch
H	Planar	Polyethelyne.	0.250 x 0.250 x 0.006 inch	0.210 x 0.210 x 0.005 inch

Note: Specimen series A1 through H1 are finish ground and series A2 through H2 are as-fired.

Table 2. Nondestructive evaluation method summary table.

METHOD	DEFECTS DETECTED	TYPE OF DEFECT MOST DIFFICULT TO DETECT	DEFECT SHOWN TRUE SIZE	ACCESS TO CENTER OF COMPONENT REQUIRED	PORTABLE	AVAILABILITY	COST	RECOMMENDED INSPECTION LEVEL	IN-SERVICE INSPECTION
X-ray film radiography	D,E,F H barely	planar and < 0.052	Yes	Yes	No	High	Low	3 (2–D)	No
Digitization and enhancement	D,E,F C barely H barely	planar and ≤0.030	Yes	N/A	N/A	Fair	Low	3 (2–D)	No
Digital radiography	D,E,F,G,H C barely	planar and ≤ 0.030	Yes	No	No	Limited	Medium	3 (2–D)	No
Computed tomography	C,D,E,F,G,H	< 0.030	Yes	No	No	Limited	High	3 (3–D) and 4	No
Full immersion pulse-echo	B,C,D,E,F,G, H	Near surface defects	No	No	No	High	Medium	1 and 2 (3–D)	Yes
Waterjet through-transmission	C,D,E,F,G,H	< 0.030	No	Yes	Yes	High	Medium	1 and 2 (2–D)	Yes
Scanning acoustic microscopy	B,D,F,G,H C & E not attempted	≤ 0.015	No	No	No	Limited	High	None	No

THE AUTHORS

RAMON R. KURKCHUBASCHE is a Research Engineer for the Ocean Engineering Division and has worked since November 1990 in the field of deep submergence pressure housings fabricated from ceramic materials. His education includes a B.S. in Structural Engineering from the University of California at San Diego, 1989; and an M.S. in Aeronautical/Astronautical Engineering from Stanford University in 1990. His experience includes conceptual design, procurement, assembly, testing, and documentation of ceramic housings. Other experience includes buoyancy concepts utilizing ceramic, nondestructive evaluation of ceramic components. He is a member of the Marine Technology Society, and has published "Elastic Stability Considerations for Deep Submergence Ceramic Pressure Housings," *Intervention '92*, and "Nondestructive Evaluation Techniques for Deep Submergence Housing Components Fabricated from Alumina Ceramic," *MTS '93 Proceedings.*

RICHARD P. JOHNSON is an Engineer for the Ocean Engineering Division. He has held this position since 1987. Before that, he was a Laboratory Technician for the Ocean Engineering Laboratory, University of California at Santa Barbara from 1985–1986, and Design Engineer in the Energy Projects Division of SAIC from 1986–1987. His education includes a B.S. in Mechanical Engineering from the University of California at Santa Barbara in 1986, and an M.S. in Structural Engineering from the University of California, San Diego, in 1991. He is a member of the Marine Technology Society and has published "Stress Analysis Considerations for Deep Submergence Ceramic Pressure Housings," *Intervention '92*, and "Structural Design Criteria for Alumina-Ceramic Deep Submergence Pressure Housings," *MTS '93 Proceedings.*

DR. JERRY STACHIW is Staff Scientist for Marine Materials in the Ocean Engineering Division. He received his undergraduate engineering degree from Oklahoma State University in 1955 and graduate degree from Pennsylvania State University in 1961.

Since that time he has devoted his efforts at various U.S. Navy Laboratories to the solution of challenges posed by exploration, exploitation, and surveillance of hydrospace. The primary focus of his work has been the design and fabrication of pressure resistant structural components of diving systems for the whole range of ocean depths. Because of his numerous achievements in the field of ocean engineering, he is considered to be the leading expert in the structural application of plastics and brittle materials to external pressure housings.

Dr. Stachiw is the author of over 100 technical reports, articles, and papers on design and fabrication of pressure resistant viewports of acrylic plastic, glass, germanium, and zinc sulphide, as well as pressure housings made of wood, concrete, glass, acrylic plastic, and ceramics. His book on "Acrylic Plastic Viewports" is the standard reference on that subject.

For the contributions to the Navy's ocean engineering programs, the Navy honored him with the Military Oceanographer Award and the NCCOSC's

RDT&E Division honored him with the Lauritsen-Bennett Award. The American Society of Mechanical Engineers recognized his contributions to the engineering profession by election to the grade of Life-Fellow, as well as the presentation of Centennial Medal, Dedicated Service Award and Pressure Technology Codes Outstanding Performance Certificate.

Dr. Stachiw is past-chairman of ASME Ocean Engineering Division and ASME Committee on

Safety Standards for Pressure Vessels for Human Occupancy. He is a member of the Marine Technology Society, New York Academy of Science, Sigma Xi and Phi Kappa Honorary Society.